Karl-Franzens-Universität Graz
Institut für Physik

The physical spectrum of theories with a Brout-Englert-Higgs effect

Pascal Törek

Dissertation zur Erlangung des
Doktorgrades der Naturwissenschaften

Betreut durch Univ.-Prof. Dipl.-Phys. Dr.rer.nat. Axel Maas

Graz, 2017

Abstract

The physical, observable spectrum in gauge theories is made up from gauge-invariant states. In the standard model of particle physics the Fröhlich-Morchio-Strocchi mechanism shows that these states can be adequately mapped to the gauge-dependent, elementary W, Z, and Higgs as well as fermionic states. In theories with a more general gauge group and Higgs sector this is no longer necessarily the case.

We classify and predict the physical spectrum for a wide range of such theories and show that discrepancies between the spectrum of elementary fields and physical particles frequently arise. We discuss in detail $\mathrm{SU}(N)$ gauge theories with single scalar fields in the fundamental and adjoint representation of the gauge group. We also investigate models for grand unified theories where usually more scalar fields appear in the theory.

The validity of these predictions can only be tested using non-perturbative methods. This is done using the method of lattice gauge theory for the special case where the gauge group is $\mathrm{SU}(3)$ with one single fundamental scalar. We first determine the phase diagram of this theory and compute the spectrum of bound states in a regime where a Brout-Englert-Higgs effect takes place. Then the spectrum of gauge-variant, elementary fields is computed and compared to the gauge-invariant, physical spectrum. We find that our computations seem to confirm the predictions of the Fröhlich-Morchio-Strocchi mechanism.

Kurzfassung

Das physikalische, beobachtbare Spektrum von Eichtheorien besteht aus eichinvarianten Zuständen. Im Standard Modell der Teilchenphysik zeigt der Fröhlich-Morchio-Strocchi Mechanismus, dass diese Zustände angemessen auf die eichvarianten, elementaren W, Z, Higgs und fermionische Zustände abgebildet werden können. In Theorien mit allgemeinerer Eichgruppe und Higgs-Sektor muss das nicht notwendigerweise der Fall sein.

Wir klassifizieren und vorhersagen das physikalische Spektrum für eine große Bandbreite von Theorien. Wir zeigen, dass es häufig Unterscheide zwischen dem Spektrum der elementaren Felder und dem der physikalischen Teilchen auftauchen. Wir diskutieren im Detail $\mathrm{SU}(N)$ Eichtheorien mit skalaren Feldern in der fundamentalen und der adjungierten Darstellung der Eichgruppe, sowie Modelle für große vereinheitlichte Theorien, wo üblicherweise mehrere skalare Felder in der Theorie auftauchen.

Diese Vorhersagen können mit nicht-störungstheoretischen Methoden getestet werden. Dafür wählen wir den Spezialfall eines fundamentalen skalaren Feldes mit der Eichgruppe $\mathrm{SU}(3)$ und studieren diesen Fall mit Hilfe von Gittereichtheorie. Zuerst wird das Phasendiagramm dieser Theorie berechnet und anschließend das physikalische Spektrum der Bindungszustände, in einem Regime wo ein Brout-Englert-Higgs Effekt stattfindet, bestimmt. Danach wird das Spektrum der eichvarianten, elementaren Feldern bestimmt. Wir finden, dass unsere Berechnung die Vorhersagen des Fröhlich-Morchio-Strocchi Mechanismus zu bestätigen scheinen.

to Hanna

Contents

1 Introduction 9

2 Theoretical foundations 15
- 2.1 Perturbative treatment of the standard model Higgs sector . . . 15
- 2.2 Gauge-invariant perturbation theory . . . 20
- 2.3 A recipe . . . 22

3 SU(N) gauge theories with scalars in several representations 25
- 3.1 SU(N) gauge theories with a fundamental scalar . . . 25
  - 3.1.1 Gauge-variant description in a fixed gauge . . . 25
  - 3.1.2 Gauge-invariant spectrum . . . 27
- 3.2 SU(N) gauge theories with an adjoint scalar . . . 30
  - 3.2.1 Gauge-variant description in a fixed gauge . . . 31
  - 3.2.2 Gauge-invariant spectrum . . . 32
  - 3.2.3 SU(2) gauge theory . . . 35
  - 3.2.4 SU(3) gauge theory . . . 36
  - 3.2.5 SU(4) gauge theory . . . 39
- 3.3 SU(5) GUT as a toy model . . . 41
  - 3.3.1 Gauge-variant description in a fixed gauge . . . 41
  - 3.3.2 Gauge-invariant description . . . 42
- 3.4 SU(3) with two scalars in the fundamental representation . . . 43

4 Lattice field theory 47
- 4.1 Gauged scalar field theory on the lattice . . . 47
- 4.2 Generating configurations . . . 49
- 4.3 Spectroscopy . . . 50
  - 4.3.1 Zero momentum projection and time slice averaging . . . 51
  - 4.3.2 Variational analysis . . . 51
  - 4.3.3 Smearing of the fields . . . 52
- 4.4 Gauge fixing on the lattice . . . 53

4.5 Propagators of gauge variant quantities and running coupling 55
4.5.1 Gauge field and scalar propagator 55
4.5.2 Definition of the renormalization scheme 56
4.5.3 Ghost propagator 57
4.5.4 Schwinger functions 57
4.5.5 Running coupling 58

5 SU(3) lattice gauge theory with a fundamental scalar 59
5.1 Phase diagram of the theory 59
5.2 Physical spectrum 61
5.2.1 Definition of interpolators 62
5.2.2 Spectroscopy results 64
5.3 Test of the Fröhlich-Morchio-Strocchi mechanism 72
5.3.1 Predictions from the FMS mechanism 72
5.3.2 Spectrum of gauge-variant quantities 72
5.3.3 Comparison between the spectra 78

6 Conclusions 81

A The structure of the state space 85

B Analysis of open U(1) states 89

C Global gauge transformation for the space-time averaged scalar field 91

D Lattice versions of the open U(1) operators 93

E Data and fit tables 95
E.1 Numerical values 95
E.2 Tables of fit parameters 96

F Determining critical exponents and Wilson coefficients for clock models 99
F.1 Introduction 99
F.2 The q-states clock-model 99
F.3 Generating configurations 100
F.4 Observables 102
F.5 Critical couplings 103
F.6 Critical exponents and finite size scaling 104
F.7 Wilson coefficients 106

References 108

Chapter 1

Introduction

The standard model of particle physics successfully describes nearly all phenomena and processes which involve particle energies up to a few TeV. This theory is impressively well established by today's collider-based experiments, and thus serves as one cornerstone of our understanding of nature. The standard model classifies all known elementary particles and describes how they interact electromagnetically, weakly, and strongly with each other using the mathematical framework of quantum field theory [1–4].

The most prominent experiments to test predictions from the standard model are nowadays located at CERN within its large hadron collider (LHC). So far, no experimental observation of physics beyond the standard model has been detected at the LHC. A discrepancy of about three standard deviations to the standard model prediction is discovered in the branching ratio of the decay of B_c^+ mesons [5] signaling a possible violation of so-called lepton universality. Currently, it is just speculation if this is a sign for new physics, an underestimation of hadronic effects, or turns out to be yet another prominent statistical fluctuation [6, 7].

Nonetheless, despite the extraordinary accomplishment of explaining the LHC experiments with the standard model theory, it is known that there must be a more fundamental theory of nature. For instance, the standard model describes only three of the known four fundamental interactions. The currently best description of the fourth force, i.e., gravity, is given by general relativity [8]. At the microscopic scale of elementary processes gravitational effects are presumably negligible compared to the other three fundamental forces, until the energy scale of the considered process moves towards the Planck scale $M_{\mathrm{P}} \approx 10^{19}$ GeV. At these large scales, effects of quantum gravity probably become important and eventually dominate the physical processes. Prominent attempts to formulate consistent quantum theories of gravity are string theory [9], supergravity [10], loop quantum gravity [11], asymptotic safety [12], or causal dynamical triangulation [13]. The pure standard model should therefore be only considered as a low energy effective theory of an extended model. However, the standard model is a theory with a consistent quantum field theoretical formulation of the other three fundamental forces using the concept of gauge invariance [3]. We introduce this formulation briefly here.

Quantum electrodynamics (QED) was the first successful implementation of gauge invariance [14–19]. This theory is invariant under the gauge group $\mathrm{U}(1)_{\mathrm{em}}$, with the electric charge being the generator of this group. All electrically charged particles interact with each other via the exchange of a gauge boson, the so-called photon. Theoretical predictions from QED are in extraordinary agreement with corresponding experiments giving strong evidence that the gauge principle could indeed be a fundamental concept of nature, see, e.g., [20–22] for a computation and experimental determination to a very high precision of the so-called anomalous magnetic moment of the electron.

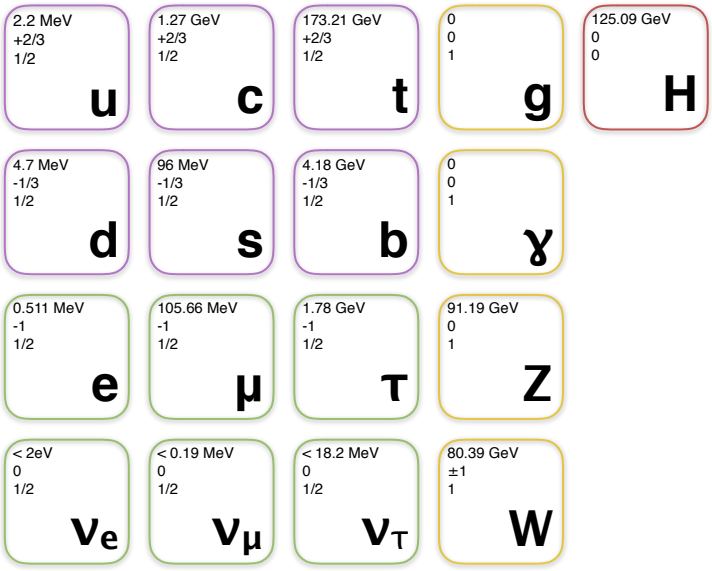

Figure 1.1: Sketch of the elementary particles of the standard model. In each box we list the mass, electric charge, and spin of the corresponding particle taken from [31]. In the violet boxes we display the six quark flavors: up (u), down (d), charm (c), strange (s), top (t), and bottom (b). Below the quarks the group of leptons is shown: electron (e) and electron neutrino (ν_e), muon (μ) and muon neutrino (ν_μ), as well as tau (τ) and tau neutrino (ν_τ). The yellow boxes indicate the gauge bosons of the strong interaction (gluons g), the weak interaction ($W^\pm$, Z), as well as of the electromagnetic interaction (photon γ). The Higgs particle (H) is located in the red box.

Guided by the success of this principle in QED, the concept of gauge invariance has been applied to formulate quantum chromodynamics (QCD), which describes the interplay between quarks and gluons [23]. It is the theory of strong interactions describing how quarks and gluons interact to finally form hadrons. The gauge group of QCD is $\mathrm{SU}(3)_\mathrm{C}$, where the index denotes the corresponding quantum number 'color'. QCD is asymptotically free [24] due to its non-Abelian nature and the six quark flavors, which manifests itself in the negative beta function of the gauge coupling. Therefore, the interaction strength between quarks and gluons decreases as the energy scale is increased. Another feature of this theory is quark confinement [25] explaining why free quarks and gluons are not observed and only exist within hadrons or plasmas. There is no rigorous definition of confinement and a lot of effort is invested in the investigation of this issue, see, e.g., [26] for an overview, and [27] for recent developments.

The research area of QCD also paved the way for so-called Euclidean lattice quantum field theory [25]. This approach is a non-perturbative tool to study quantum systems on a discrete spacetime lattice, and is optimally suited for numerical simulations using Monte Carlo methods. Lattice quantum field theory is one of the most successful methods to compute static properties of particles. A brief introduction to lattice field theory is given in Chapter 4. For a detailed theoretical background, see, e.g., [28–30].

The third fundamental interaction, the weak interaction, can actually be 'unified' with the electromagnetic one. The theory which describes these interactions is called Glashow-Salam-Weinberg (GWS) theory [32–34]. The underlying gauge group of this theory is the direct product $\mathrm{SU}(2)_\mathrm{L} \times \mathrm{U}(1)_\mathrm{Y}$. The hypercharge Y is the generator of the Abelian gauge group. The value of Y differs for

left- and right-handed particles. The index L of the non-Abelian $\mathrm{SU}(2)_\mathrm{L}$ gauge group attributes the fact that only the left-handed particles are gauged, and the right-handed ones are gauge singlets with respect to this group. The GWS theory incorporates the so-called Higgs mechanism [35–39] explaining how the gauge bosons of the weak interaction, W, and Z, obtain their mass as well as how the fermion masses are generated. Also, a fundamental scalar particle, the Higgs boson, is predicted by the GWS theory whose existence has been confirmed by the ATLAS and CMS collaborations [40, 41]. Colloquially, one speaks of spontaneous break down of the gauge symmetry $\mathrm{SU}(2)_\mathrm{L} \times \mathrm{U}(1)_\mathrm{Y}$ to $\mathrm{U}(1)_\mathrm{em}$, see Section 2.1.

The full standard model is now the product group $\mathrm{SU}(3)_\mathrm{C} \times \mathrm{SU}(2)_\mathrm{L} \times \mathrm{U}(1)_\mathrm{Y}$ which is broken by the Brout-Englert-Higgs effect to $\mathrm{SU}(3)_\mathrm{C} \times \mathrm{U}(1)_\mathrm{em}$. We show a sketch of the elementary particles described by the standard model and some of their properties in Figure 1.1.

Beside of not explaining gravity, there are issues within the standard model as well. Some of them are explicitly related to the Higgs sector. So far it seems that the only consistent four-dimensional quantum field theory of a scalar field is a non-interacting theory [42, 43]. This is the so-called triviality problem. However, since this problem can be suspended to energy scales of the order of the GUT scale, $M_\mathrm{GUT} \approx 10^{15}$ GeV, this question is not necessarily of practical relevance. One can define an interacting scalar field theory with a (large) intrinsic cutoff [44–46], which serves as an additional parameter of the theory, thus yielding a still useful low-energy effective theory [47].

Furthermore, there is the so-called hierarchy problem which states that there is no reason why the masses of the fermions are so different. Only the top quark is of the order of the electroweak scale $M_\mathrm{ew} \approx 246$ GeV and all the other fermion masses are well below this scale. Within the standard model it is not possible to explain this hierarchy of fermion masses.

One peculiar feature of the standard model is that the running gauge couplings of the standard model interactions almost meet at a scale of about M_GUT, suggesting a unification of the strong and the electroweak interaction [48]. Theories which implement a crossing of the gauge couplings are called grand unified theories (GUTs). The idea of these kind of theories is, that one uses Lie groups which contain the standard model group $\mathrm{SU}(3)_\mathrm{C} \times \mathrm{SU}(2)_\mathrm{L} \times \mathrm{U}(1)_\mathrm{Y}$ as a subgroup. The fact that the standard model has rank 4 excludes already, e.g., $\mathrm{SU}(4)$ with rank 3 and G_2 with rank 2 as grand unified groups. The GUT group must also allow for complex fermion representations, since they are described by complex spinors. This excludes groups which only allow for real representations as, e.g., again G_2. The simplest Lie groups are the rank 4 groups $\mathrm{SU}(5)$ and $\mathrm{SO}(10)$, as well as the popular exceptional Lie groups E_6, E_7, and E_8, where the subscripts indicate their respective ranks. GUTs can explain the quantization of charges, which cannot be explained within the standard model, since $\mathrm{U}(1)_\mathrm{em}$ is an Abelian group allowing for arbitrary charge values. Therefore, GUTs are able to explain the anomaly cancellation in the standard model.

There are also other suggestions for beyond the standard model extensions as, e.g., technicolor, little Higgs, and hidden sectors. Technicolor avoids the hierarchy problem by treating the Higgs boson as a composite object. It is a strongly interacting additional sector to the standard model with an energy scale of around 1 TeV which has similar features as QCD. The general setup is to introduce an $\mathrm{SU}(N_\mathrm{T})$ gauge group with N_f additional so-called techniquarks, transforming in the fundamental representation of $\mathrm{SU}(N_\mathrm{T})$. Together with technigluons the techniquarks form technihadrons. The Higgs is then a scalar technimeson similar to the σ meson in QCD. The simplest models suffer from some issues, and therefore more advanced technicolor theories, as extended technicolor or minimal walking technicolor are needed. For an overview see, e.g., [49].

The idea that the Higgs particle could be a pseudo-Goldstone boson of a spontaneously broken global symmetry at a TeV scale is used by little Higgs models. The (approximate) global symmetry would then stabilize the Higgs mass. For a review see, e.g., [50].

Models with hidden sectors contain additional particles, which couple only weakly or even not at all to the known standard model particles. Heavy messenger particles, with masses in the TeV range, connect the hidden sector with the standard model. Therefore, these models are a rich source for dark matter candidates [51].

The physical states of gauge theories, as the standard model as well as all the candidates [1] for beyond standard model theories discussed above, need to be gauge-invariant. This almost tautological insight has a realization which is far from obvious in the standard model and in beyond standard model theories. In QCD, the aforementioned confinement mechanism takes care of this issue [2], while for QED dressings by Dirac phases create observable states [52]. A third type of realization is encountered in the weak sector, where the same necessity applies [53–57]. At first sight, this seems surprising, as a perturbative description using the BRST-invariant, but still gauge-dependent, elementary states of the Lagrangian, the W, the Z, the Higgs, and the fermion fields, describe experimental results remarkably well, as mentioned above [31].

The subtle reason for this is the mechanism described by Fröhlich, Morchio, and Strocchi (FMS) [56, 57]: Under certain conditions, met by the standard model, the properties of the physical states can be mapped to the gauge-dependent states which appear in the Lagrangian, see Section 2.2. This FMS mechanism has been confirmed in lattice calculations for the bosonic sector [58, 59]. A review of this can be found in [60, 61]. While this also applies to the fermion sector in principle [56, 57, 62], the involved technical complications have yet made an explicit test not possible. Still, the excellent agreement of the predictions of the FMS mechanism with experimental results is already good evidence for its validity.

However, the conditions mentioned are quite specific, and the standard model is special to fulfill them, as the local symmetry group is the same as the global symmetry group in the weak sector. This issue is further exemplified in Section 2. In general, beyond the standard model theories cannot be expected to accomplish this particular requirement [63]. If such a theory does not satisfy certain conditions, discrepancies between the actual physical spectrum and the one described by perturbation theory arise. Investigations of explicit examples have found both types of behaviors [64, 65]. In particular, this can imply that the low-lying observable spectrum is different from the standard model, even if a model features perturbatively the W and Z bosons and a light Higgs. Such theories would therefore not be suitable extensions of the standard model.

The aim of this work is to classify a set of theories according to their physical spectrum. This will be done using the FMS mechanism in Chapter 3. These results are analytical predictions, valid in a similar range as conventional perturbation theory. We then test the mechanism using lattice field theory for a particular theory, i.e., an $\mathrm{SU}(3)$ gauge theory with a scalar field in the fundamental representation of the gauge group, see Chapter 5. In this case the gauge group is larger than the global symmetry group, which is $\mathrm{U}(1)$. We are able to construct states which are neutral or charged with respect to this global symmetry. It is the latter case which gives rise to quantum numbers which are not sustainable by the elementary fields. As long as no statistically reliable experimental indication of new physics arise, these predictions can be tested only theoretically, e.g., using lattice simulations along the lines of [58, 59, 65].

This thesis is organized as follows: In Chapter 2 we introduce the theoretical foundations of this work. We further discuss the gauge-Higgs sector of the standard model. We first focus on the standard perturbative treatment of this sector and discuss which fundamental problem arises in this analysis. We change the point of view when we consider so-called gauge-invariant perturbation theory, where we combine the Fröhlich-Morchio-Strocchi mechanism with standard perturbation theory. A recipe

[1] This does not have to be the case for an ungauged hidden-sector theory.

on how one should apply this procedure to general gauge-Higgs theories is given at the end of this chapter.

In Chapter 3 we apply this recipe to $\mathrm{SU}(N)$ gauge theories with scalar fields in several representations of the gauge group. We first consider a scalar in the fundamental representation. The gauge-dependent spectrum of this theory is discussed in the beginning, followed by the prediction of the spectrum using gauge-invariant perturbation theory. We then discuss the case of a scalar field in the adjoint representation. Again, we consider the gauge-variant spectrum first, before we switch to the gauge-invariant description. Furthermore, we examine several specific gauge groups in this section. The subsequent section is dedicated to one of the most prominent grand unified theories, i.e., an $\mathrm{SU}(5)$ gauge theory where two different scalar fields appear, one field in the fundamental and one in the adjoint representation of $\mathrm{SU}(5)$. We conclude this chapter by considering an even simpler version of the $\mathrm{SU}(5)$ grand unified theory, namely an $\mathrm{SU}(3)$ gauge theory with two different scalars in the fundamental representation. We will see that with increasingly complex structures in the Higgs sectors a full discussion quickly proliferates into an involved group-theoretical problem.

Chapter 4 is dedicated to an introduction to lattice field theory. We introduce and discuss all the techniques used to perform a Monte Carlo simulation of a distinct lattice field theory which are needed to test the FMS mechanism. We especially discuss in detail how configurations are created via Markov chains, how spectroscopy is performed, as well as how we fix the gauge on the lattice. This is needed to determine the propagators of the elementary and gauge-variant fields.

We apply these lattice techniques to an $\mathrm{SU}(3)$ gauge theory with a scalar field in the fundamental representation in Chapter 5. We show how the phase diagram of this theory is obtained, and how the spectrum in the Higgs-like regime looks like. The propagators of the gauge-variant, elementary fields are studied on gauge-fixed configurations to compare to the gauge-invariant spectrum and investigate whether the predictions of the FMS mechanism apply.

Finally, we conclude our work and give an outlook to possible future studies regarding the application of the FMS mechanism to other theories as well as further tests of this mechanism on the lattice.

The Appendix F is devoted to a project I worked on during a stay abroad at the Friedrich-Schiller University in Jena, Germany, under the supervision of Andreas Wipf in collaboration with Martin Ammon and André Sternbeck. The project was about determining critical exponents and Wilson coefficients for certain spin models, so-called q-states clock-models. This chapter is located at the end of this thesis.

Additionally, I should note that also some results from Chapter 3 find their origin from this stay. This work has been done in collaboration with Axel Maas and René Sondenheimer.

Chapter 2

Theoretical foundations

In this chapter, we review some of the theoretical concepts regarding Higgs physics needed for the rest of the thesis. This content can be found in almost every textbook about theoretical particle physics and quantum field theory, e.g., see [3, 4]. The main purpose of the following sections is to introduce our conventions and notations as well as for the sake of completeness.

First we discuss the standard model Higgs sector, or, to be more precise, the gauge-Higgs part of this sector. We give an overview of the perturbative treatment of this sector, introducing the most important concepts. This is followed by an introduction to the Fröhlich-Morchio-Strocchi mechanism and to so-called gauge-invariant perturbation theory in Section 2.2.

At the end of this chapter we present a general recipe on how gauge-invariant perturbation theory can be used for more general gauge groups and scalar field representations.

The following sections follow closely parts of [60] as well as [61, 66].

2.1 Perturbative treatment of the standard model Higgs sector

For simplicity we only consider the weak sector of the standard model here, where we neglect the $\mathrm{U}(1)$ gauge group as well as fermions. Therefore, we deal with a model which describes an $\mathrm{SU}(2)$ gauge theory coupled to a complex scalar field in the fundamental representation. Of course, this is a significant simplification of the intricate standard model-Higgs sector, but sufficient for the following considerations. The gauge-invariant Lagrangian is given by

$$\mathcal{L} = -\frac{1}{4}\, W^a_{\mu\nu}\, W^{a\,\mu\nu} + \big(D_\mu\phi\big)^\dagger \big(D^\mu\phi\big) - V\big(\phi^\dagger\phi\big)\ , \tag{2.1}$$

with the field strength tensor $W^a_{\mu\nu}$ and the covariant derivative D_μ defined as,

$$W^a_{\mu\nu} = \partial_\mu W^a_\nu - \partial_\nu W^a_\mu - g\,\epsilon^{abc}\, W^b_\mu\, W^c_\nu \quad \text{and} \quad D_\mu = \partial_\mu + \mathrm{i}\, g\, W^a_\mu\, \frac{\sigma^a}{2}\ , \tag{2.2}$$

where ϵ^{abc} is the totally antisymmetric Levi-Civita symbol, i.e., the structure constants of the Lie algebra of $\mathrm{SU}(2)$. The generators T^a of the Lie algebra can be chosen to be proportional to the standard Pauli matrices σ^a, $T^a = \frac{\sigma^a}{2}$. The gauge coupling g gives rise to a 3- and a 4-point interaction between the gauge bosons as well as for an interaction of the scalar field with the gauge bosons.

The fields transform under gauge transformations $U(x) \in \mathrm{SU}(2)$ as

$$\phi(x) \to U(x)\,\phi(x) \quad , \quad W_\mu(x) \to U(x)\,W_\mu(x)\,U(x)^\dagger + \frac{\mathrm{i}}{g}\left(\partial_\mu U(x)\right)U(x)^\dagger \,, \tag{2.3}$$

with the matrix-valued gauge fields $W_\mu(x) = W_\mu^a(x)\,T^a$.

The potential of the Lagrangian (2.1) is a function of the gauge invariant quantity $\phi^\dagger\phi$ only. For our discussions we use a Mexican hat-type potential,

$$V\left(\phi^\dagger\phi\right) = \lambda\left(\phi^\dagger\phi - f^2\right)^2 \,, \tag{2.4}$$

where λ and f are the couplings of the potential. The parameter λ has to be positive for stability reasons. In principle f^2 can be negative, but then the system would be in the symmetric phase in which no symmetry breaking can occur at tree level. Therefore, we set $f^2 > 0$ such that the potential has the desired Mexican hat-like form.

In total there are four real degrees of freedom of the complex scalar field, and thus, due to the pseudo- reality of $\mathrm{SU}(2)$, the Lagrangian (2.1) has besides the gauge symmetry an additional global custodial symmetry group $\mathrm{SU}(2)_\mathrm{c}$ in the pure Higgs sector. There is also another way to see this fact: Consider the pure scalar field theory only, i.e., the ungauged system. This theory exhibits a global $O(4)$ symmetry, which is isomorphic to $\mathrm{SU}(2)_\mathrm{L} \times \mathrm{SU}(2)_\mathrm{R}$. Gauging, e.g., $\mathrm{SU}(2)_\mathrm{L}$ leaves $\mathrm{SU}(2)_\mathrm{R}$ as a global symmetry. The custodial symmetry group is then identified with the global $\mathrm{SU}(2)_\mathrm{R}$ group.

To make the invariance explicit, it is useful to rewrite the Lagrangian (2.1) by using the matrix representation of the scalar field [67],

$$X = \begin{pmatrix} \phi_1 & -\phi_2^\star \\ \phi_2 & \phi_1^\star \end{pmatrix} \,, \tag{2.5}$$

where ϕ_i, $i = 1, 2$, are the complex components of the doublet ϕ. This representation will be particularly useful in the next section. The full symmetry group of the Higgs sector is $\mathrm{SU}(2) \times \mathrm{SU}(2)_\mathrm{c}$, and thus the theory is invariant under the transformations

$$X(x) \to U(x)\,X(x)\,M^\dagger \quad , \quad W_\mu \to U(x)\,W_\mu(x)\,U(x)^\dagger + \frac{\mathrm{i}}{g}\left(\partial_\mu U(x)\right)U(x)^\dagger \,, \tag{2.6}$$

where the gauge transformation $U(x) \in \mathrm{SU}(2)$ acts as left multiplication, and the custodial transformation $M \in \mathrm{SU}(2)_\mathrm{c}$ as a right multiplication on the matrix-valued field X. The gauge field W_μ does not transform under custodial transformations. The Lagrangian (2.1) in this notation now reads

$$\mathcal{L} = -\frac{1}{4}\,W_{\mu\nu}^a\,W^{a\,\mu\nu} + \frac{1}{2}\,\mathrm{tr}\Big[\left(D_\mu X\right)^\dagger\left(D^\mu X\right)\Big] - \lambda\left(\frac{1}{2}\,\mathrm{tr}\big[X^\dagger X\big] - f^2\right)^2 \,, \tag{2.7}$$

where the invariance under $\mathrm{SU}(2) \times \mathrm{SU}(2)_\mathrm{c}$ transformation is manifest. The gauge-invariant condition for the potential to be minimal is $\phi^\dagger\phi = f^2$. These minima are invariant under custodial as well as under gauge transformations. The minima make the custodial symmetry metastable against external perturbations, but never break the global symmetry as argued in [60]. Having now the minimum of the potential, the next step is to split the scalar field as $\phi(x) = \frac{v}{\sqrt{2}}\,n + \varphi(x)$, with $\varphi(x)$ being a fluctuation field around the spacetime-independent quantity $\frac{v}{\sqrt{2}}\,n$, where n is some unit vector, $n^\dagger n = 1$. In the standard approach [3] one sets $v = \sqrt{2}f$ and therefore $\langle\varphi\rangle = 0$. One calls

$\frac{v}{\sqrt{2}}\, n$ the vacuum expectation value of the field ϕ in this case. It is usually said that the split hides the gauge symmetry. We will further discuss this issue below.

In terms of the matrix-valued scalar field (2.5), the condition for a minimal potential is $\frac{1}{2}\mathrm{tr}\left[X^\dagger X\right] = f^2$. The matrix valued field X is then split into $X(x) = v\alpha + \chi(x)$, where $v = f$, α is some arbitrary $\mathrm{SU}(2)$ matrix, and $\chi(x)$ the fluctuation field with $\langle\chi\rangle = 0$.

It is possible to select a certain direction n or equivalently α of the vev in the classical case. A convenient choice is $\alpha = \mathbb{1}$ for the $\mathrm{SU}(2)$ gauge theory. This choice breaks the $\mathrm{SU}(2) \times \mathrm{SU}(2)_\mathrm{c}$ symmetry and only the diagonal global subgroup $\mathrm{SU}(2)_\mathrm{diag}$ corresponding to $U(x) = M$, where M is spacetime independent, remains unbroken, since $v\mathbb{1} \to v\, M\, \mathbb{1}\, M^\dagger = v\, \mathbb{1}$. Therefore, the breaking pattern reads

$$\mathrm{SU}(2) \times \mathrm{SU}(2)_\mathrm{c} \to \mathrm{SU}(2)_\mathrm{diag}\ . \tag{2.8}$$

However, as already mentioned, the Lagrangian (2.1) or equivalently (2.7) is invariant under the full symmetry group $\mathrm{SU}(2)\times\mathrm{SU}(2)_\mathrm{c}$, and the path integral is an integral over all field configurations, i.e.,

$$Z = \int \mathcal{D}[\phi, W]\, \mathrm{e}^{\mathrm{i}\int \mathrm{d}^4x\, \mathcal{L}[\phi,W]} = \int \mathcal{D}[\phi, W]\, \mathrm{e}^{\mathrm{i}S[\phi,W]}\ . \tag{2.9}$$

This implies that every expectation value with one or more open indices vanishes identically [68]. The reason is that the minimization of the potential (2.4) only fixes the length $\phi^\dagger\phi$, but not the direction n of the configuration, and thus an average over all equally possible directions is performed in the path integral yielding a zero expectation value for such observables. One example is the vev of the scalar field $\langle\phi\rangle$ which averages to zero in the path integral.

To perform standard perturbation theory, gauge fixing is required to single out a preferred direction such that $\langle\phi\rangle \neq 0$. We follow the Faddeev-Popov method [69] and use the vector representation of the scalar field for clarity. Following the steps described in, e.g., [3], gives rise to an effective Lagrangian including a gauge-fixing term as well as a ghost term,

$$\mathcal{L}_\mathrm{eff} = \mathcal{L} + \mathcal{L}_\mathrm{gf} + \mathcal{L}_\mathrm{ghost}\ , \tag{2.10}$$

where the first term is the Lagrangian from (2.1). We implement the so-called 't Hooft gauge condition, $\partial^\mu W^a_\mu + \frac{\mathrm{i}gv\zeta}{\sqrt{2}}\, \phi_i\, T^a\, n_j = 0$, in order to make a perturbative expansion around the vev possible [3, 70–72]. Thus, the gauge-fixing part of the Lagrangian reads

$$\mathcal{L}_\mathrm{gf} = -\frac{1}{2\xi}\left|\partial^\mu W^a_\mu + \frac{\mathrm{i}g\zeta v}{\sqrt{2}}\left(n^\dagger\, T^a\, \varphi - \varphi^\dagger\, T^a\, n\right)\right|^2\ , \tag{2.11}$$

with the independent gauge parameters ξ and ζ. The ghost term is given by

$$\mathcal{L}_\mathrm{ghost} = -\bar{c}^a\Big(\partial^\mu D^{ab}_\mu - \frac{\zeta g^2 v}{\sqrt{2}}\left(n^\dagger\, T^a\, T^b\, \phi + \phi^\dagger\, T^a\, T^b\, n\right)\Big)c^b\ , \tag{2.12}$$

where c and $\bar{c}$ are the ghost and anti-ghost fields, respectively, and again $\phi(x) = \frac{v}{\sqrt{2}}n + \varphi(x)$. The ghost fields are Grassmann-valued complex scalar fields and thus anti-commuting. The covariant derivative in the adjoint representation D^{ab}_μ appears in the first term of the bracket. It is defined by [1]

[1] For the gauge group $\mathrm{SU}(N > 2)$ the definition of the covariant derivative in the adjoint representation stays essen-

$D_\mu^{ab} = \delta^{ab}\partial_\mu + g\,\epsilon^{abc}\,W_\mu^c$. The full gauge fixed path integral is now given by

$$Z = \int \mathcal{D}[\phi, W, c, \bar{c}]\; \mathrm{e}^{\mathrm{i}\left(S[\phi,W]+S_{\mathrm{gf}}[\phi,W]+S_{\mathrm{ghost}}[\phi,W,c,\bar{c}]\right)}\;, \tag{2.13}$$

where the actions S, S_{gf}, and S_{ghost} are obtained by integrating the corresponding Lagrangians over spacetime.

At this point we would like to make some remarks:

- Usually one sets $\xi = \zeta$ to avoid a mixing term of the Goldstone field and the gauge field at tree-level. However, the quantum corrections are different for both. Thus, it is necessary to enforce the equality to circumvent mixing at loop level by introducing this condition as a part of the renormalization scheme [3]. We always do this in the following.

- Since n is a constant vector, the 't Hooft gauge explicitly prefers a distinct direction. Therefore, it follows that $\langle\phi\rangle \neq 0$, and at tree-level $\langle\phi\rangle = \frac{v}{\sqrt{2}}n$. As before, $v^2 = 2f^2$, bearing in mind that the vector $\frac{v}{\sqrt{2}}n$ changes under gauge transformations, whereas the number f is a parameter of the theory and a parameter of the gauge choice in the 't Hooft gauge condition.

- If the Brout-Englert-Higgs effect is not active in the theory, then $\langle\phi\rangle = 0$, and the gauge condition becomes $\partial^\mu W_\mu^a = 0$, i.e., a linear covariant gauge. If $\frac{v}{\sqrt{2}}n$ is identified with the vev, it changes under transformations as, e.g., custodial transformations. In this case it is a dynamical decision of the theory, whether $\frac{v}{\sqrt{2}}n$ is zero or nonzero, i.e., the gauge condition depends on the parameters of the theory.

- The direction of the vev is usually not invariant under the custodial group, as we have discussed in the paragraph above Equation (2.8). In order to preserve the gauge condition every custodial transformation is compensated by a global gauge transformation. Thus, the theory is invariant under the diagonal subgroup which is in our case $\mathrm{SU}(2)_{\mathrm{diag}}$. This group contains partly the global gauge symmetry, and thus is not observable.

Let us now focus on the tree-level mass spectrum of the theory (2.1), with the potential (2.4). We first split the scalar field $\phi(x) = \frac{v}{\sqrt{2}}n + \varphi(x)$, with $\langle\varphi\rangle = 0$, and fix to 't Hooft gauge. The resulting Lagrangian is the effective one (2.10) where the gauge fixing term (2.11) and the ghost term (2.12) enter. However, the direction n is not invariant under custodial transformations as argued above. The split hides the symmetry. The gauge symmetry is broken explicitly by the gauge-fixing procedure. The resulting theory is not invariant under the full symmetry $\mathrm{SU}(2) \times \mathrm{SU}(2)_{\mathrm{c}}$ anymore.

We now perform a rewriting of (2.10) using the split of the scalar field in the vev $\frac{v}{\sqrt{2}}n$ and in the

tially the same, but ϵ^{abc} has to be replaced by the corresponding structure constants f^{abc}.

fluctuations around the vev φ, which yields

$$\begin{aligned}\mathcal{L}_{\text{eff}} = &- \frac{1}{4}\, W^a_{\mu\nu}\, W^{a\,\mu\nu} + \left(\partial_\mu \varphi^\dagger\right)\left(\partial^\mu \varphi\right) \\ &+ \frac{g^2 v^2}{2}\left(n^\dagger\, T^a\, T^b\, n\right) W^a_\mu\, W^{b\,\mu} - 2\lambda v^2\, \mathrm{Re}\big[n^\dagger\, \varphi\big]^2 \\ &- \frac{g^2 v^2 \xi}{2}\, \mathrm{Im}\big[n^\dagger\, T^a\, \varphi\big]^2 + \xi g^2 v^2 \left(n^\dagger\, T^a\, T^b\, n\right) \bar{c}^a\, c^b \\ &+ \sqrt{2} g^2 v\, \mathrm{Re}\big[n^\dagger\, T^a\, T^b\, \varphi\big]\, W^a_\mu\, W^{b\,\mu} - 2\sqrt{2}\lambda v \left(\varphi^\dagger \varphi\right) \mathrm{Re}\big[n^\dagger \varphi\big] - \lambda \left(\varphi^\dagger \varphi\right)^2 \\ &+ 2g\, \mathrm{Re}\Big[\left(\partial_\mu \varphi^\dagger\right) W^\mu \varphi\Big] + g^2\, \varphi^\dagger\, W_\mu W^\mu\, \varphi + \sqrt{2}\xi g^2 v\, \mathrm{Re}\big[n^\dagger\, T^a\, T^b\, \varphi\big]\, \bar{c}^a\, c^b \\ &- \frac{1}{2\xi}\left(\partial^\mu W^a_\mu\right)^2 - \bar{c}^a\, \partial^\mu D^{ab}_\mu\, c^b\ ,\end{aligned} \tag{2.14}$$

where we have set $v^2 = 2f^2$. The first two terms in the first line are the kinetic terms for the gauge field and the fluctuation field as well as the three- and four-point interactions of the gauge bosons. The four terms in the second and third lines are mass terms for the gauge bosons W^a_μ, the fluctuation fields φ_i, and the ghosts c^a, respectively. The mass of all three gauge bosons is $\frac{1}{2}gv$, and thus they are not independent, which is a signal for an explicit symmetry. This degeneracy is a consequence of the remaining unbroken global diagonal subgroup $\mathrm{SU}(2)_{\text{diag}}$ of the theory (2.14). The second term in the second line is a mass term for the so-called Higgs field $h \equiv \sqrt{2}\, \mathrm{Re}\big[n^\dagger \varphi\big]$, which is a singlet with respect to the diagonal subgroup. [2] The Higgs field is identified with the fluctuation field in the direction of the vev. The mass of the Higgs field is $m_{\text{h}} = \sqrt{\lambda} v$.

The first term in the third line contains the would-be Goldstone fields, which are the remaining degrees of freedom of the fluctuation field not involved in the Higgs part. The mass of the would-be Goldstones is $\frac{1}{2\sqrt{2}}\sqrt{\xi} gv$, where all Goldstone fields are mass degenerated. The fact that the mass matrix of the would-be Goldstone fields is proportional to the one of the gauge bosons [3] in 't Hooft gauge with the proportionality factor $\sqrt{\xi}$ is a general feature [3]. The mass depends on the gauge parameter ξ and thus revealing that they are nonphysical objects. The last term in this line gives rise to a mass of the ghost-fields given by $\sqrt{\xi} gv$, and thus makes them also unphysical as the Goldstone fields.

The fourth and fifth line contain interactions between scalars (cubic and quartic), scalars and ghosts, as well as between scalars and gauge bosons. In total there are six of them, which have three coupling constants. They are combinations of the gauge coupling g, and the parameters of the potential $f^2 = v^2/2$, λ. Those relations between the couplings is yet another sign for a hidden symmetry [73]. The last line involves the familiar gauge fixing terms from linear covariant gauges. The first term in this line also provides an additional gauge-dependent mass pole to the gauge boson propagator.

To summarize, the standard model Higgs sector exhibits, in the perturbative treatment, three degenerate massive gauge bosons and one massive Higgs boson. The other degrees of freedom have masses which depend on the gauge parameter. It can be shown by BRST construction, that these degrees of freedom cancel in perturbatively physical amplitudes [3].

The issue of the Gribov-Singer ambiguity [74, 75] is likely to be quantitatively irrelevant for these

[2] Note that in our conventions we distinguish between the scalar field ϕ and the Higgs field h. The Higgs field is part of the fluctuation field φ after splitting the scalar field into $\phi(x) = \frac{v}{\sqrt{2}} n + \varphi(x)$.

[3] To be more precise, we speak of the gauge bosons corresponding to broken generators, i.e., $\big\{W^a_\mu \,\big|\, T^a\, n \neq 0,\ a = 1, 2, \ldots, N^2 - 1\big\}$.

type of models and is not discussed here, see [76, 77] as well as [78] for an explicit lattice calculation.

2.2 Gauge-invariant perturbation theory

The Higgs and the gauge bosons belong to BRST singlets [3], and are considered to be physical states. This suggests that they are observable particles. However, those fields do not transform trivially under gauge transformations, since they have an open gauge index. Moreover, it seems that the construction of a gauge-invariant local gauge charge is inaccessible in non-Abelian [4] gauge theories [52, 79, 81, 82]. Therefore, it is impossible to observe objects with an open gauge index in nature. As a consequence gauge-dependent correlation functions vanish identically if no gauge fixing condition is enforced.

A physical observable can be a gauge-invariant and scheme-invariant state only. In a non-Abelian gauge theory these are described by composite operators [52, 56, 57, 83], i.e., bound-state operators and not the elementary fields present in the Lagrangian.

Instantly one question arises:

Why is the description of experiments in the standard model in terms of the Higgs and the weak gauge bosons as if they are observable particles working so well? [3, 31, 84]

The answer can be given in the framework of gauge-invariant perturbation theory [85]. In the next section a general recipe for this procedure is given. But for now we explain this method in the following for the weak sector of the standard model.

First, we want to mention that any composite operator, and thus observable state, can be characterized by its J^{PC} quantum numbers, where J is the total angular momentum, P the parity and C the charge parity. They are obtained from the corresponding J^{PC} quantum numbers of the constituents and from possible relative momenta between them. We outline some constructions in Chapter 5 for a special lattice gauge theory. The bound states can also have custodial quantum numbers additionally to the J^{PC} quantum numbers.

The next step is to determine the masses of the bound states. Generally non-perturbative methods are needed to compute bound-state masses, due to their non-perturbative nature [86, 87]. However, if one deals with a theory where a Brout-Englert-Higgs effect is active, one can compute them analytically [56, 57] with the aforementioned method of gauge-invariant perturbation theory. The main concept is described in [61, 62, 88].

Consider again the weak sector of the standard model with an $\mathrm{SU}(2)$ gauge symmetry and an $\mathrm{SU}(2)_\mathrm{c}$ custodial symmetry. In this case all physical observable states are characterized by the quantum numbers $J^P_{\mathrm{SU}(2)_\mathrm{c}}$, where the subscript indicates the custodial quantum number. Since $\mathrm{SU}(2)$ is a pseudo-real group, charge parity is trivial there.

As a simple example, let us consider a composite operator in the scalar singlet channel, i.e., $J^P_{\mathrm{SU}(2)_\mathrm{c}} = 0^+_1$,

$$O_{0^+_1}(x) = \left(\phi^\dagger\phi\right)(x) \ , \tag{2.15}$$

which is evidently gauge-invariant. The next step is to employ the Fröhlich-Morchio-Strocchi mechanism [56, 57], which we briefly outline in the following and describe in more detail in the following

[4] In Abelian gauge theories it is possible to construct a gauge-invariant charge using a Dirac phase factor [52, 79, 80]. This construction creates a physical observable charge.

section. Therefore, we fix to a gauge with a Higgs vev and make the split $\phi(x) = \frac{v}{\sqrt{2}} n + \varphi(x)$, with $n^\dagger n = 1$. Then, the correlator $\left\langle O_{0_1^+}(x)\, O^\dagger_{0_1^+}(y)\right\rangle$ is rewritten in terms of the fluctuation field and the vev,

$$\begin{aligned}\left\langle O_{0_1^+}(x)\, O^\dagger_{0_1^+}(y)\right\rangle = \frac{v^4}{4} &+ \frac{v^3}{2}\left\langle h(x) + h(y)\right\rangle \\ &+ v^2\left\langle h(x)\, h(y)\right\rangle + \frac{v^2}{2}\left\langle \left(\varphi^\dagger\varphi\right)(x) \;+ \left(\varphi^\dagger\varphi\right)(y)\right\rangle \\ &+ v\left\langle h(x)\left(\varphi^\dagger\varphi\right)(y) + \left(\varphi^\dagger\varphi\right)(x)\, h(y)\right\rangle + \left\langle \left(\varphi^\dagger\varphi\right)(x)\left(\varphi^\dagger\varphi\right)(y)\right\rangle\,,\end{aligned} \tag{2.16}$$

where we used again the definition of the Higgs field $h = \sqrt{2}\,\mathrm{Re}\left[n^\dagger\varphi\right]$. This is an exact rewriting of the correlator. Note that, since the left-hand side is gauge-invariant, also the sum of the right-hand side is gauge-invariant. But, each individual term on the right-hand side is gauge-variant. No approximation has been applied and Equation (2.16) is an exact identity.

The remaining task is to calculate the properties of the correlation functions. While the left-hand side involves the propagation of a gauge-invariant but complicated bound state operator, the FMS mechanism provides a mapping to gauge-dependent elementary correlation functions in a fixed gauge. Approximations for the latter can be calculated by a variety of tools, e.g., perturbation theory, lattice, or functional methods.

For the moment, we will restrict the calculations to the simplest possible approximation, a tree-level analysis. Computing the n-point functions on the right-hand side at tree-level (tl), we get

$$\left\langle O_{0_1^+}(x)\, O^\dagger_{0_1^+}(y)\right\rangle = \text{const.} + v^2\left\langle h(x)\, h(y)\right\rangle_{\text{tl}} + \left\langle h(x)\, h(y)\right\rangle^2_{\text{tl}} + \mathcal{O}(\varphi^3, g^2, \lambda)\,, \tag{2.17}$$

where we collected all spacetime-independent quantities in a constant. A single propagating Higgs particle is described by the term proportional to v^2. The last term describes the propagation of two non-interacting Higgs particles. It is obtained by the fact that at lowest order the full four-point function decomposes by cluster decomposition into a product of two tree-level Higgs propagators, since there is no connected vertex function at order λ^0. The mass of the bound state is now determined by the poles of the right-hand side. This side has a pole at the tree-level Higgs mass $m_{0_1^+} = m_{\text{h}} = \sqrt{\lambda} v$ and a cut starting from twice the same mass. Comparing poles on both sides, gauge-invariant perturbation theory predicts that the physical, gauge-invariant left-hand side should have a mass equal to the tree-level mass of the Higgs and the next state should then be a scattering state of twice the same particle. Thus, the gauge-invariant singlet scalar state has the same ground state mass as the gauge-dependent elementary Higgs.

Higher-order corrections can be included by going to higher orders in conventional perturbation theory on the right-hand side of Equation (2.17). Studies on the lattice [89, 90] show that those corrections are small. However, the mass of the Higgs becomes scheme-dependent at loop order. This requires a suitable scheme, like the pole scheme [3, 91].

Naturally, there are different bound state operators which carry the same quantum numbers. For example, one could just square the operator (2.15) yielding again a scalar singlet state. Or one could also include appropriate Wilson lines into the operator (2.15), such that this new operator is again gauge-invariant and does not alter the $J^P_{\text{SU}(2)_\text{c}}$ quantum numbers. All these operators involve scalar fields. But there are also operators where those fields are absent, still forming a scalar singlet. For

instance, a so-called W-ball

$$O'_{0_1^+}(x) = \left(W^a_{\mu\nu}\, W^{a\,\mu\nu}\right)(x) \ , \tag{2.18}$$

which is the equivalent of a glueball in QCD. Since there is no scalar field involved, the expansion in fluctuation fields just reproduces the ordinary operator. The leading contribution from the usual perturbative expansion gives two non-interacting gauge boson propagators. Therefore, there should also exist a scattering state with twice the gauge boson mass in this channel.

Of course, all operators with the same quantum numbers mix, and thus, in principle, all these operators have to be included in an operator basis describing the specific channel in order to find the mass eigenbasis. In this basis there exists a linear combination such that this combination expands into the Higgs propagator, and all other orthogonal combinations expand into additional bound states, resonances and/or scattering states.

In standard perturbation theory, the gauge bosons W^a_μ are viewed as physical observable states. However, they have an open gauge index, indicating that they cannot be a physical observable. In order to coincide with experiments [31], where a vector triplet is observed, we have to construct a vector triplet out of the global symmetry group. The simplest one is given by [58, 59, 92]

$$O^{\bar{a}\,\mu}_{1_3^-}(x) = \mathrm{tr}\left[T^{\bar{a}}\, \frac{X^\dagger}{\sqrt{\det X}}\, D^\mu\, \frac{X}{\sqrt{\det X}}\right](x) \ , \tag{2.19}$$

where $T^{\bar{a}}$, $\bar{a} = 1, 2, 3$, are the generators of $\mathrm{SU}(2)_\mathrm{c}$. Using $X(x) = v\alpha + \chi(x)$, $\alpha \in \mathrm{SU}(2)$, yields for the corresponding correlator to leading order in the FMS expansion

$$\left\langle O^{\bar{a}\,\mu}_{1_3^-}(x)\, O^{\bar{b}\,\nu\,\dagger}_{1_3^-}(y)\right\rangle = g^2\, c^{\bar{a}a}\, c^{\bar{b}b} \left\langle W^{a\,\mu}(x)\, W^{b\,\nu}(y)\right\rangle + \mathcal{O}(\chi) \ , \tag{2.20}$$

where $c^{\bar{a}a} = \mathrm{tr}\left[T^{\bar{a}}\, \alpha^\dagger\, T^a\, \alpha\right] \in \mathbb{R}$. If one uses the gauge choice $\alpha = \mathbb{1}$, then $c^{a\bar{a}} = \frac{1}{2}\delta^{a\bar{a}}$. This shows, that the gauge boson propagator is obtained to leading order in the FMS expansion. Thus, following the same arguments as before, the composite operator on the left-hand side has the same mass as the gauge-variant right-hand side, i.e., the mass of the elementary W boson.

To summarize, gauge-invariant perturbation theory predicts the same spectrum as standard perturbation theory, i.e., a single massive scalar and three degenerate massive vector bosons. The remaining states are trivial scattering states. These consideration can be also extended to the full standard model [56, 57] and has been confirmed in explicit lattice calculations [58, 59].

2.3 A recipe

In the previous section we have seen, that the gauge-invariant spectrum of the gauge-Higgs theory can be mapped to the gauge-variant spectrum of standard perturbation theory by employing the FMS mechanism to composite operators built from elementary fields of the Lagrangian. We described the procedure of gauge-invariant perturbation theory using an $\mathrm{SU}(2)$ gauge theory with a scalar field in the fundamental representation. This section explains how to generalize this method to, in principle, arbitrary gauge groups and scalar field representations.

In the following we will consider gauge theories coupled to scalar fields equipped with a potential

that allows for a Brout-Englert-Higgs effect,

$$\mathcal{L} = -\frac{1}{2}\mathrm{tr}(F_{\mu\nu}F^{\mu\nu}) + (D_\mu\phi_f^r)^\dagger_{\tilde{a}}(D^\mu\phi_f^r)_{\tilde{a}} - V(\phi_f^r) \ . \tag{2.21}$$

The gauge field A_μ with field-strength tensor $F_{\mu\nu}$ couple through the covariant derivative D_μ to the Higgs fields ϕ_f^r, which are in some representation r of the gauge group. For the Higgs potential V, we allow for any gauge-invariant scalar term build from the components of the scalar fields which is renormalizable by power-counting and which is required to have classically one or more minima at non-zero Higgs field. We allow further for multiple Higgs fields in the same representation, counted by the index f. The precise structure of the potential will determine whether the theory contains global symmetries between the Higgs fields of a given representation, i.e., an enlarged global custodial symmetry. However, we will restrict the discussion to only one flavor in the fundamental representation or one flavor in the adjoint representation in the following sections, yielding $\mathrm{U}(1)$ and $\mathbb{Z}_2$ as custodial symmetries, respectively. We outline the strategy for multiple Higgs fields in the same representation at the end of Chapter 3. The index $\tilde{a}$ in the kinetic term has to be understood as a multi-index running over all possible components of the Higgs fields in a certain representation such that a gauge-invariant real scalar term is formed.

The basic principle of the FMS mechanism is now straightforward [56, 57]. The first step is to classify all possible gauge-invariant bound states of interest with respect to these global quantum numbers. A straightforward example is given by the operator $O_{0^+}(x) = (\phi^\dagger_{\tilde{a}}\phi_{\tilde{a}})(x)$ which is the simplest operator in the 0^+ channel.

The second step is to choose a gauge in which the Higgs fields acquire nonvanishing vacuum expectation values $\langle\phi\rangle = \phi_0$. This requirement is necessary to perform perturbative calculations within the FMS prescription. A convenient choice is given by the class of R_ξ or also called 't Hooft gauges which will be used throughout this work. We would like to emphasize at this point again that whether the scalar field acquires a vev is a pure gauge choice and only within these gauges perturbation theory is applicable [54, 70]. Even if the Higgs potential has a Mexican-hat structure, gauges are possible in which the vev of the scalar field vanishes identically, e.g., by averaging over all possible minima of the potential [88]. Within such a gauge the mass of the elementary W field would vanish identically to all orders in perturbation theory. However, the observable gauge-invariant vector state which characterizes the physical W remains massive due to nonperturbative effects.

All physical relevant information of an operator is stored in its n-point function. In order to extract the mass, we can investigate the propagator $\langle O(x)\, O^\dagger(y)\rangle$. The last step of the FMS prescription is to expand the Higgs fields in fluctuations φ around the gauge-dependent vev, $\phi(x) = \phi_0 + \varphi(x)$, within the correlators of the gauge-invariant states. This yields

$$\left\langle O_{0^+}(x)\, O^\dagger_{0^+}(y)\right\rangle = \left\langle \left(\phi^\dagger_{0\,\tilde{a}}\,\varphi_{\tilde{a}}\right)(x)\, \left(\phi^\dagger_{0\,\tilde{a}}\,\varphi_{\tilde{a}}\right)^\dagger(y)\right\rangle + \dots \ , \tag{2.22}$$

for our simple example in the 0^+ channel. The right-hand side is just an ordinary fluctuation-field propagator corresponding to the propagator of an elementary Higgs excitation in a given representation and flavor along the radial direction of the vev. Comparing poles on both sides implies that the physical scalar has the same mass as the elementary fluctuation field. This explains as argued in the last section why the observable particle has the same mass as the elementary Higgs field in the standard model, and is thus well described by perturbation theory.

The neglected parts in Equation (2.22) can also contribute to the spectrum of the 0^+ operator. Whether these additional contributions are further bound states, resonances or scattering states de-

pends on the actual considered theory. Further, Equation (2.22) stresses the necessity to choose a gauge with a nonvanishing vev for the scalar field in order to use the FMS prescription to predict the mass. For a vanishing vev, the FMS expansion would trivially reproduce the original bound-state operator which leads, of course, to a true but non-illuminating statement.

Because of gauge invariance there are also no gauge multiplets in the physical spectrum. The only possible multiplets arise if there are global symmetries. Then, the physical states can be multiplets in such global symmetries. In this work, we consider only custodial multiplets. If other global symmetries are present, this may also involve these symmetries [63].

The particular consequences of a custodial symmetry depend on the specific example. For instance, in the standard model with its $\mathrm{SU}(2)_c$ custodial symmetry, discussed in the previous section, a custodial triplet with spin 1 is found to have the same mass as the W and Z bosons, forming their physical equivalents [56, 57], which has also been confirmed on the lattice [58, 59]. As will be seen in the following, the global multiplet structure plays a central role for the particle spectrum, as has already been seen in explicit examples [63–65]. It also plays an important role in the fermion sector [56, 57, 61, 62], though this sector will not be considered in what follows.

While the FMS expansion is always possible, it does not necessarily lead for every operator and/or every quantum number channel to a single elementary particle state at leading order as in Equation (2.22). In fact, the first non-vanishing term can be a scattering state for some operators, i.e., a state involving two or more elementary fields. Such states may yield, just as in the quark model, an additional bound state mass made up from the combined masses of the particles in the scattering state. We will come back to this in the following Chapters.

In principle, the FMS mechanism can be expected to work well if the gauge-dependent propagators are described well by perturbation theory for any gauge with a non-vanishing Higgs condensate. This condition can, unfortunately, not be self-consistently guaranteed in perturbation theory alone, as has been seen in explicit lattice calculations [89]. However, this is exactly the same kind of condition applying to ordinary perturbation theory.

In the remainder of this work we use this general recipe to determine the physical spectrum of different classes of theories, as well as for some particular explicit examples.

Chapter 3

SU(N) gauge theories with scalars in several representations

This chapter is dedicated to the discussion of $\mathrm{SU}(N)$ gauge theories with scalar fields in the fundamental representation and in the adjoint representation.

First, we discuss the case of a single scalar field in the fundamental representation. We will constrain our discussion to the case $N > 2$. Next, a section about scalar fields in the adjoint representation follows, where we discuss several examples for different values of N. Having discussed these cases, we focus on two models for grand unified theories, i.e., an $\mathrm{SU}(5)$ gauge theory, where an adjoint as well as a fundamental scalar appears, and a toy version, i.e., $\mathrm{SU}(3)$ gauge theory with two scalars in the fundamental representation.

In all those discussions we first look at the spectrum of standard perturbation theory and then compare this to the predictions from the FMS mechanism.

This chapter follows [66].

3.1 SU(N) gauge theories with a fundamental scalar

We consider an $\mathrm{SU}(N > 2)$ gauge theory coupled to a single scalar field in the fundamental representation.[1] This is a special case of the Lagrangian (2.21), where the scalar field ϕ denotes a complex N-component vector transforming as $\phi(x) \to U(x)\,\phi(x)$ with $U(x) = \mathrm{e}^{\mathrm{i}T^a\alpha^a(x)} \in \mathrm{SU}(N)$, $\alpha^a(x) \in \mathbb{R}$, and T^a are the generators of the associated Lie algebra. The latter can be constructed explicitly by the generalized Gell-Mann matrices for the fundamental representation. The scalar potential depends only on the invariant $\phi^\dagger\phi$ and the scalar kinetic term reads $(D_\mu\phi)^\dagger\,(D^\mu\phi)$.

3.1.1 Gauge-variant description in a fixed gauge

The precise shape of the scalar potential determines whether a non-zero (unique) vacuum expectation value is classically possible.[2] In order to render the functional integral well-defined[3] we imple-

[1] See [56, 57, 59, 64] for the $\mathrm{SU}(2)$ fundamental case and the discussion in Chapter 2.

[2] We assume here and in the following always implicitly that this is still possible at the quantum level. This is not guaranteed, as lattice calculations have shown explicitly [89]. However, only in this case the gauge condition (3.1) can be chosen and the FMS mechanism meaningfully applied, as discussed in Section 2.3.

[3] The issue of the Gribov-Singer ambiguity [74, 75] is likely to be irrelevant for these type of models, see [76, 77] as well as [78] for an explicit lattice calculation.

ment the convenient R_ξ gauge condition as before by

$$\mathcal{L}_{\rm gf} = -\frac{1}{2\xi}\left|\partial^\mu A^a_\mu + \frac{\mathrm{i}\, g\, v\, \xi}{\sqrt{2}}\left(n^\dagger\, T^a\, \varphi - \varphi^\dagger\, T^a\, n\right)\right|^2 , \tag{3.1}$$

where n is a unit vector in gauge space, $n^\dagger n = 1$, pointing in the direction of the vev, and v is its absolute value, $\phi_0^\dagger\, \phi_0 = v^2/2$. The vacuum expectation value satisfies $\partial_\phi V|_{\phi=\phi_0=\frac{v}{\sqrt{2}}n} = 0$. A mass term for the would-be Goldstone bosons is introduced as well for the class of R_ξ gauges. This mass term is proportional to the gauge fixing parameter, but since the would-be Goldstone bosons form a BRST quartet with the ghost sector and time-like gauge bosons they will not appear in the physical spectrum, and in particular drop out in any vacuum correlator [3]. They will therefore play no role in the following as already argued for the standard model case in Chapter 2.

To investigate the mass spectrum of the elementary fields in a fixed gauge with a nonvanishing vev for the scalar field, a split of the scalar field into its vev and a fluctuation part φ around the vev is useful:

$$\phi(x) = \frac{v}{\sqrt{2}}\, n + \varphi(x)\ . \tag{3.2}$$

The spectrum contains one real-valued massive scalar degree of freedom and $(2N-1)$ would-be Goldstone modes. The non-Goldstone Higgs boson which is the excitation of the scalar field along n, as well as the would-be Goldstones can be described in a gauge-covariant (but not gauge-invariant) manner without specifying n by $h \equiv \sqrt{2}\,\mathrm{Re}(n^\dagger\varphi)$ and $\breve{\varphi} \equiv \phi - \mathrm{Re}(n^\dagger\phi)\, n = \varphi - \mathrm{Re}(n^\dagger\varphi)\, n$, respectively. However, in the following we will usually make the explicit choice $n_i = \delta_{i,N}$. Without loss of generality this is always possible as we can perform locally a gauge transformation such that the vev is in the real part of the $N^{\rm th}$ component at every spacetime point.[4]

Rewriting the scalar kinetic term in the Lagrangian (2.21) by splitting the scalar field into the vev and the fluctuation part, Equation (3.2), we obtain

$$\begin{aligned}\left(D_\mu\phi\right)^\dagger\left(D^\mu\phi\right) = \left(\partial_\mu\varphi^\dagger\right)\left(\partial^\mu\varphi\right) + \frac{g^2v^2}{2}\, n^\dagger\, T^a\, T^b\, n\, A^a_\mu\, A^{b\,\mu} \\ + \sqrt{2}gv\,\mathrm{Im}\big(n^\dagger\, T^a\, \partial^\mu\, \varphi\big)\, A^a_\mu + \dots\ ,\end{aligned} \tag{3.3}$$

where we have the usual [3] mass matrix for the gauge bosons in the first line and the mixing between the longitudinal parts of the gauge bosons and the Goldstone bosons in the second line. The neglected part describes the three and four point vertices between the scalar and gauge field. Note that only those gauge bosons mix with the Goldstone bosons which acquire a mass, i.e., which correspond to the broken generators of the gauge group. These mixing terms are removed by the gauge fixing condition (3.1) in which the additional part proportional to the Goldstone fields is exactly constructed in such a way to obtain a propagator diagonal in field space. This is analogous to the discussion in Chapter 2.

The mass matrix $(M_A^2)^{ab}$ of the gauge bosons is already diagonal for our convenient choice of the

[4] This might change once nonperturbative solutions of the equations of motion of the elementary fields like instantons are considered as well and/or in the presence of gauge defects. For simplicity, we do not consider these type of additional nonperturbative effects in the following.

direction of the vev, $n_i = \delta_{i,N}$, and is given by,

$$(M_{\mathrm{A}}^2)^{ab} = \frac{g^2 v^2}{2}\, n^\dagger \{T^a, T^b\}\, n = \frac{g^2 v^2}{4}\, \mathrm{diag}\Big(\underbrace{0,\ldots,0}_{(N-1)^2-1}, \underbrace{1,\ldots,1}_{2(N-1)}, \frac{2}{N}(N-1)\Big)^{ab} . \tag{3.4}$$

Thus, we obtain $\big((N-1)^2-1\big)$ massless gauge bosons, $2(N-1)$ degenerated massive gauge bosons with mass $m_{\mathrm{A}} = \frac{1}{2} g v$ and one with mass $M_{\mathrm{A}} = \sqrt{2(N-1)/N}\, m_{\mathrm{A}}$. Moreover, the elementary Higgs field has a mass $m_{\mathrm{h}}^2 = \lambda v^2$, where λ is the coupling from Equation (2.4).

The situation is now that which is, in an abuse of language, usually called 'spontaneously broken' in case the system is in the Brout-Englert-Higgs phase.The breaking pattern reads $\mathrm{SU}(N) \to \mathrm{SU}(N-1)$. With respect to the subgroup $\mathrm{SU}(N-1)$ the gauge bosons are in the adjoint representation (massless), a fundamental and an anti-fundamental representation (mass m_{A}) and a singlet representation (mass M_{A}), explaining their degeneracy pattern.

3.1.2 Gauge-invariant spectrum

So far, the construction was the standard perturbative one. We now turn to the observable gauge-invariant states of the theory and apply the FMS mechanism to predict the physical mass spectrum. We construct the gauge-invariant spectrum according to the multiplets of the global symmetries of the theory. The Lagrangian exhibits a global $\mathrm{U}(1)$ symmetry, acting only on the scalar field, besides the local $\mathrm{SU}(N)$ gauge symmetry.

It is straightforward to construct a gauge-invariant state for the Higgs boson, which should be a scalar with positive parity and a singlet under the global symmetry, $J^P_{\mathrm{U}(1)} = 0^+_0$. Therefore, we consider the following gauge-invariant composite operator,

$$O_{0^+_0}(x) = \big(\phi^\dagger \phi\big)(x) \ , \tag{3.5}$$

which exhibits the demanded quantum numbers. This is essentially the same discussion we already had in Section 2.2, with the only difference that we treated an $\mathrm{SU}(2)$ custodial singlet scalar. We apply the FMS prescription according to Section 2.3, to predict the mass of the state provided by the mapping from the gauge-invariant to the elementary states. The expanded correlation function in the scalar fluctuations is of the same form as given in Equation (2.16) in Section 2.3, and thus the same discussion as made there applies here. Especially, the bound state has the same mass as the perturbative Higgs boson $m_{0^+_1} = m_{\mathrm{h}} = \sqrt{\lambda} v$.

Next we construct a singlet vector operator and apply the FMS procedure:

$$O^\mu_{1^-_0}(x) = \mathrm{i}\, \big(\phi^\dagger\, D^\mu\, \phi\big)(x) = -\frac{v^2 g}{2}\, \big(n^\dagger\, A^\mu\, n\big)(x) + \mathcal{O}(\varphi) \ . \tag{3.6}$$

The correlator is given by

$$\begin{aligned} \big\langle O^\mu_{1^-_0}(x)\, O^{\nu\,\dagger}_{1^-_0}(y)\big\rangle &= \frac{v^4 g^2}{4}\, \big\langle n^\dagger\, A^\mu(x)\, n n^\dagger\, A^\nu(y)\, n\big\rangle + \mathcal{O}(\varphi) \\ &\overset{n_i=\delta_{i,N}}{=} \frac{(N-1) v^4 g^2}{8N}\, \big\langle A^{\mu\, N^2-1}(x)\, A^{\nu\, N^2-1}(y)\big\rangle + \mathcal{O}(\varphi) \ , \end{aligned} \tag{3.7}$$

to leading order in the FMS expansion. We project generically on the heaviest elementary state due to the projector $nn^\dagger$ between the gauge fields in the propagator. Thus, this predicts a single vector

particle with the mass of the heaviest gauge boson, $m_{1_0^-} = M_{\mathrm{A}}$. For the case of $\mathrm{SU}(3)$, this has been confirmed in lattice calculations [65] and will also be seen in Chapter 5. [5] Here, we predict this to be true for any $N \geq 3$.

Besides the gauge-invariant prescription of the observable Higgs boson with the operator (3.5) which has the mass of an elementary Higgs field, we also obtain a state which can be mapped on an elementary gauge boson in the 1^- channel. Our analysis for the simplest operator in the 0^+ channel might tempt to the conclusion that it is sufficient for the calculation of the ground state mass to truncate the FMS expansion after the first nontrivial elementary field which leads to an elementary propagator on the right-hand side. For the 0^+ channel this is the elementary Higgs field $O_{0_0^+}(x) = v^2/2 + v\, h(x) + \mathcal{O}\big(\varphi^2\big)$ and propagators coming from the neglected parts indeed contribute only to scattering states. However, the situation can be more involved for more intricated bound states in other channels.

In order to illustrate this, we take the next-to-leading order of the FMS prescription for the vector operator (3.6) into account. At this level, the vector operator reads

$$O^{\mu}_{1_0^-} = -\frac{v^2 g}{2}\left(n^\dagger\, A_\mu\, n\right) + \mathrm{i}\frac{v}{\sqrt{2}}\, n^\dagger\, \partial_\mu \varphi - \sqrt{2} g\, \mathrm{Re}\big(n^\dagger\, A^\mu\, \varphi\big) + \mathcal{O}\big(\varphi^2\big)\ . \tag{3.8}$$

While the third and fourth term on the right-hand side indeed give scattering states of the elementary Higgs with the massive gauge bosons once the correlator of the 1_0^- operator is investigated, the first term linear in φ also contributes to the pole structure of the gauge-invariant operator. Thus, the actual propagator of the vector operator $O_{1_0^-}$ reads to lowest order in the elementary n-point functions:

$$\begin{aligned}\big\langle O^{\mu}_{1_0^-}(x)\, O^{\nu\,\dagger}_{1_0^-}(y)\big\rangle = {}& \frac{(N-1)v^4 g^2}{8N}\, \big\langle A^{\mu\, N^2-1}(x)\, A^{\nu\, N^2-1}(y)\big\rangle_{\mathrm{tl}} \\ & + \frac{v^2}{2}\, \partial^\mu_x\, \partial^\nu_y\, \big\langle h(x)\, h(y)\big\rangle_{\mathrm{tl}} + \dots\ ,\end{aligned} \tag{3.9}$$

where the $\dots$ contain the $(n \geq 3)$-point functions. Identifying poles on the right-hand side, we not only get a pole at the mass of the heaviest gauge boson M_{A} but also of the elementary Higgs field m_{h} to this order in the FMS expansion.

Nonetheless, this additional pole structure does not necessarily imply that an additional particle in the vector channel is predicted as it does not exhibit the expected Lorentz structure of a massive vector boson as this pole appears only in the longitudinal part of the correlator. It rather reflects the fact, that a derivative acting on scalar operators transforms as a vector and therefore mix with vector operators in the 1^- channel but does not indicate a next-level state in this channel, at least to this order in the approximation. In general a detailed variational analysis including various operators with a sufficiently large overlap with the ground as well as the first excited states within a specific channel is required to make a definite statement about potential higher excitations.

Nevertheless, higher-order terms in the fluctuating elementary fields can in principle also lead to nonvanishing 2-point functions which contribute to the spectrum of an operator in certain cases even if this was not the case in the previous example. Whether this leads to an additional particle either in terms of an additional bound state or a resonance, or just a nontrivial scattering state within the

[5] Note that the situation for $\mathrm{SU}(2)$ is different because of the differing global symmetry, but also there the results from the FMS mechanism have been confirmed on the lattice [58, 59].

Table 3.1: *Left*: Gauge-variant spectrum of an $\mathrm{SU}(N)$ gauge theory with a single scalar field in the fundamental representation. Here m_{h} denotes the mass of the elementary Higgs field, M_{A} is the mass of the heaviest elementary gauge boson and m_{A} the mass of the degenerated lighter massive gauge bosons.
Right: Gauge-invariant (physical) spectrum of the theory. We assign a custodial $\mathrm{U}(1)$ charge of $1/N$ to the scalar field ϕ. The column 'next-level state' lists the masses of possible additional bound states or resonances, see the discussion in the main text and in Appendix B. Whether these states are indeed bound states or resonances or only non-trivial scattering states can only be decided once the full analytical structure of the correlator is investigated. Trivial scattering states are ignored. The definition of the fields and operators can be found in the main text.

elementary spectrum				gauge-invariant spectrum				
J^P	Field	Mass	Deg.	U(1)	Op.	Mass	Next-level state	Deg.
0^+	h	m_{h}	1	0	$O_{0^+_0}$	m_{h}	-	1
				± 1	$O_{0^+_{\pm 1}}$	$(N-1)m_{\mathrm{A}}$	$(N-1)m_{\mathrm{A}} + M_{\mathrm{A}}$	$1/\bar{1}$
1^-	$A_\mu^{1,\ldots,(N-1)^2-1}$	0	$(N-1)^2-1$	0	$O^\mu_{1^-_0}$	M_{A}	-	1
	$A_\mu^{(N-1)^2,\ldots,N^2-2}$	m_{A}	$2(N-1)$	± 1	$O^\mu_{1^-_{\pm 1}}$	$(N-1)m_{\mathrm{A}}$	$(N-1)m_{\mathrm{A}} + M_{\mathrm{A}}$	$1/\bar{1}$
	$A_\mu^{N^2-1}$	M_{A}	1					

considered channel depends on the precise properties of the model.[6] We illustrate such an example in the following.

Besides the $\mathrm{U}(1)$ singlet states, we can also construct states with open $\mathrm{U}(1)$ quantum numbers. This is important as the lightest such state is absolutely stable in the theory as this charge is conserved.

For $\mathrm{SU}(3)$ an explicit example for a vector state is given by

$$O^\mu_{1^-_1}(x) = \left[\epsilon_{ijk}\, \phi_i \left(D^\mu \phi\right)_j \left(D^2 \phi\right)_k\right](x) \ , \tag{3.10}$$

where we assigned a $\mathrm{U}(1)$ charge $1/N = 1/3$ to the scalar field ϕ. To leading order in the FMS mechanism as well as in perturbation theory, the correlator of this operator expands to a product of three propagators.

As a simple-minded constituent model, we interpret the mass of the gauge-invariant operator by the sum of the masses of the three propagators on the right-hand side of the expansion.

The mass of this state is given by $m_{1^-_1} = 2m_{\mathrm{A}}$ as in leading order one of the massless elementary gauge boson as well as two gauge bosons with mass m_{A} contribute to this state. We expect also a higher order excitation with mass $m^\star_{1^-_1} = 2m_{\mathrm{A}} + M_{\mathrm{A}}$. There exists, of course, an anti-particle of the same mass but opposite U(1) charge described by $O^\mu_{1^-_{-1}} = O^{\mu\ \dagger}_{1^-_1}$.

Besides the presented gauge-invariant operators, it is of course also possible to construct other operators within a specific channel. We expect that those operators have the largest overlap with the

[6] For the rest of this paper, we will use the term *next-level state* in case the state is not the ground state or a trivial scattering state of n times the mass of the ground state. As more sophisticated analyses beyond these simple considerations are needed to identify whether this state is an additional bound state, a scattering state, or a resonance, we will simply stick to the term next-level state, keeping in mind that this state can also predict an additional particle in case it is a bound state or a resonance.

ground state of a given channel, which have the least field content. For the $\mathrm{U}(1)$-singlet operators the unique solution to this requirement is given. However, there are ambiguities regarding the other channels. For instance, the operators $\epsilon_{ijk}\,\phi_i\,\left(D^\nu\phi\right)_j\,\left(D_{\{\nu}D_{\mu\}}\phi\right)_k$ and $\epsilon_{ijk}\,\phi_i\,\left(D^\nu\phi\right)_j\,\left(F_{\nu\mu}\phi\right)_k$ equally describe a vector state with nonvanishing $\mathrm{U}(1)$ quantum number. The advantage of the latter is that it can be straightforwardly generalized to an arbitrary $\mathrm{SU}(N)$ theory. An explicit prescription for these operators is given by

$$O^{\mu}_{1^-_1} = \epsilon_{i_1\ldots i_N}\,\phi_{i_1}\,\left(D_{\nu_1}\,\phi\right)_{i_2}\,\left(F^{\nu_1}{}_{\nu_2}\,\phi\right)_{i_3}\,\ldots\,\left(F^{\nu_{N-2}\mu}\,\phi\right)_{i_N}\,. \tag{3.11}$$

It is straightforward to convince oneself that the lightest pole of this operator is given by $(N-1)m_{\mathrm{A}}$ for any $N>2$. Moreover, we get several excited states. For instance a next-level state is predicted with mass $(N-1)m_{\mathrm{A}}+M_{\mathrm{A}}$ in case $M_{\mathrm{A}}<m_{\mathrm{h}}$. A sketch of the analysis of the FMS description of these operators can be found in Appendix B.

In contrast to the scalar channel for the elementary fields, we can also construct scalar operators with an open $\mathrm{U}(1)$ quantum number. These read for instance

$$O_{0^+_1} = \epsilon_{i_1\ldots i_N}\,\phi_{i_1}\,\left(D_{\mu_1}\,\phi\right)_{i_2}\,\left(F^{\mu_1}{}_{\mu_2}\,\phi\right)_{i_3}\,\ldots\,\left(F^{\mu_{N-3}}{}_{\mu_{N-2}}\,\phi\right)_{i_{N-1}}\,\left(D^{\mu_{N-2}}\,\phi\right)_{i_N}\,, \tag{3.12}$$

for $N>3$ and $\epsilon_{i_1i_2i_3}\,\phi_{i_1}\,(D_\mu\,\phi)_{i_2}\,(D_\nu F^{\mu\nu}\,\phi)_{i_3}$ for $N=3$ and we predict them to have a ground-state mass of $m_{0^+_1}=(N-1)m_{\mathrm{A}}$ as well as a mass of $(N-1)m_{\mathrm{A}}+M_{\mathrm{A}}$ for the next-level state for $M_{\mathrm{A}}<m_{\mathrm{h}}$.

To briefly summarize our results of this section, we observed a qualitative difference of the elementary spectrum which is usually used to describe the physical states of a gauge theory with a Brout-Englert-Higgs effect and of the gauge-invariant observable spectrum for $\mathrm{SU}(N>2)$ gauge theories with a scalar field in the fundamental representation. The two different spectra are recapped in Table 3.1. While the elementary spectrum contains only one field with mass m_{h} in the 0^+ channel, the gauge-invariant spectrum contains at least three states. One of them is a singlet regarding the global $\mathrm{U}(1)$ symmetry group, also with mass m_{h}. The other two are the particle and anti-particle state with open $\mathrm{U}(1)$ quantum number and thus have the same mass. Furthermore, the spectra differ in the 1^- channel. The elementary spectrum contains $(N-1)^2-1$ massless gauge bosons, degenerated $2(N-1)$ massive ones and one gauge boson with a generically heavier mass. The gauge-invariant observables are given by a $\mathrm{U}(1)$-singlet and one state plus the corresponding antiparticle with open $\mathrm{U}(1)$ quantum number. Moreover, it is possible that more particles in the gauge-invariant spectrum arise which can manifest as further bound states or resonances. We would like to emphasize, that the degrees of freedom of the gauge-invariant spectrum do not change once the gauge group is altered. Only the masses and other physical properties like decay constants change, in contrast to the elementary spectrum where also the number of degrees of freedom increase once N increase.

3.2 SU(N) gauge theories with an adjoint scalar

After the detailed discussion of the fundamental case, we now consider an $\mathrm{SU}(N)$ gauge theory coupled to a scalar field in the adjoint representation. In this case, it is useful to formulate the Lagrangian (2.21) as

$$\mathcal{L} = -\frac{1}{4}F^a_{\mu\nu}F^{a\,\mu\nu} + \mathrm{tr}\left[(D_\mu\Sigma)^\dagger\,(D^\mu\Sigma)\right] - V(\Sigma)\,. \tag{3.13}$$

The scalar field $\Sigma = \Sigma^a T^a$ transforms as $\Sigma(x) \to U(x)\,\Sigma(x)\,U(x)^\dagger$ and its components Σ^a form a N^2-1 dimensional real-valued vector. The covariant derivative acting on Σ is given by $D^\mu\Sigma = \partial^\mu\Sigma + \mathrm{i}g\,[A^\mu, \Sigma]$. The scalar potential V contains all possible couplings up to fourth order in the scalar field spanned by the invariant Casimirs of the gauge group, i.e.,

$$V = -\mu^2 \operatorname{tr}\Sigma^2 + \gamma \operatorname{tr}\Sigma^3 + \frac{\lambda}{2}\left(\operatorname{tr}\Sigma^2\right)^2 + \tilde{\lambda}\operatorname{tr}\Sigma^4 \,. \tag{3.14}$$

For most of the time, we will enforce the action to be invariant under a discrete $\mathbb{Z}_2$ symmetry, i.e., $\gamma = 0$. The case of a nonvanishing γ will be exemplified in Section 3.2.4.

It is important to note that the adjoint case induces a very different structure than the fundamental case where the only little group is $\mathrm{SU}(N-1)$ and all minima of the potential belong to the same gauge orbit [93]. By contrast, different directions of the vev can belong to different little groups and thus to different physical theories with different mass spectra for the elementary fields as not all directions of the vev can be connected via a gauge transformation for a scalar in the adjoint representation. This also induces further subtleties in the FMS prescription for the gauge-invariant spectrum which are discussed in more detail in Appendix A.

3.2.1 Gauge-variant description in a fixed gauge

Assuming that the (effective) potential allows for a Brout-Englert-Higgs effect and choosing a gauge with a nonvanishing vev, we again split the scalar field in its vev and fluctuations around it:

$$\Sigma(x) = \langle\Sigma\rangle + \sigma(x) \equiv w\,\Sigma_0 + \sigma(x) \,. \tag{3.15}$$

The breaking pattern depends on the direction of the vev Σ_0^a with $\Sigma_0^a\,\Sigma_0^a = 1$. We again implement the gauge condition such that it removes the mixing between the gauge bosons and the would-be Goldstones, leading to a gauge-fixing Lagrangian

$$\mathcal{L}_{\mathrm{gf}} = \frac{1}{\xi}\operatorname{tr}\big(\partial_\mu A^\mu + \mathrm{i}\,g\,\xi\,[\Sigma_0, \Sigma]\big)^2 \,. \tag{3.16}$$

We can always choose a gauge in which Σ_0 is diagonal due to the fact that every unitary matrix can be diagonalized by a suitable unitary transformation. Thus, it is sufficient to consider vevs spanned by the generators of the Cartan subalgebra as every element of the $\mathrm{SU}(N)$ algebra can be rotated to an element of the diagonal generators.

The mass matrix for the gauge fields is given by

$$\left(M_{\mathrm{A}}^2\right)^{ab} = -2(gw)^2 \operatorname{tr}\big([T^a, \Sigma_0]\,[T^b, \Sigma_0]\big) \,. \tag{3.17}$$

Whether a gauge boson acquires a mass or remains massless depends on whether the generator which is associated to that gauge boson commutes with Σ_0.

To identify all possible breaking patterns for a given group $\mathrm{SU}(N)$ corresponds to the identification of all possible little groups. This can be mapped on the combinatorial problem of finding all partitions $p(N)$ of the number N. The function $p(N)$ can be extracted from the formal Taylor series of the inverse Euler function $\prod_{k=1}^{\infty} 1/(1-x)^k = \sum_{N=0}^{\infty} p(N)x^N$. However, when it comes to the actual minimization of the potential energy of the scalar field, it can be shown that the potential has extrema only if the vev Σ_0 has at most two different eigenvalues [94–96]. Therefore,

the only relevant breaking patterns which can lead to a minimum of the potential are $\mathrm{SU}(N) \to \mathrm{S}\big(\mathrm{U}(P) \times \mathrm{U}(N-P)\big)$ with $P < N$ and one only has to consider $\lfloor N/2 \rfloor$ breaking patterns.[7]

Thus, we obtain $\big(N^2 - 1 - 2P(N-P)\big)$ massless and $2P(N-P)$ massive gauge fields in the spectrum of the elementary fields. The masses of the massive gauge bosons are given by

$$m_{\mathrm{A}}^2 = \frac{1}{2}\,\frac{N}{P(N-P)}\,g^2\,w^2\ . \tag{3.18}$$

Correspondingly, we obtain $2P(N-P)$ would-be Goldstone modes which are not present in the elementary spectrum as they are BRST non-singlets and $\big(N^2 - 1 - 2P(N-P)\big)$ real scalar degrees of freedom which are the Higgs fields. They correspond to the unbroken generators and have mass $m \geq 0$. Moreover, we can already predict that $\big(P^2 - 1\big)$ of these scalar fields have the same mass denoted by m_{P} and $\big((N-P)^2 - 1\big)$ masses $m_{\mathrm{N-P}}$ are degenerated as well due to the group theoretical structure. These scalar fields belong to the $\mathrm{SU}(P)$ and $\mathrm{SU}(N-P)$ subgroups, respectively. Finally, there is the massive Higgs field corresponding to the generator of the vev and thus to the invariant $\mathrm{U}(1)$ subgroup. We denote its mass by m_{H} in the following. These masses read[8]

$$m_{\mathrm{H}}^2 = \lambda\,w^2 + 2\,\frac{(N-P)^3 + P^3}{N^2 P(N-P)}\,\tilde{\lambda}\,w^2\ , \tag{3.19}$$

$$m_{\mathrm{P}}^2 = \frac{2N-3P}{P(N-P)}\,\tilde{\lambda}\,w^2 \quad , \quad m_{\mathrm{N-P}}^2 = \frac{3P-N}{P(N-P)}\,\tilde{\lambda}\,w^2\ . \tag{3.20}$$

Thus, the elementary mass spectrum of $\mathrm{SU}(N)$ gauge theories is more involved than in the fundamental case, especially for increasing N. We will discuss some specific examples and particularities of some models below. Moreover, the different physical theories given by the different gauge orbits influence the physical gauge-invariant spectrum.

3.2.2 Gauge-invariant spectrum

Before, we turn to the breaking patterns of some example groups and their precise spectrum, we discuss some of the properties of the gauge-invariant spectrum in general. Neglecting the cubic term in Equation (3.14), the global symmetry group is given by a discrete $\mathbb{Z}_2$ symmetry. Thus, we classify our states in $\mathbb{Z}_2$ even $(+)$ and $\mathbb{Z}_2$ odd $(-)$ states. The lightest $\mathbb{Z}_2$ odd state is again necessarily absolutely stable.

We start the discussion of the gauge-invariant spectrum with the 1^- channel. Inspired from the fundamental case, an operator with minimal field content which is $\mathbb{Z}_2$ even is given by $\mathrm{tr}[\Sigma\, D_\mu\, \Sigma]$. The simplest $\mathbb{Z}_2$ odd state is $\mathrm{tr}[\Sigma^2\, D_\mu\, \Sigma]$. [9]

However, those states do not expand to an elementary gauge field A_i^μ, since $\mathrm{tr}[\Sigma^n D_\mu \Sigma] = \mathrm{tr}[\Sigma^n \partial_\mu \Sigma] = \partial_\mu \mathrm{tr}\Sigma^{n+1}/(n+1)$, but in leading order to an elementary scalar field. Of course, they contribute to the pole structure of the 1^- channel but do not give rise to a vector particle as they have a pole only

[7] Moreover, it can be shown that the global minimum of the potential is given by the breaking pattern $P = \lfloor N/2 \rfloor$ for $\tilde{\lambda} > 0$ and $P = 1$ for $\tilde{\lambda} < 0$ [94]. Nevertheless, we will determine the spectrum also for the minima in which the theory is in a metastable state as this minima can become global once other fields are coupled to the theory.

[8] Note some particularities. For sufficiently large N and $(N-1) > P > 2N/3$, the potential obeys only a saddle point as the condition that Σ_0 exhibits at most two different eigenvalues is a necessary but not sufficient condition that the potential has an extremum in that direction. For $P = N-1$, a minimum can only be obtained in case $\tilde{\lambda} < 0$. In this case there are no scalar fields with mass $m_{\mathrm{N-P}}$.

[9] The even simpler state $\mathrm{tr}[D_\mu \Sigma]$ vanishes identically.

in the longitudinal component due to the partial derivative. This is similar to the fundamental case where we also observed that the mass pole of the scalar fields appears in the gauge-invariant vector state.

Nevertheless, it is also possible to construct operators which expand to a single gauge field in leading order, following the SU(2) fundamental case in [57]. These (non-local) operators read

$$O^{\mu}_{1^-_-}(x) = \frac{\partial_\nu}{\partial^2}\,\mathrm{tr}\big[\Sigma\, F^{\mu\nu}\big](x)\ , \tag{3.21}$$

$$O^{\mu}_{1^-_+}(x) = \frac{\partial_\nu}{\partial^2}\,\mathrm{tr}\big[\Sigma^2\, F^{\mu\nu}\big](x)\ , \tag{3.22}$$

for the $\mathbb{Z}_2$ odd and even state, respectively.[10] These states expand in leading order in the FMS expansion and in leading order in the elementary gauge field to

$$O^{\mu}_{1^-_-}(x) = -w\,\mathrm{tr}\big[\Sigma_0\, A^{\mu}_{\perp}\big](x) + \mathcal{O}\big(A^2,\sigma\big)\ , \tag{3.23}$$

$$O^{\mu}_{1^-_+}(x) = -w^2\,\mathrm{tr}\big[(\Sigma_0)^2\, A^{\mu}_{\perp}\big](x) + \mathcal{O}\big(A^2,\sigma\big)\ , \tag{3.24}$$

where $A^{\mu}_{\perp} = (\delta^{\mu}_{\nu} - \partial^{\mu}\partial_{\nu}/\partial^2)\, A^{\nu}$ is the transversal component of the gauge field. Both operators expand to massless gauge fields as only those gauge fields survive the trace which are associated to generators of the Cartan algebra and thus are diagonal. More precisely, the right-hand side for both operators in Equation (3.24) is given by the elementary gauge field that corresponds to the unbroken $\mathrm{U}(1)$ group given by the generator Σ_0.[11] Thus the FMS mechanism predicts two massless physical states in the gauge-invariant vector channel of an arbitrary $\mathrm{SU}(N > 2)$ gauge theory with a scalar in the adjoint representation and discrete $\mathbb{Z}_2$ symmetry. Note that for $\mathrm{SU}(2)$ all $\mathbb{Z}_2$ even operators vanish identically in the vector channel and thus for $\mathrm{SU}(2)$ we get only a single massless vector state, see also the discussion in Section 3.2.3.

The results of Equation (3.24) are a prediction of massless composite vector states. Moreover, this appears at the current time within the gauge-invariant setting to create massless vector states as physically observable particles. This is particularly interesting in the setting of grand-unified theories, where a $\mathrm{U}(1)$ with a massless vector particle has to be 'broken out' of a non-Abelian gauge theory [3, 97].

Further, we would like to emphasize that also a term quadratic in the gauge fields occurs to leading order in the FMS expansion. However, these as well as the higher order terms from the FMS expansion and the elementary scalar contribution from the operator $\mathrm{tr}[\Sigma^n\, D_\mu\, \Sigma]$ will not alter the ground state pole structure as these terms will correspond to scattering states or resonances in the 1^- channel or might even be massless, depending on the precise parameters and gauge group. Thus, the situation is different from the fundamental case, where the ground state mass of the 1^- channel is either M_{A} or m_{h}. Here, we predict always two massless vector states.

[10] Note that similar operators can also be constructed in the fundamental case for an arbitrary $\mathrm{SU}(N)$ theory, e.g., given by $\frac{\partial_\nu}{\partial^2}(\phi^\dagger\, F^{\mu\nu}\, \phi)$. However, the operator (3.6) provided in Section 3.1.2 has less field content and is sufficient to get a prediction for the ground state mass of the vector channel. Of course, the operator in Equation (3.6) and the one constructed from the field strength tensor as well as others have to be investigated in a detailed spectroscopy of the states as they carry the same quantum numbers.

[11] There is only one particular exception for the $\mathbb{Z}_2$ even state for even N for the breaking pattern $\mathrm{SU}(N) \to \mathrm{SU}(N/2) \times \mathrm{SU}(N/2) \times \mathrm{U}(1)$, see the discussion at the end of this section. Nonetheless, the ground state of this operator remains massless as it is given by two propagating massless gauge fields.

In the 0^+ channel, the simplest possible (minimal field content) operator is given by

$$O_{0^+_+}(x) = \mathrm{tr}\big[\Sigma^2\big](x) \ . \tag{3.25}$$

This operator expands in the FMS description as

$$O_{0^+_+}(x) = \frac{w^2}{2} + w\, H(x) + \frac{1}{2}\, \sigma^a(x)\sigma^a(x) \ . \tag{3.26}$$

Thus, we obtain in leading order the Higgs excitation $H(x) = \Sigma^a_0 \sigma^a(x)$. However, the situation is more subtle than in the fundamental case, as the term $\sigma^a(x)\sigma^a(x)$ does not only contain the product of two massive Higgs fields $H(x)$ but also the scalar degrees of freedom belonging to the unbroken generators forming the invariant $\mathrm{SU}(P)$ and $\mathrm{SU}(N-P)$ subgroups which are not would-be Goldstone bosons and therefore present in the elementary spectrum. Whether these are massive or even massless depends on the details of the considered theory. In most cases, they have a mass given by Equation (3.20). For some particular theories, however, they can be massless, e.g., see the discussion in Section 3.2.4 or consider the case $P = 2N/3$ or $P = N/3$ in Equation (3.20).

Therefore, the correlator $\big\langle O_{0^+_+}(x)\, O^\dagger_{0^+_+}(y)\big\rangle$ contains also the propagation of two degrees of freedom with mass m_{P} from position x to position y as well as two degrees of freedom with mass $m_{\mathrm{N-P}}$ which is a bound state operator with mass $2m_{\mathrm{P}}$ or $2m_{\mathrm{N-P}}$, respectively. We can suppose $N/2 \leq P < N$ without loss of generality. Then, $0 \leq m_{\mathrm{P}} \leq m_{\mathrm{N-P}}$. In case $m_{\mathrm{H}} < 2m_{\mathrm{P}}$ the ground state mass is given by the mass of the scalar field radial to the direction of Σ^a_0. However, in case $m_{\mathrm{H}} > 2m_{\mathrm{P}}$ the ground state mass is given by $2m_{\mathrm{P}}$ and an excited state is predicted at mass m_{H} as well as a trivial scattering state with twice this mass. Which scenario is realized depends on the ratio of the couplings λ and $\tilde{\lambda}$ as well as on the gauge group and the breaking pattern characterized by the numbers N and P, respectively.

Moreover, we have the $\mathbb{Z}_2$ odd state in the 0^+ channel given by

$$O_{0^+_-}(x) = \mathrm{tr}\big[\Sigma^3\big](x) \ . \tag{3.27}$$

This operator can show distinct results for the different physical phases of the theory. Similar to the considerations above, this state can expand to elementary states which are massless or massive. We exemplify its different realizations by the following investigation.

The FMS expansion of the scalar $\mathbb{Z}_2$ odd operator is given by

$$O_{0^+_-} = w^3\, \mathrm{tr}\big[{\Sigma_0}^3\big] + 3w^2\, \mathrm{tr}\big[{\Sigma_0}^2\sigma\big] + 3w\, \mathrm{tr}\big[\Sigma_0\sigma^2\big] + \mathrm{tr}\big[\sigma^3\big] \ . \tag{3.28}$$

To analyze its spectrum, it is convenient to perform a basis change of the generators of the Cartan subalgebra, i.e., a field redefinition of the fields in the Cartan. We leave the first $(P-1)$ elements of the Cartan algebra unchanged, i.e., they are given by the first $(P-1)$ diagonal matrices of the generalized Gell-Man matrices with rank two to P. For the Cartan elements P to $(N-2)$, we choose the following block-diagonal matrices,

$$T = \begin{pmatrix} 0 & 0 \\ 0 & t \end{pmatrix} \ , \tag{3.29}$$

with t one of the $(N-P-1)$ Cartan generators of the $(N-P)$ subgroup. For the remaining

generator, we use the actual direction of the vev Σ_0, which can be parameterized as

$$\Sigma^0 = \frac{1}{2}\sqrt{\frac{2}{NP(N-P)}}\begin{pmatrix}(N-P)\,\mathbb{1}_P & 0\\ 0 & -P\,\mathbb{1}_{N-P}\end{pmatrix}\,, \tag{3.30}$$

with $\mathbb{1}_n$ the $n \times n$ unit matrix.

Now, it is straightforward to check that the leading order contribution in the fluctuating field is only given by the Higgs excitation associated to the vev, $\mathrm{tr}\big({\Sigma_0}^2\sigma\big) = H\ \mathrm{tr}\big({\Sigma_0}^3\big)$. Thus, we generically get a pole at m_{H} except for two cases. The first exception manifests for $\mathrm{SU}(3)$ and is discussed in Section 3.2.4. The second is given for even N and the breaking pattern $\mathrm{SU}(N) \to \mathrm{SU}(N/2)\times\mathrm{SU}(N/2)\times\mathrm{U}(1)$. For this particular choice of the vev, $\mathrm{tr}\big({\Sigma_0}^2\sigma\big)$ vanishes identically as ${\Sigma_0}^2 \sim \mathbb{1}$. At next to leading order, $\mathrm{tr}\big(\Sigma_0\sigma^2\big)$, we obtain two fluctuating elementary fields propagating from x to y. For the latter breaking pattern, these will make up the ground state mass for the $\mathbb{Z}_2$ odd operator. For all other theories, it depends again on the precise couplings as to whether m_{H} is smaller than $2m_{\mathrm{P}}$ (or $2m_{\mathrm{N-P}}$) and defines the ground state mass, similar to the $\mathbb{Z}_2$ even operator.

In addition to the predicted ground state masses of both scalar operators at tree level, these two operators can also have various additional excitations. Suppose, $m_{\mathrm{H}} < 2m_{\mathrm{P}} < 2m_{\mathrm{N-P}} < 2m_{\mathrm{H}}$. Then, the ground state mass is given by m_{H} and each operator has a next-level state with mass $2m_{\mathrm{P}}$ and a next-to-next- level state with mass $2m_{\mathrm{N-P}}$. All these states are either nontrivial scattering states or resonances as every state in the scalar channel can decay to at least two of the massless ground states in the vector channel. Of course, similar conclusions hold for $2m_{\mathrm{P}} < m_{\mathrm{H}}$ or other mass ratios.

Thus, the adjoint case has a much broader variety in the spectrum than the fundamental case. Depending on the physical realization of the theory, also see Appendix A, such a theory can have different numbers of observable states.

3.2.3 SU(2) gauge theory

After these general considerations on the spectra of gauge theories with an adjoint scalar field, we will now discuss some example theories to illustrate the different spectra for different realizations of the physical theories as well as some particularities of $\mathrm{SU}(2)$ and $\mathrm{SU}(3)$.

We start with the almost trivial example $\mathrm{SU}(2)$. The only nontrivial breaking pattern is $\mathrm{SU}(2) \to \mathrm{U}(1)$. The cubic term of the potential vanishes identically and the quartic $\mathrm{tr}\Sigma^4$ can be written as $\big(\mathrm{tr}\Sigma^2\big)^2$, as $\mathrm{tr}\Sigma^2$ is the only invariant Casimir of $\mathrm{SU}(2)$. Thus, we set $\tilde{\lambda} = 0$ without loss of generality.

The elementary spectrum is given by one massive Higgs excitation with mass $m_{\mathrm{H}}^2 = \lambda w^2$, two massive gauge bosons with mass $m_{\mathrm{A}}^2 = g^2 w^2$ and one massless gauge boson. A convenient choice for the vev is $\Sigma_0^a = \delta^{a,3}$.

Considering the gauge-invariant bound-state spectrum, we first note that all $\mathbb{Z}_2$ odd operators in the scalar channel, $\mathrm{tr}\big(\Sigma^{2n+1}\big)$, and $\mathbb{Z}_2$ even operators in the vector channel, $\mathrm{tr}\big(\Sigma^{2n}\ F^{\mu\nu}\big)$, vanish identically due to the properties of the Pauli matrices. Thus, we have only one state within the 0^+ as well as 1^- channel, modulo higher excitations. For the scalar channel, the operator (3.25) expands to,

$$O_{0_+^+}(x) = \frac{w^2}{2} + w\,H(x) + \frac{1}{2}\,H^2(x)\,, \tag{3.31}$$

where we have omitted the contributions from the would-be Goldstone modes, given by $\sigma^a\,\Sigma_0^a = 0$ in this specific model, as these cancel anyway once the physical spectrum is considered. Thus, we get

Table 3.2: *Left*: Gauge-variant spectrum of an $\mathrm{SU}(2)$ gauge theory with a single scalar field in the adjoint representation.
Right: Gauge-invariant (physical) spectrum of the theory. $m_{\mathrm{H}} = \sqrt{\lambda} w$ denotes the mass of the Higgs, $m_{\mathrm{A}} = gw$ is the mass of the two charged elementary gauge bosons. The next- level state of the vector channel will always be a scattering state or a resonance. The definitions of the fields and operators can be found in the main text.

	elementary spec.				gauge-invariant spec.			
J^P	Field	Mass	Deg.	$\mathbb{Z}_2$	Op.	Mass	Next-level state	Deg.
0^+	H	m_{H}	1	$+$	$O_{0^+_+}$	m_{H}	-	1
1^-	A^μ_3	0	1	$-$	$O^\mu_{1^-_-}$	0	$2m_{\mathrm{A}}$	1
	$A^\mu_{1,2}$	m_{A}	2					

a pole at the mass of the elementary Higgs field as well as a trivial scattering state at twice its mass, similar to the fundamental case.

For the vector channel, we predict generically a massless state as the ground state for the operator (3.21). Going beyond the leading order contribution in the fluctuating fields, we also predict two next-level states, being either nontrivial scattering states or resonances, at the mass of the elementary Higgs and of twice the mass of the elementary massive gauge fields. A brief summary of the spectra can be found in Table 3.2.

There exists exploratory confirmation of the existence of a massless composite vector state in this model [98]. In this work the energy extracted from the exponential decay of the correlator of the operator (3.21) with nonvanishing (lowest lattice) momentum has been compared to the energy of a massless free particle in a finite volume. The authors of this work found agreement with a massless state as predicted by the FMS mechanism, even though polynomial volume corrections play a role.

3.2.4 SU(3) gauge theory

The next example is the $\mathrm{SU}(3)$ case, which has a variety of new features compared to the $\mathrm{SU}(2)$ case. Most important, the $\mathbb{Z}_2$ odd and even operators are nonvanishing in the scalar and vector channel, respectively. Thus, new states, i.e., observable particles, are present. In addition, we get two different breaking patterns and a second invariant Casimir can be constructed, $\mathrm{tr}\Sigma^3$. So further properties of the spectrum for the adjoint case can be exemplified but also particularities which are only present in this model.

Although $\mathrm{tr}\Sigma^3 \neq 0$, we first demand a $\mathbb{Z}_2$ invariant Lagrangian in order to analyze the spectrum. Thus, we set $\gamma = 0$ in the scalar potential (3.14) as well as $\tilde{\lambda} = 0$ without loss of generality in analogy to the $\mathrm{SU}(2)$ case. Note, that the pure scalar part of the action has an enhanced $\mathrm{O}(8)$ symmetry in this case as the potential is only build up from the invariant $\mathrm{tr}\Sigma^2 = \Sigma^a\Sigma^a/2$.

The two breaking patterns of $\mathrm{SU}(3)$ are given by $\mathrm{SU}(2)\times\mathrm{U}(1)$ and $\mathrm{U}(1)\times\mathrm{U}(1)$. Parameterizing all possible vevs by $\Sigma_0 = \Sigma_0^3 T^3 + \Sigma_0^8 T^8$ with $\left(\Sigma_0^3\right)^2 + \left(\Sigma_0^8\right)^2 = 1$, the former breaking pattern can be realized by the three particular combinations $\left(0, 1\right)$, $\left(\sqrt{3}/2, 1/2\right)$, and $\left(\sqrt{3}/2, -1/2\right)$ regarding the tupel $\left(\Sigma_0^3, \Sigma_0^8\right)$. All other combinations result in an invariant $\mathrm{U}(1)\times\mathrm{U}(1)$ subgroup. Note that also the latter breaking pattern minimizes the potential due to the enhanced symmetry of the scalar potential even if Σ^0 has three different eigenvalues. This is a particularity of $\mathrm{SU}(3)$ with a discrete $\mathbb{Z}_2$

symmetry and will be no longer the case once a nonvanishing γ in the potential is allowed or larger gauge groups are considered where $\mathrm{tr}\Sigma^4$ is another invariant Casimir for $N > 3$.

While the spectrum of the elementary vector states differs for both breaking patterns, the gauge invariant spectrum of the vector states remains the same. The mass spectrum of the elementary gauge bosons reads

$$M_{\mathrm{A}}^2 = g^2 w^2 \,\mathrm{diag}\left(\left(\Sigma_0^3\right)^2, \left(\Sigma_0^3\right)^2, 0, \frac{\left(\Sigma_0^3 + \sqrt{3}\Sigma_0^8\right)^2}{4}, \frac{\left(\Sigma_0^3 + \sqrt{3}\Sigma_0^8\right)^2}{4}, \frac{\left(\Sigma_0^3 - \sqrt{3}\Sigma_0^8\right)^2}{4}, \frac{\left(\Sigma_0^3 - \sqrt{3}\Sigma_0^8\right)^2}{4}, 0\right) . \tag{3.32}$$

Thus in general, the theory contains at least two massless gauge bosons corresponding to the two generators of the Cartan subalgebra and at most six massive fields, which we can group in three pairs where the mass of the gauge bosons of each pair is degenerated. In case of a breaking to $\mathrm{SU}(2)\times\mathrm{U}(1)$, e.g., by choosing $\Sigma_0^3 = 0$ and $\Sigma_0^8 = 1$, we obtain four massless gauge bosons corresponding to the invariant subgroup and four degenerated massive gauge bosons with mass $m_{\mathrm{A}} = \sqrt{3}/2\, gw$. For completeness, there are also three particular directions, $\left(1, 0\right)$, $\left(1/2, \sqrt{3}/2\right)$, and $\left(1/2, -\sqrt{3}/2\right)$, with little group $\mathrm{U}(1) \times \mathrm{U}(1)$, for which two of the mass pairs further degenerate such that the spectrum contains two massive vector bosons with mass $m_{\mathrm{A}^1} = gw$ and four degenerated fields with mass $m_{\mathrm{A}^4} = gw/2$.

Even though the spectrum of the elementary vector states is different for the different physical realizations of the theory characterized by the different directions of the vev in the Cartan algebra, the gauge-invariant spectrum always contains two massless vector states distinguished by their global $\mathbb{Z}_2$ parity as described in Section 3.2.2.

For the scalar channel, the elementary spectrum is much clearer. First, we have four or six would-be Goldstone bosons, depending on the respective breaking pattern, which mix with the longitudinal parts of the massive gauge bosons. Second, there is always one massive Higgs field with mass $m_{\mathrm{H}} = \sqrt{\lambda} w$, corresponding to the generator proportional to the vev, $H = \Sigma_0^a\, \sigma^a$. The remaining three or one scalar field(s) belong to the elementary spectrum of the theory and are Higgs fields as well. They are massless for the $\mathrm{SU}(3)$ case with a discrete $\mathbb{Z}_2$ symmetry imposed on the scalar potential. We emphasize at this point that they are not Goldstone bosons as they belong to the remaining unbroken generators of the gauge group, $[T^a, \Sigma_0] = 0$. The fact that they are massless is an accident due to the enhanced $\mathrm{O}(8)$ symmetry of the scalar potential.

The presence of massless fields in the elementary spectrum has a direct impact on the gauge-invariant spectrum of the composite operators (3.25) and (3.27). Although, the $\mathbb{Z}_2$ even operator (3.25) expands in leading order to the massive elementary Higgs field H, it also contains the propagation of two massless scalar degrees of freedom at next-to-leading order in the FMS expansion. Thus, the FMS mechanism predicts at least at tree level a massless bound state for this operator.[12] Similar conclusions can be drawn for the $\mathbb{Z}_2$ odd operator. Depending on the actual direction of the vev in the Cartan space, either the leading order or next-to-leading order expands to massless scalar fields. For instance, the leading order expansion contains the massless field σ^8 for $\Sigma_0 = T^3$ and thus the ground state mass is $m_{0^+_-} = 0$. The next-to leading order in the FMS expansion predicts the mass of the next-level state which is $2m_{\mathrm{H}}$. For $\Sigma_0 = T^8$ the leading order in the FMS expansion contains

[12] Of course, it is possible that also this as well as other massless bound state acquires a non-vanishing mass due to quantum corrections, e.g., in analogy to glueballs.

Table 3.3: Gauge-variant and gauge-invariant spectrum of an $\mathrm{SU}(3)$ gauge theory with a single scalar field in the adjoint representation with discrete $\mathbb{Z}_2$ symmetry for the two different breaking patterns.
Top table: The breaking pattern is given by $\mathrm{SU}(3) \to \mathrm{U}(1) \times \mathrm{U}(1)$ and the gauge orbit is characterized by $\Sigma_0^3 = 1, \Sigma_0^8 = 0$. The masses are given by $m_{\mathrm{H}} = \sqrt{\lambda} w, m_{\mathrm{A}^1} = gw$, and $m_{\mathrm{A}^4} = gw/2$.
Bottom table: The breaking pattern is given by $\mathrm{SU}(3) \to \mathrm{SU}(2) \times \mathrm{U}(1)$ and the gauge orbit is characterized by $\Sigma_0^3 = 0, \Sigma_0^8 = 1$. The mass $m_{\mathrm{A}} = \sqrt{3}/2\, gw$.

	elementary spectrum				gauge-invariant spectrum			
J^P	Field	Mass	Deg.	$\mathbb{Z}_2$	Op.	Mass	Next-level state	Deg.
0^+	$\sigma^3 \equiv H$	m_{H}	1	$+$	$O_{0^+_+}$	0	m_{H}	1
	σ^8	0	1	$-$	$O_{0^+_-}$	0	$2m_{\mathrm{H}}$	1
1^-	$A_\mu^{3,8}$	0	2	$+$	$O^\mu_{1^-_+}$	0	$2m_{\mathrm{A}^4}$	1
	$A_\mu^{1,2}$	m_{A^1}	2	$-$	$O^\mu_{1^-_-}$	0	$2m_{\mathrm{A}^4}$	1
	$A_\mu^{4,5,6,7}$	m_{A^4}	4					

breaking pattern: $\mathrm{SU}(3) \to \mathrm{U}(1) \times \mathrm{U}(1)\, (\Sigma_3^0 = 1)$

	elementary spectrum				gauge-invariant spectrum			
J^P	Field	Mass	Deg.	$\mathbb{Z}_2$	Op.	Mass	Next-level state	Deg.
0^+	$\sigma^{1,2,3}$	0	3	$+$	$O_{0^+_+}$	0	m_{H}	1
	$\sigma^8 \equiv H$	m_{H}	1	$-$	$O_{0^+_-}$	0	m_{H}	1
1^-	$A_\mu^{1,2,3,8}$	0	4	$+$	$O^\mu_{1^-_+}$	0	$2m_{\mathrm{A}}$	1
	$A_\mu^{4,5,6,7}$	m_{A}	4	$-$	$O^\mu_{1^-_-}$	0	$2m_{\mathrm{A}}$	1

breaking pattern: $\mathrm{SU}(3) \to \mathrm{SU}(2) \times \mathrm{U}(1)\, (\Sigma_8^0 = 1)$

also only σ^8 but which is this time massive. However, the next to-leading-order contribution $\mathcal{O}(\sigma^2)$ contains products of the massless fields $\sigma^{1,2,3}$ such that the 2-point function of this operator has a pole at vanishing mass on the right hand side. A summary of these two example breaking patterns can be found in Table 3.3.

So far, we only investigated the spectrum for theories with a discrete $\mathbb{Z}_2$ symmetry for the scalar field. Allowing for an explicit breaking term will not only influence the gauge-invariant spectrum indirectly as the elementary spectrum is changed. It also has a direct impact as transitions between the $\mathbb{Z}_2$ even and odd states are allowed. Therefore, the number of observable gauge-invariant states is altered as less different channels exist. A straightforward example for this is the vector channel of the theory. The former two massless states distinguished by their $\mathbb{Z}_2$ quantum number are now in the same 1^- channel and thus have overlap with the same ground state. Thus, the FMS description predicts only one massless state for any $\mathrm{SU}(N)$ gauge theory with a scalar in the adjoint representation once the Lagrangian does not exhibit a $\mathbb{Z}_2$ symmetry.

The same statement can be formulated for the scalar channel. In addition, the situation is more involved for $\gamma \neq 0$ in the scalar potential given in Equation (3.14). In this case, the potential has minima only in the three equivalent directions which lead to a breaking pattern $\mathrm{SU}(3) \to \mathrm{SU}(2) \times \mathrm{U}(1)$ according to the lemma of [95]. The elementary scalar spectrum has a Higgs field with mass

Table 3.4: Gauge-variant and gauge-invariant spectrum of an $\mathrm{SU}(3)$ gauge theory with a single scalar field in the adjoint representation. The scalar potential exhibits an explicit $\mathbb{Z}_2$ breaking term, $\gamma\ \mathrm{tr}\Sigma^3$. Thus, there is no $\mathbb{Z}_2$ classification of the gauge-invariant spectrum. We have assumed $m_{\mathrm{H}} < 2m_{\mathrm{P}=2}$ for the ground state mass of the scalar channel otherwise the ground state mass would be $2m_{\mathrm{P}}$ and the next-level state has mass m_{H}.

	elementary spectrum			gauge-invariant spectrum			
J^P	Field	Mass	Deg.	Op.	Mass	Next-level state	Deg.
0^+	H	m_{H}	1	O_{0^+}	m_{H}	$2m_{\mathrm{P}}$	1
	$\sigma^{1,2,3}$	$m_{\mathrm{P}=2}$	3				
1^-	$A_\mu^{1,2,3,8}$	0	4	$O^\mu_{1^-}$	0	$2m_{\mathrm{A}}$	1
	$A_\mu^{4,5,6,7}$	m_{A}	4				

breaking pattern: $\mathrm{SU}(3) \to \mathrm{SU}(2) \times \mathrm{U}(1)$

$m_{\mathrm{H}}^2 = \lambda w^2 - \frac{\sqrt{3}}{2}\,\gamma w$ and three degenerated Higgs fields with mass $m_{\mathrm{P}=2}^2 = \frac{\sqrt{27}}{2}\,\gamma w$. Thus, the gauge-invariant ground state in the scalar channel is now massive and either m_{H} for $2\,\lambda w < \sqrt{75}\,\gamma$ or $2\,m_{\mathrm{P}=2}$ for $2\,\lambda w > \sqrt{75}\,\gamma$. A brief summary of the spectrum is given in Table 3.4 for the former case.

3.2.5 SU(4) gauge theory

Finally, we discuss the spectrum of $\mathrm{SU}(4)$. This is the smallest group for which we have the full set of invariant Casimirs regarding perturbative renormalizability and we are able to directly apply the formulas provided in Section 3.2.1. For simplicity, we again impose a discrete $\mathbb{Z}_2$ symmetry on the Lagrangian, i.e., $\gamma = 0$. The nonvanishing coupling $\tilde{\lambda}\ \mathrm{tr}\Sigma^4$ will induce nonvanishing masses for the elementary scalar fields which belong to the unbroken generators of the theory but are not the Higgs excitation radial to Σ_0^a. Even if $\tilde{\lambda}$ is zero at the classical level, it will be generated due to quantum corrections from the gauge bosons as it is not protected by a symmetry. The scalar potential has minima only for the breaking patterns $\mathrm{SU}(4) \to \mathrm{SU}(3) \times \mathrm{U}(1)$ and $\mathrm{SU}(4) \to \mathrm{SU}(2) \times \mathrm{SU}(2) \times \mathrm{U}(1)$. While the latter corresponds to the global minimum for $\tilde{\lambda} > 0$, the former breaking pattern is favored for $\tilde{\lambda} < 0$. The other directions in the Cartan space associated to little groups $\mathrm{SU}(2) \times \mathrm{U}(1)^2$ and $\mathrm{U}(1)^3$ are not extrema of the potential and can be ignored.

For the breaking pattern $\mathrm{SU}(4) \to \mathrm{SU}(3) \times \mathrm{U}(1)$ the elementary spectrum is given by nine massless gauge fields and six massive ones with mass $m_{\mathrm{A}}^2 = \frac{2}{3}\,g^2 w^2$. Moreover, we obtain a massive Higgs with mass $m_{\mathrm{H}}^2 = (6\lambda + 7\tilde{\lambda})w^2/6$ and eight degenerated scalar fields invariant under the remaining $\mathrm{SU}(3)$ subgroup with mass $m_{\mathrm{P}=3}^2 = -\tilde{\lambda}w^2/3$. In order that the scalar potential exhibits a minimum, the couplings have to fulfill the relation $6\lambda > -7\tilde{\lambda}$ and $\tilde{\lambda} < 0$. The ground state mass of the gauge-invariant 0_+^+ or 0_-^+ operator is given by either m_{H} or $2m_{\mathrm{P}}$, depending on the ratios of the coupling constants. In the vector channel two massless vector bosons are predicted as discussed in detail above. The spectra are summarized in Table 3.5.

For the breaking pattern $\mathrm{SU}(4) \to \mathrm{SU}(2) \times \mathrm{SU}(2) \times \mathrm{U}(1)$ the elementary spectrum is given by seven massless gauge fields and eight massive ones with mass $m_{\mathrm{A}}^2 = g^2 w^2/2$. In the scalar sector, we have a massive Higgs, $m_{\mathrm{H}}^2 = (\lambda + \tilde{\lambda}/2)\,w^2$, three massive scalar fields invariant under the first $\mathrm{SU}(2)$ subgroup with mass $m_{\mathrm{P}=2}^2 = \tilde{\lambda}w^2/2$ and three scalar fields invariant with respect to the

Table 3.5: Gauge-variant and gauge-invariant spectrum of an $\mathrm{SU}(4)$ gauge theory with a single scalar field in the adjoint representation with discrete $\mathbb{Z}_2$ symmetry for the breaking pattern $\mathrm{SU}(4) \to \mathrm{SU}(3) \times \mathrm{U}(1)$, e.g., realized by $\Sigma_0 = T^{15}$. We assume $m_{\mathrm{H}} < 2m_{\mathrm{P}=3}$ for the gauge invariant spectrum, here.

	elementary spectrum				gauge-invariant spectrum			
J^P	Field	Mass	Deg.	$\mathbb{Z}_2$	Op.	Mass	Next-level state	Deg.
0^+	H	m_{H}	1	$+$	$O_{0^+_+}$	m_{H}	$2m_{\mathrm{P}=3}$	1
	$\sigma^{1,\ldots,8}$	$m_{\mathrm{P}=3}$	8	$-$	$O_{0^+_-}$	m_{H}	$2m_{\mathrm{P}=3}$	1
1^-	A^{15}_μ	0	1	$+$	$O^\mu_{1^-_+}$	0	$2m_{\mathrm{A}}$	1
	$A^{1,\ldots,8}_\mu$	0	8	$-$	$O^\mu_{1^-_-}$	0	$2m_{\mathrm{A}}$	1
	$A^{9,\ldots,14}_\mu$	m_{A}	6					

Table 3.6: Gauge-variant and gauge-invariant spectrum of an $\mathrm{SU}(4)$ gauge theory with a single scalar field in the adjoint representation with discrete $\mathbb{Z}_2$ symmetry for the breaking pattern $\mathrm{SU}(4) \to \mathrm{SU}(2)^2 \times \mathrm{U}(1)$, e.g., realized by $\Sigma^0 = \sqrt{2/3}\,T^8 + \sqrt{1/3}\,T^{15}$. We assume $m_{\mathrm{H}} < 2m_{\mathrm{P}=2}$ for the gauge invariant spectrum, here. The field $\sigma^{\mathrm{SU}(2)}$ encodes the fields $\sigma^{1,2,3}$ which belong to the first remaining $\mathrm{SU}(2)$ group, while $\bar{\sigma}^{\mathrm{SU}(2)}$ encodes the three scalar fields which belong to the other remaining $\mathrm{SU}(2)$ group given by σ^{13}, σ^{14}, and $-\sqrt{1/3}\,\sigma^{18} + \sqrt{2/3}\,\sigma^{15}$, for the exemplified Σ_0. Similar considerations hold for the gauge bosons.

	elementary spectrum				gauge-invariant spectrum			
J^P	Field	Mass	Deg.	$\mathbb{Z}_2$	Op.	Mass	Next-level state	Deg.
0^+	H	m_{H}	1	$+$	$O_{0^+_+}$	m_{H}	$2m_{\mathrm{P}=2}$	1
	$\sigma_{\mathrm{SU}(2)}$	$m_{\mathrm{P}=2}$	3	$-$	$O_{0^+_-}$	$2m_{\mathrm{P}=2}$	$2m_{\mathrm{H}}$	1
	$\bar{\sigma}_{\mathrm{SU}(2)}$	$m_{\mathrm{P}=2}$	3					
1^-	$A^{\mathrm{U}(1)}_\mu$	0	1	$+$	$O^\mu_{1^-_+}$	0	$2m_{\mathrm{A}}$	1
	$A^{\mathrm{SU}(2)}_\mu$	0	3	$-$	$O^\mu_{1^-_-}$	0	$2m_{\mathrm{A}}$	1
	$A^{\mathrm{SU}(2)}_\mu$	0	3					
	$A^{4,\ldots,7,9,\ldots,12}_\mu$	m_{A}	8					

second $\mathrm{SU}(2)$ subgroup with the same mass $m^2_{\mathrm{N-P}=2} = \tilde{\lambda} w^2/2$. The gauge invariant spectrum for the scalar $\mathbb{Z}_2$ even operator depends on the ratio of the two quartic couplings. For $2\lambda < 3\tilde{\lambda}$, the ground state mass is given by m_{H} and we obtain a further next-level state with mass $2m_{\mathrm{P}}$ at tree level and vice versa for $2\lambda > 3\tilde{\lambda}$. The ground state of the $\mathbb{Z}_2$ odd operator is generically given by $2m_{\mathrm{P}=2}$ for positive quartic couplings. The only possibility to obtain a ground state mass of $2m_{\mathrm{H}}$ for this operator is given by $\lambda < 0$. In this case $(2\lambda + \tilde{\lambda}) > 0$ has to hold to have a minimum as well as a potential bounded from below. For a brief summary of the gauge-variant and gauge-invariant spectrum for this particular breaking pattern see Table 3.6.

3.3 SU(5) GUT as a toy model

Moving away from the basic ingredients, we consider in this section the scalar-gauge sector of the prototype of grand unified theories, namely an $\mathrm{SU}(5)$ gauge theory with one scalar field in the adjoint representation Σ and one in the fundamental representation ϕ, but ignore the fermionic sector for simplicity [48]. The Lagrangian has at least a global $\mathrm{U}(1)$ symmetry acting on ϕ. Depending on the precise form of the scalar potential, this symmetry can be enhanced to a $\mathbb{Z}_2 \times \mathrm{U}(1)$ custodial symmetry in case it is invariant under the discrete transformation $\Sigma \to -\Sigma$.

Table 3.7: *Left*: Gauge-variant spectrum of an $\mathrm{SU}(5)$ gauge theory with one scalar field in the fundamental representation and one in the adjoint representation. The fields listed here are all mass-eigenstates. The 8 massless gluons which correspond to the unbroken $\mathrm{SU}(3)$ gauge group are not listed.
Right: Gauge-invariant (physical) spectrum of the theory. In case the $\mathbb{Z}_2$ symmetry is explicitly broken, we obtain only one ground state within the different $\mathrm{U}(1)$ channels. For simplicity, we only indicate the order of magnitude for the masses of the heavy gauge invariant states.

	elementary spectrum				gauge-invariant spectrum			
J^P	Field	Mass	Deg.	$(\mathrm{U}(1), \mathbb{Z}_2)$	Operator	Mass	Next-level state	Deg.
0^+	h	m_{h}	1	$(0,+)$	$O_{0^+_{0+}}$	m_{h}	$\sim w$	1
	$\varphi_{1,\dots,6}$	$m_{\varphi_{1,\dots,6}}$	6	$(0,-)$	$O_{0^+_{0-}}$	m_{h}	$\sim w$	1
	$\sigma^{1,\dots,8}$	$m_{\sigma^{1,\dots,8}}$	8	$(\pm1,+)$	$O_{0^+_{\pm1+}}$	$\sim w$	$\sim w$	1
	$\sigma^{21,22,23}$	m_σ	3	$(\pm1,-)$	$O_{0^+_{\pm1-}}$	$\sim w$	$\sim w$	1
	σ^{24}	M_σ	1					
1^-	A_μ	$m_{\mathrm{A}} = 0$	1	$(0,+)$	$O_{1^-_{0+}}$	m_{A}	m_Z	1
	$W^\pm_\mu$	m_W	2	$(0,-)$	$O_{1^-_{0-}}$	m_{A}	m_Z	1
	Z_μ	m_Z	1	$(\pm1,+)$	$O_{1^-_{\pm1+}}$	$\sim w$	$\sim w$	1
	$A^{9,\dots,14}_\mu$	m_L	6	$(\pm1,-)$	$O_{1^-_{\pm1-}}$	$\sim w$	$\sim w$	1
	$A^{15,\dots,20}_\mu$	M_L	6					

3.3.1 Gauge-variant description in a fixed gauge

The perturbative construction is as follows: First the adjoint scalar acquires a vev $\langle\Sigma\rangle \sim T^{24}$, where T^{24} is the following element of the Cartan subalgebra, $T^{24} = \frac{1}{2}\sqrt{\frac{3}{5}}\mathrm{diag}(-2/3, -2/3, -2/3, 1, 1)$. This choice of the vev of the scalar field in the adjoint representation breaks at some high scale, much larger than the electroweak scale, $\mathrm{SU}(5)$ to $\mathrm{SU}(3)_{\mathrm{C}} \times \mathrm{SU}(2)_{\mathrm{L}} \times \mathrm{U}(1)_{\mathrm{Y}}$ which is the standard model gauge group. The fundamental scalar acquires a vev $\langle\phi\rangle = v/\sqrt{2}\, n$, where v is of the order of the electroweak scale. It is sufficient to consider a complex unit-vector of the form $n = (0, 0, n_3, 0, n_5)$ with $n_5 \in \mathbb{R}$ as we are still allowed to perform appropriate $\mathrm{SU}(3)$ and $\mathrm{SU}(2)$ gauge transformations. In order to leave the strong interaction unbroken, it is important to impose constraints on the parameters of the scalar potential in such a way, that the potential energy of the scalar fields is minimized for a field configuration with $n = (0, 0, 0, 0, 1)$. In this case, the fundamental scalar field

breaks the standard model group to $\mathrm{SU}(3)_\mathrm{C} \times \mathrm{U}(1)_\mathrm{em}$. To achive this, we can consider the following special realization of the Lagrangian (2.21)

$$\begin{aligned}\mathcal{L} = &- \frac{1}{4}\, F^a_{\mu\nu}\, F^{a\,\mu\nu} + \mathrm{tr}\big[(D_\mu\,\Sigma)^\dagger\,(D^\mu\,\Sigma)\big] + (D_\mu\,\phi)^\dagger\,(D^\mu\,\phi) \\ &- V_\Sigma(\Sigma) - V_\phi(\phi^\dagger\phi) - \beta\,\phi^\dagger\,\Sigma^2\,\phi\ ,\end{aligned} \tag{3.33}$$

where V_Σ is defined in Equation (3.14). The Lagrangian is invariant under the discrete $\mathbb{Z}_2$ transformation for $\gamma = 0$. For nonvanishing γ also the interaction term $\phi^\dagger\Sigma\phi$ has to be considered as this term will be at least generated by radiative corrections in case the $\mathbb{Z}_2$ symmetry is explicitly broken. The part of the potential which contains only the self interactions of the fundamental scalar V_ϕ is of the usual Mexican-hat form. The term proportional to β, mixing both scalar fields, is responsible for driving the system into the appropriate minimum where the strong interaction remains unbroken. A necessary condition is $\beta < 0$. Moreover, we dropped the remaining possible perturbatively renormalizable term given by $\phi^\dagger\phi\ \mathrm{tr}\Sigma^2$ as this term leads only to an unimportant mass shift in the elementary scalar spectrum but does not influence the main results of the following section.

All together this leads to the following (perturbative) elementary particle spectrum: From the breaking of $\mathrm{SU}(5)$ to the standard model group we get 12 heavy gauge bosons called leptoquarks and 12 heavy Higgs bosons. From the breaking of the standard model group to $\mathrm{SU}(3)_\mathrm{C} \times \mathrm{U}(1)_\mathrm{em}$ we obtain 3 light gauge bosons, the $W^\pm$ and the Z, and 7 additional Higgs bosons. Of course, there is fine tuning at work, such that only one of the 19 Higgs bosons will be the standard model Higgs and the others will have masses of the order of the GUT scale denoted by w in the following, as do the leptoquarks [3].

We want to point out that the last term in Equation (3.33) gives rise to an off-diagonal mass matrix for the Σ fields leading to a mixture of Σ^{23} and Σ^{24} depending on the parameters of the potential. Thus, a suitable field redefinition has to be performed such that a diagonal mass matrix is achieved. These redefined fields are used in the next subsection to identify the poles of the gauge-invariant states.

The gauge-variant spectrum of this theory is sketched on the left-hand side of Table 3.7. The lightest scalar field with mass of the electroweak scale $m_\mathrm{h} \sim v$ is denoted by h. We do not provide the explicit masses in terms of the masses of the elementary fields for all heavy gauge-invariant states for better readability. As these masses are of the order of the GUT scale, we simply indicate that they are $\sim w$.

3.3.2 Gauge-invariant description

We begin the analysis of the gauge-invariant spectrum for a Lagrangian with a $\mathbb{Z}_2 \times \mathrm{U}(1)$ custodial symmetry. Therefore, we can group the states into $\mathrm{U}(1)$ singlets and non-singlets which can have $\mathbb{Z}_2$ even or odd parity.

Due to the increased field content several gauge-invariant operators can be constructed to analyze the spectrum of the different channels. For instance, some of the possible classes of operators for the scalar $\mathrm{U}(1)$-singlet $\mathbb{Z}_2$-even channel 0^+_{0+} are $\left(\phi^\dagger\phi\right)^n$, $\mathrm{tr}\Sigma^{2n}$, $\left(\phi^\dagger\,\Sigma^{2n}\,\phi\right)^m, \ldots$, with $n, m \in \mathbb{N}$. Analyzing these operators with the aid of the FMS prescription, we conclude that the ground state mass is given by the mass of the lightest fundamental perturbative Higgs h. Further, there are a number of excited states with mass of the order of the GUT scale w, e.g., with the mass of the fields σ^{23} and σ^{24} or twice the masses of the other elementary scalar fields. A similar spectrum appears for the $\mathrm{U}(1)$-singlet $\mathbb{Z}_2$-odd channel 0^+_{0-}. The operator $\phi^\dagger\ \Sigma\ \phi$ can be used to straightforwardly

compute that the mass of the ground state is again the mass of the lightest elementary fundamental Higgs excitation h. Thus, the gauge- invariant spectrum contains not only one but two scalar fields with mass of the order of the electroweak scale, while the elementary spectrum has only one light scalar field.

The situation becomes even more problematic once the vector channel is investigated. The vector $\mathrm{U}(1)$-singlet channel can be analyzed by the operators $\frac{\partial^\nu}{\partial^2}\,\mathrm{tr}\big(F_{\mu\nu}\,\Sigma^{2n}\big)$, $\mathrm{i}\,\phi^\dagger\,\Sigma^{2n}\,D_\mu\phi, \ldots$, or $\frac{\partial^\nu}{\partial^2}\,\mathrm{tr}\big(F_{\mu\nu}\,\Sigma^{2n+1}\big)$, $\mathrm{i}\,\phi^\dagger\,\Sigma^{2n+1}\,D_\mu\phi, \ldots$, for the $\mathbb{Z}_2$ even and odd case, respectively. These are inspired by the investigations in the previous sections but even more involved singlet operators can be studied, e.g., $\epsilon_{ijklm}\,\epsilon_{i'j'k'l'm'}\,(D^\mu\,\phi)_i\,\big(\phi^\dagger\big)_{\bar{i}}\,\Sigma_{j'j}\,\Sigma_{k'k}\,\Sigma_{l'l}\,\Sigma_{m'm}$ where fields with indices with a prime transform with respect to the anti-fundamental representation. Also, similar operators contribute to the spectrum of the scalar channel. Performing the FMS prescription, we obtain that the leading order contribution comes from the elementary massless photon and the next-level state has the mass of the Z boson in both cases. Thus, the gauge-invariant spectrum consists of two massless vector fields which are not observed in nature in case the theory exhibits a discrete $\mathbb{Z}_2$ symmetry.

At first glance, these problems can be solved by introducing a $\mathbb{Z}_2$ breaking term on the level of the Lagrangian. Then, we can classify the states only according to the global $\mathrm{U}(1)$ quantum number and the spectrum would contain only one low lying scalar with the mass of the lightest elementary Higgs as well as one massless vector particle with a possible resonance which could be interpreted as the Z boson. However, there is no obvious way to construct gauge-invariant composite states that expand to only one elementary $W^\pm$ field.

It is possible to construct states with open $\mathrm{U}(1)$ quantum number according to Equation (3.11). However, these are generically too heavy as they contain at least three leptoquarks (as well as an elementary W) at leading order and thus, their mass is of the order of the GUT scale. Of course, there are many other potential operators within this channel, e.g., $\epsilon_{ijklm}\,\phi_i\,\big(\Sigma\,\phi\big)_j\,\big(\Sigma^2\,\phi\big)_k\big(\Sigma^3\,\phi\big)_l\,\big(D^\mu\,\phi\big)_m$ which contain only a single gauge field. Unfortunately, the leading order contribution in the fluctuating fields vanishes identically due to the antisymmetric properties of the epsilon tensor if the QCD vacuum shall be unbroken. Therefore, this state will generically be heavier than the mass of the lightest elementary Higgs. As we only have the fundamental vectors ϕ and $\Sigma^n\,\phi$ which do not contain an elementary gauge field, we do not see any comparatively simple operator which can expand to an object with the desired properties.

Thus, the number and masses of the gauge-invariant states are actually incompatible with the standard model, as the low-lying charged gauge bosons, the $W^\pm$, are not appropriately reproduced. Moreover, the FMS analysis demonstrates that $\mathbb{Z}_2$ violating interactions are needed to avoid a doubling of the photon and light Higgs state, which are only distinguished by their global $\mathbb{Z}_2$ parity, in contrast to the elementary spectrum. For these reasons, the bosonic sector of $\mathrm{SU}(5)$ is likely not a proper extension of the bosonic sector of the standard model already from a pure field theoretical point of view.

3.4 SU(3) with two scalars in the fundamental representation

We sketch the spectrum of a gauge theory with two scalar fields in the fundamental representation in the following. For simplicity, we only discuss the case where the gauge group is $\mathrm{SU}(3)$ but generalize the results of [99] where a similar investigation was performed. The Lagrangian which we use is of

the form

$$\mathcal{L} = -\frac{1}{4}\, F^a_{\mu\nu} F^{a\,\mu\nu} + \sum_{\alpha=1}^{2} \left(D_\mu\, \phi_{(\alpha)}\right)^\dagger \left(D^\mu\, \phi_{(\alpha)}\right) - V\left(\phi_{(1)}, \phi_{(2)}\right) \,, \tag{3.34}$$

where α labels the different scalar flavors. Depending on the precise form of the scalar potential, the theory can have different global symmetries, e.g., a global $\mathrm{U}(1) \times \mathrm{U}(1)$ symmetry for potentials of the form $V\left(\phi^\dagger_{(1)}\, \phi_{(1)}, \phi^\dagger_{(2)} \phi_{(2)}\right)$ or a global $\mathrm{SU}(2) \times \mathrm{U}(1)$ symmetry for $V\left(|\phi_{(1)}|^2 + |\phi_{(2)}|^2\right)$. We will focus to this end on the latter case, where the potential has the largest custodial symmetry. This symmetry can be used to construct gauge-invariant states which have distinct $\mathrm{SU}(2) \times \mathrm{U}(1)$ transformation properties. As usual, we start our discussion by summarizing the gauge-variant spectrum of the theory.

Depending on the alignment of the vevs different breaking patterns exist. If the two vevs are (anti) parallel the breaking pattern reads $\mathrm{SU}(3) \to \mathrm{SU}(2)$. In all other cases the breaking pattern is $\mathrm{SU}(3) \to \mathrm{SU}(2) \to 1$. The elementary spectrum of the former case is listed in the left panel of Table 3.8. In Table 3.9 we restrict the discussion on vevs which are orthogonal. In case the second vev has a parallel as well as an orthogonal component can also straightforwardly be computed but leads only to further mass splits in the elementary spectrum and does not give new insights in the structures of the gauge-invariant spectrum.

Having settled the perturbative spectrum we can now focus on the gauge-invariant (physical) spectrum of the theory by applying the FMS mechanism. We start with operators which are $\mathrm{U}(1)$ singlets. Due to the $\mathrm{SU}(2)$ custodial symmetry we can arrange our operators in singlets and triplets for

Table 3.8: Summary table for the case with two parallel vevs. Here, we used $n_{(\alpha),i} = \delta_{i,3}$, $\alpha = 1, 2$.
Left: Gauge-variant spectrum of an $\mathrm{SU}(3)$ gauge theory with two scalar fields in the fundamental representation and $\mathrm{SU}(2) \times \mathrm{U}(1)$ custodial symmetry. The fields listed here are all mass-eigenstates.
Right: Gauge-invariant (physical) spectrum of the theory to leading order.
m_h denotes the mass of the massive Higgs, M_A is the mass of the heaviest gauge boson and m_A the mass of the degenerate lighter gauge bosons. (I, I^3) are the quantum numbers of the global symmetry group $\mathrm{SU}(2)$. We only consider $\mathrm{U}(1)$-singlet states here.

	elementary spectrum			gauge-invariant spectrum			
J^P	Field	Mass	Deg.	(I, I^3)	Op.	Mass	Deg.
0^+	$\varphi_{(1),5}$	m_h	1	$(0,0)$	$O_{0^+_0}$	m_h	1
	$\varphi_{(2),1,\ldots,6}$	0	6	$(1, I_3)$	$O_{0^+_{1,2,3}}$	0	3
1^-	A^8_μ	M_A	1	$(0,0)$	$O^\mu_{1^-_0}$	M_A	1
	$A^{4,\ldots,7}_\mu$	m_A	4	$(1, I_3)$	$O^\mu_{1^-_{1,2,3}}$	M_A	3
	$A^{1,2,3}_\mu$	0	3				

Table 3.9: Summary table for the case with orthogonal vevs. Here, we use the special choice $n_{(1),i} = \delta_{i,3}$ and $n_{(2),i} = \delta_{i,1}$.
Left: Gauge-variant spectrum of an $\mathrm{SU}(3)$ gauge theory with two scalar fields in the fundamental representation and $\mathrm{SU}(2) \times \mathrm{U}(1)$ custodial symmetry. The fields listed here are all mass-eigenstates.
Right: Gauge-invariant (physical) spectrum of the theory to leading order. m_{h} denotes the mass of the Higgs and the masses of the gauge bosons have the following ordering: $m_{\mathrm{A}} < m_{\mathrm{A}^{1,2}} < m_{\mathrm{A}^{6,7}} < m_{\mathrm{A}^{4,5}} < M_{\mathrm{A}}$. (I, I^3) are the quantum numbers of the global symmetry group $\mathrm{SU}(2)$. We only consider $\mathrm{U}(1)$-singlet states here.

	elementary spectrum			gauge-invariant spectrum			
J^P	Field	Mass	Deg.	(I, I^3)	Op.	Mass	Deg.
0^+	$\varphi_{(1),5}$	m_{h}	1	$(0,0)$	$O_{0^+_0}$	m_{h}	1
	$\varphi_{(2),1,5,6}$	0	3	$(1, I_3)$	$O_{0^+_{1,2,3}}$	0	3
1^-	A^8_μ	M_{A}	1	$(0,0)$	$O^\mu_{1^-_0}$	m_{A}	1
	$A^{6,7}_\mu$	$m_{\mathrm{A}^{6,7}}$	2	$(1, \pm 1)$	$O^\mu_{1^-_{1,2}}$	$m_{\mathrm{A}^{4,5}}$	2
	$A^{4,5}_\mu$	$m_{\mathrm{A}^{4,5}}$	2	$(1,0)$	$O^\mu_{1^-_3}$	m_{A}	1
	A^3_μ	m_{A}	1				
	$A^{1,2}_\mu$	$m_{\mathrm{A}^{1,2}}$	2				

$J^P = 0^+, 1^-$:

$$\begin{aligned} O_{0^+_{\hat{a}}} &= \phi^\dagger_{(\alpha)}\, \tau^{\hat{a}}_{\alpha\beta}\, \phi_{(\beta)} \quad , \quad O^\mu_{1^-_{\hat{a}}} = \phi^\dagger_{(\alpha)}\, \tau^{\hat{a}}_{\alpha\beta}\, D_\mu\, \phi_{(\beta)} \ , \\ \tau^{\hat{a}} &\in \left\{ \mathbb{1}, \tau_+ = \frac{\sigma^1 + \mathrm{i}\,\sigma^2}{2}, \tau_- = \frac{\sigma^1 - \mathrm{i}\,\sigma^2}{2}, \sigma^3 \right\} \ , \end{aligned} \tag{3.35}$$

with $\hat{a} = 0, 1, 2, 3$ and $\sigma^{1,2,3}$ are the usual Pauli matrices. The operators for the case $\hat{a} = 0$ are the singlets and $\hat{a} = 1, 2, 3$ are the triplet operators for both J^P-$\mathrm{U}(1)$- singlet channels.

Using again the FMS mechanism to leading order, we obtain the results listed in the right panels of Table 3.8 and 3.9.

We expect in the 0^+ channel for both, parallel and orthogonal vevs, one massive state with the mass of the perturbative Higgs in the $\mathrm{SU}(2)$-singlet channel and in the triplet we expect three degenerate massless states. In the 1^- channel there are four degenerate massive states with the mass of the heaviest gauge boson in the case of parallel vevs. In the case of orthogonal vevs there is one state in the $\mathrm{SU}(2)$-singlet channel with the mass of the lightest gauge boson which also appears in the triplet channel. In this channel there are also two degenerate states with masses of the second heaviest gauge boson(s). In both cases this is in contradiction to the elementary spectrum (cf. left panels of Table 3.8 and 3.9).

There is one interesting observation: If the vevs are parallel then the triplets in the 0^+ and in the 1^- channel are degenerate, which one would expect due to the Wigner-Eckart theorem. However, if the vevs are orthogonal then the degeneracy splits (at least in the 1^- channel). That appears due to the fact that in the case of parallel vevs there is still a $\mathrm{SU}(2)$ rotation left which can be applied to two of the three components of the vevs. This is not the case if the vevs are orthogonal.

Of course we can construct, in analogy to Section 3.1, objects similar to baryons, i.e., states with

open $\mathrm{U}(1)$ quantum numbers. An example set of these states are ($\alpha = 1, 2$):

$$\begin{aligned} O_{0_1^+,(\alpha)} &= \epsilon_{ijk}\, \phi_{(1),i}\, \phi_{(2),j} \left(D_\mu\, D^\mu\, \phi_{(\alpha)}\right)_k \quad , \quad O_{0_{-1}^+,(\alpha)} = \left(O_{0_1^+,(\alpha)}\right)^\dagger , \\ O^\mu_{1_1^-,(\alpha)} &= \epsilon_{ijk}\, \phi_{(1),i}\, \phi_{(2),j} \left(D^\mu\, \phi_{(\alpha)}\right)_k \quad , \quad O^\mu_{1_{-1}^-,(\alpha)} = \left(O^\mu_{1_1^-,(\alpha)}\right)^\dagger . \end{aligned} \tag{3.36}$$

It is easy to see that if the vevs are parallel, the leading order contribution of the FMS expansion vanishes due to the antisymmetry of the ϵ-tensor. Therefore, we discuss only on the case where the vevs are orthogonal. For simplicity we restrict on the case $v_{(1)} \gg v_{(2)}$ as it is the typical situation in GUTs. Then $m_{\mathrm{A}} = m_{\mathrm{A}^{1,2}}$ and $m_{\mathrm{A}^{4,5}} = m_{\mathrm{A}^{6,7}} \equiv m'_{\mathrm{A}}$. After expanding the corresponding correlators to leading order in FMS and in perturbation theory (similar strategy as in Appendix B) we obtain the following spectrum of states with an open $\mathrm{U}(1)$ quantum number for the theory in the above limit:

- 0^+ channel: Ground state mass of $2m_{\mathrm{A}}$ and excited states $m_{\mathrm{A}} + m'_{\mathrm{A}} < 2m'_{\mathrm{A}} < m_{\mathrm{A}} + M_{\mathrm{A}} < m'_{\mathrm{A}} + M_{\mathrm{A}}$.
- 1^- channel: Ground state mass of m_{A} and an excited state with a mass of m'_{A}.

Note that all these states have conjugated partners, describing the particle and anti-particle, respectively.

Chapter 4

Lattice field theory

In the last chapter we made analytical predictions for the particle spectra for $\mathrm{SU}(N)$ gauge theories with scalar fields in the fundamental and in the adjoint representation. For these predictions we generalized the FMS mechanism, which was introduced to investigate the electroweak sector of the standard model in a gauge-invariant manner, to theories with an extended Higgs sector. Of course these findings need to be tested. Since we are dealing with genuinely nonperturbative objects, i.e., bound states, we are required to use nonperturbative methods. We will focus on the lattice method for this purpose.

The basic setup introduced below follows closely [28, 30]. We explain how configurations of gauge and scalar fields can be generated, how masses can be extracted from lattice data and how to fix a gauge on the lattice as well as how to compute gauge-dependent objects in order to check the FMS mechanism in the end.

Since we show results for an $\mathrm{SU}(3)$ gauge theory with a scalar field in the fundamental representation of the gauge group in the next chapter, we will focus on this special case in the following. Generalization to other gauge groups and scalar representations as well as the treatment of fermions can be found in, e.g., [28].

However, this chapter is far from being a complete overview of the broad topic of lattice field theory. It should be kept in mind that we only introduce and discuss the most important techniques used in our simulations to comprehend the results presented in the next chapter.

4.1 Gauged scalar field theory on the lattice

Our task is to discretize the Lagrangian defined in Equation (2.21) as described in Section 3.1 for $N = 3$ and a fundamental scalar in Euclidean space-time for the following continuum potential:

$$V\left(\phi^\dagger\phi\right) = -m_0^2\,\phi^\dagger\phi + \lambda\left(\phi^\dagger\phi\right)^2 . \tag{4.1}$$

This is done on a 4-dimensional isotropic, hypercubic lattice with lattice constant a and volume $V = L^4$. The resulting discretized action reads [28]

$$S[U,\phi] = \sum_x \left(\frac{\beta}{3} \sum_{\mu<\nu} \mathrm{Re}\,\mathrm{tr}\big[\mathbb{1} - U_{\mu\nu}(x)\big] + \phi(x)^\dagger \phi(x) \right.$$
$$\left. + \bar{\lambda}\left(\phi(x)^\dagger\phi(x) - 1\right)^2 - \kappa \sum_{\mu=\pm1}^{\pm4} \phi(x)^\dagger\, U_\mu(x)\, \phi(x+\hat{\mu}) \right) , \tag{4.2}$$

where we have completed the terms in Equation (4.2) to a square, and added a constant (see below for the for the definition of $\bar{\lambda}$ and κ). The first sum runs over all lattice sites $x = (x_1, x_2, x_3, x_4)$, $x_i = 0, 1, \ldots, L-1$ and $\hat{\mu}$ denotes the unit vector in the μ-direction. The first term of the action is the Wilson gauge action with the plaquette variable $U_{\mu\nu}(x)$, which is a product of four link variables $U_\mu(x)$ forming a closed loop, i.e.,

$$U_{\mu\nu}(x) = U_\mu(x)\, U_\nu(x+\hat{\mu})\, U_\mu(x+\hat{\nu})^\dagger\, U_\nu(x)^\dagger \ , \tag{4.3}$$

and is essentially the field-strength tensor squared plus $\mathcal{O}(a^2)$-corrections in the naive continuum limit $a \to 0$. The links are related to the gauge fields by $U_\mu(x) = \exp(\mathrm{i}\, a\, A^c_\mu(x)\, T^c)$, with $2T^c$ being the Gell-Mann matrices. Thus, the links are elements of the gauge group $\mathrm{SU}(3)$. Note, that $U_{-\mu}(x) \equiv U_\mu(x-\hat{\mu})^\dagger$.

Both, the scalar field as well as the links, obey periodic boundary conditions, i.e.,

$$\phi(x + \hat{\nu}\, L) = \phi(x) \quad \text{and} \quad U_\mu(x) = U_\mu(x + \hat{\nu}\, L) \ , \ \ \forall\, x,\ \mu,\ \nu \ . \tag{4.4}$$

Under gauge transformations the scalar field and the gauge links transform as

$$\phi(x) \to\ g(x)\, \phi(x) \quad , \quad U_\mu(x)\ \to\ g(x)\, U_\mu(x)\, g(x+\hat{\mu})^\dagger \quad , \quad g(x) \in \mathrm{SU}(3)\ \forall\, x \ . \tag{4.5}$$

The Equation (4.2) is clearly invariant under these transformations making the action gauge invariant.

In total three parameters appear in the action (4.2): β is the inverse gauge coupling, $\bar{\lambda}$ is the coupling for the self-interaction of the scalar fields, and κ is related to the square of the inverse bare mass. Those lattice parameters are related to the continuum ones by

$$\beta = \frac{6}{g^2} \quad , \quad a^2 m_0^2 = \frac{1-2\bar{\lambda}}{\kappa} - 8 \quad , \quad \lambda = \frac{\bar{\lambda}}{\kappa^2} \ , \tag{4.6}$$

where the scalar field was rescaled by $1/\sqrt{\kappa}$ and the gauge field by $1/\sqrt{\beta}$ making the action (4.2) dimensionless. In the following we will use λ for the quartic coupling in (4.2) instead of $\bar{\lambda}$. We will only use $\bar{\lambda}$ if confusion could arise.

The full partition function is given by

$$Z = \int \mathcal{D}[U,\phi]\, \mathrm{e}^{-S[U,\phi]} \quad \text{with} \quad \mathcal{D}[U,\phi] = \left(\prod_x \prod_{\mu=1}^{4} \mathrm{d}U_\mu(x) \right) \left(\prod_x \mathrm{d}\phi(x) \right) , \tag{4.7}$$

where the gauge field measure is the so-called Haar measure which is a measure for integration over a compact continuous group, see, e.g., [30], and the integration over the scalar field is an integration

over $\mathbb{C}^3$ at every lattice site x. Both measures are invariant under the gauge transformations (4.5) and thus, the theory is completely gauge invariant.

Evaluating the partition sum involves the computation of a high dimensional integral which can be done efficiently using Monte Carlo techniques.

4.2 Generating configurations

The vacuum expectation value of a gauge-invariant observable[1] O in Euclidean spacetime on the lattice is given by the functional integral

$$\langle O \rangle = \frac{1}{Z} \int \mathcal{D}[U,\phi]\, \mathrm{e}^{-S[U,\phi]}\, O[U,\phi] \ , \tag{4.8}$$

with Z defined in Equation (4.7). Since this expression cannot be evaluated analytically, except for very small lattices, we use a Monte Carlo simulation to approximate the integral by an average of the observable O computed on N sample configurations $U_{(n)}$, $\phi_{(n)}$, distributed according to the probability distribution density

$$\mathrm{d}P(U,\phi) = \frac{1}{Z}\, \mathrm{e}^{-S[U,\phi]}\, \mathcal{D}[U,\phi] \ , \tag{4.9}$$

which is the so-called Gibbs measure. The expectation value of the observable is then given by

$$\langle O \rangle = \lim_{N\to\infty} \frac{1}{N} \sum_{n=1}^{N} O[U_{(n)}, \phi_{(n)}] \ . \tag{4.10}$$

In actual computations the integral is approximated by using a finite sample of configurations. The statistical error of the observable is then proportional to $1/\sqrt{N}$.

In order to generate configurations following the probability distribution $P(U,\phi) \propto \mathrm{e}^{-S[U,\phi]}$ the idea of Markov-chain Monte Carlo is used. This essentially boils down to finding a transition probability $T(U',\phi'|U,\phi)$ which leads from one configuration U, ϕ to a new configuration U', ϕ', and which fulfills the so-called detailed balance condition, i.e.,

$$T(U',\phi'|U,\phi)\, P(U,\phi) = T(U,\phi\,|U',\phi')\, P(U',\phi') \ . \tag{4.11}$$

One algorithm which fulfills this condition is the Metropolis algorithm [100]. This method of generating configurations is the procedure of our choice.[2] The transition probability in our case is

$$T(U',\phi'|U,\phi) = \min\big[1, \exp(-\Delta S)\big] \quad \text{with} \quad \Delta S = S[U',\phi'] - S[U,\phi] \ . \tag{4.12}$$

For the links we use one multi-hit Metropolis sweep, where 5 attempts are made to update one link by standard techniques [30] before moving to the next link, and one subsequent Metropolis sweep for the scalar field using a Gaußian proposal. We tuned the widths of the proposals adaptively to achieve a 50% acceptance rate for both updates. After every 5 sweeps through the lattice, a reprojec-

[1] A gauge-variant observable would vanish identically as a consequence of the theorem in [68].

[2] Note that, a heat bath algorithm could be used for SU(3) with a fundamental scalar as well, see, e.g., [101]. This kind of update can very efficiently be used if the gauge group is SU(2), see [102] for details, or if adjoint scalars are used.

tion step of the gauge links to $\mathrm{SU}(3)$ matrices is performed by a standard Gram-Schmidt procedure [30] in order to keep rounding errors under control.

For completeness we list the changes ΔS of the action used in (4.12) for both consecutive updates:

1. Change in the action for the link update: $U_\mu(x) \to U'_\mu(x)$

$$\begin{aligned}\Delta S = S[U',\phi] - S[U,\phi] = -\frac{\beta}{3}\,\mathrm{Re}\,\mathrm{tr}\Big[\big(U'_\mu(x) - U_\mu(x)\big)\sum_{\nu\neq\mu} C_{\mu\nu}(x)\Big] \\ -2\kappa\,\mathrm{Re}\left[\phi(x)^\dagger\,\big(U'_\mu(x) - U_\mu(x)\big)\,\phi(x+\hat\mu)\right]\,,\end{aligned} \tag{4.13}$$

with the so-called staple

$$\begin{aligned}C_{\mu\nu}(x) = U_\nu(x+\hat\mu)\,U_\mu(x+\hat\nu)^\dagger\,U_\nu(x)^\dagger \\ + U_\nu(x+\hat\mu-\hat\nu)^\dagger\,U_\mu(x-\hat\nu)^\dagger\,U_\nu(x-\hat\nu)\,.\end{aligned} \tag{4.14}$$

2. Change in the action for the scalar field update: $\phi(x) \to \phi'(x)$

$$\begin{aligned}\Delta S = S[U,\phi'] - S[U,\phi] = \lambda\Big[\big(\phi'(x)^\dagger\phi'(x) - 1\big)^2 - \big(\phi(x)^\dagger\phi(x)\big)^2\Big] \\ + \phi'(x)^\dagger\phi'(x) - \phi(x)^\dagger\phi(x) - 2\kappa\sum_{\mu=\pm1}^{\pm4}\mathrm{Re}\left[\big(\phi'(x)-\phi(x)\big)^\dagger\,U_\mu(x)\,\phi(x+\hat\mu)\right]\,.\end{aligned} \tag{4.15}$$

4.3 Spectroscopy

In this section we concentrate on determining masses of bound states, as the ones described in Chapter 3, i.e., we focus on a spectroscopy calculation. The initial step for this kind of calculation is to identify interpolators O and $O^\dagger$ such that the corresponding operators $\hat O$ and $\hat O^\dagger$ annihilate and create states that have overlap with particle states we want to analyze. An interpolator is a functional of the lattice fields with the quantum numbers of the state one is interested in. These interpolators are by construction gauge invariant. Usually, 'operator' and 'interpolator' are used synonymoulsy.

Physically allowed states can be observed in the spectral decomposition of the correlators of these interpolators ($x_4 \equiv t$),

$$\begin{aligned}\big\langle O(t)\,O^\dagger(t')\big\rangle &= \sum_k \langle 0|\hat O|k\rangle\langle k|\hat O^\dagger|0\rangle\,\mathrm{e}^{-a\,(t-t')\,E_k} \\ &= A\,\mathrm{e}^{-a\,(t-t')\,E_\mathrm{B}}\left(1 + \mathcal{O}\big(\mathrm{e}^{-a\,(t-t')\,\Delta E}\big)\right)\,,\end{aligned} \tag{4.16}$$

where A is a constant, E_B the energy of the lowest state $|B\rangle$ with $\langle 0|\hat O|B\rangle \neq 0$, and ΔE is the energy difference to the first excited state. From the leading exponential decay we thus can extract the energy E_B of the state.

4.3.1 Zero momentum projection and time slice averaging

The bound states we want to study should have definite spatial momentum $\boldsymbol{p}$. Therefore, we Fourier transform the interpolator,

$$O(\boldsymbol{p}, t) = \frac{1}{\sqrt{L^3}} \sum_{\boldsymbol{x}} O(\boldsymbol{x}, t)\, \mathrm{e}^{-\mathrm{i}\, a\, \boldsymbol{x}\cdot\boldsymbol{p}} \,, \tag{4.17}$$

where the sum runs only over the spatial components $\boldsymbol{x} = (x_1, x_2, x_3)$ and the momenta $\boldsymbol{p}$ are spatial momenta with components $p_i = 2\pi k_i/(aL)$, $k_i = -L/2+1, \ldots, L/2$. Therefore, the operator $O(\boldsymbol{p}, t)$ is located on a single time slice t and is projected to a definite spatial momentum $\boldsymbol{p}$. Computing the correlator for definite momenta $\boldsymbol{p}$ and $\boldsymbol{q}$ yields

$$\begin{aligned} \left\langle O(\boldsymbol{p}, t)\, O^\dagger(\boldsymbol{q}, t') \right\rangle &= \frac{1}{L^3} \sum_{\boldsymbol{x},\boldsymbol{y}} \mathrm{e}^{-\mathrm{i}\, a\, (\boldsymbol{x}-\boldsymbol{y})\cdot\boldsymbol{p}} \left\langle O(\boldsymbol{x}, t)\, O^\dagger(\boldsymbol{y}, t') \right\rangle \delta^{(3)}(\boldsymbol{p}-\boldsymbol{q}) \\ &= A\, \mathrm{e}^{-a\,(t-t')\,E(\boldsymbol{p})} \left(1 + \mathcal{O}\big(\mathrm{e}^{-(t-t')\,a\,\Delta E}\big)\right) \delta^{(3)}(\boldsymbol{p}-\boldsymbol{q}) \,, \end{aligned} \tag{4.18}$$

where we have used translational invariance in the spatial coordinates giving rise to the δ-function enforcing $\boldsymbol{p} = \boldsymbol{q}$, and where $E(\boldsymbol{p}) = \sqrt{m^2 + \boldsymbol{p}^2}$, the relativistic dispersion relation, with m being the physical mass of the state and thus $E(\boldsymbol{0}) = m$.

In order to increase statistics, we can make use of the time translation invariance of Equation (4.16) or (4.18) and perform time slice averaging [92]. For operators with zero spatial momentum ($O(\boldsymbol{p} = \boldsymbol{0}, t) \equiv O(t)$) this method yields the correlation function $C(t)$ given by

$$\begin{aligned} C(t) &= \frac{1}{L} \sum_{t'=0}^{L-1} \left\langle O(t')\, O^\dagger(t+t') \right\rangle_{\mathrm{c}} \\ &\equiv \frac{1}{L} \sum_{t'=0}^{L-1} \left\langle \Big(O(t') - \langle O(t') \rangle\Big) \Big(O^\dagger(t+t') - \langle O^\dagger(t+t') \rangle\Big) \right\rangle \,, \end{aligned} \tag{4.19}$$

where we subtracted the vacuum contribution $\langle O(t) \rangle$ from the correlator, i.e., we only consider the connected contributions $\langle \cdots \rangle_{\mathrm{c}}$ of the correlator. This is necessary since states with the quantum numbers $J^{PC} = 0^{++}$ mix with the vacuum, which has exactly these quantum numbers, and thus adds additional noise to the correlator.

4.3.2 Variational analysis

One is often interested in computing excited states. This can be done by considering not only a single correlator, but by computing a matrix of cross correlators

$$C_{ij}(t) = \frac{1}{L} \sum_{t'=0}^{L-1} \left\langle O_i(t')\, O_j^\dagger(t+t') \right\rangle_{\mathrm{c}} \,, \tag{4.20}$$

for a set of N basis interpolators O_i, $i = 1, 2, \ldots, N$, all with the quantum numbers of the state one is interested in. One can show that the eigenvalues $\lambda_k(t)$ of the correlation matrix behave as

[103–105]

$$\lambda_k(t) \propto \mathrm{e}^{-a\,t\,E_k}\left(1+\mathcal{O}\big(\mathrm{e}^{-a\,t\,\Delta E_k}\big)\right)\,,\;\; k=0,1,\ldots,N-1\,, \tag{4.21}$$

where ΔE_k is the distance of E_k to nearby energy levels. Usually the generalized eigenvalue problem

$$C(t)\,\boldsymbol{v} = \lambda(t)\,C(t_0)\,\boldsymbol{v}\,, \tag{4.22}$$

is solved for $t_0 < t$. The eigenvalues behave again as in Equation (4.21) but the amplitude of the correction term is typically smaller. Due to the normalization at one time slice t_0, the contributions from higher states are suppressed and the signal is therefore improved.

If the number of different interpolators is increased, the method improve if all interpolators have good overlap with the eigenstates of the system. The information about the overlap can be retrieved from the eigenvectors $\boldsymbol{v}$.

The energy levels are extracted as

$$a\,E_k\big(t+\tfrac{1}{2}\big) = \ln\frac{\lambda_k(t)}{\lambda_k(t+1)}\,, \tag{4.23}$$

where the ground state energy E_0 is usually called effective mass, i.e., $E_0 \equiv m_{\text{eff}}$.

Since all our fields appearing in the action (4.2) obey periodic boundary conditions, the propagation in t and $(L-t)$ of all our states O is identical and thus we fit the eigenvalues or correlators to

$$\lambda_k(t) = A_k^{(1)}\,\cosh\left(a\,E_k^{(1)}\,\big(t-L/2\big)\right) + A_k^{(2)}\cosh\left(a\,E_k^{(2)}\,\big(t-L/2\big)\right)\,, \tag{4.24}$$

where we take into account a possible excitation of the level E_k, since heavier states still can contribute for small values of t to this level after the variational analysis. The energy levels are then extracted from the fits.

4.3.3 Smearing of the fields

In most theories short distances are entirely dominated by quantum effects. Therefore, using operators which are evaluated on a single lattice site are strongly afflicted by these quantum fluctuations, which increases the noise. One is able to substantially improve the signal of correlation functions by smearing the fields. The typical smearing procedure replaces gauge links by local averages over paths connecting the endpoints of the link. Since smearing is gauge covariant, operators with different levels of smearing can be used to construct a basis for a spectroscopical analysis as discussed before. There are several methods on the market such as APE, HYP and stout smearing. For a general overview see [30].

In our case we apply stout smearing to the gauge links according to the procedure described in [106]. We choose this approach due to fact that with this method a projection back to the gauge group is not necessary. The new link after one stout smearing step is

$$U'_\mu(x) = \mathrm{e}^{\mathrm{i}Q_\mu(x)}\,U_\mu(x)\,, \tag{4.25}$$

where $Q_\mu(x)$ is a hermitian and traceless matrix which is constructed from staples (4.14), i.e.,

$$\begin{aligned} Q_\mu(x) &= \frac{\mathrm{i}}{2}\left(\Omega_\mu(x)^\dagger - \Omega_\mu(x) - \frac{\mathbb{1}}{3}\,\mathrm{tr}\big[\Omega_\mu(x)^\dagger - \Omega_\mu(x)\big]\right) , \\ \Omega_\mu(x) &= \left(\sum_{\nu\neq\mu} \rho_{\mu\nu}\, C_{\mu\nu}(x)^\dagger\right) U_\mu(x)^\dagger , \end{aligned} \tag{4.26}$$

where we set $\rho_{\mu 4} = \rho_{4\mu} = 0$, $\rho_{ij} = \rho$ since we want to measure correlations in the Euclidean time direction and thus only spatial links are allowed to be smeared. In all our simulations we set $\rho = 0.1$, see [106]. Of course, this procedure can be iterated. Therefore, the new link after $(n+1)$ stout smearing steps is given by

$$U_\mu^{(n+1)}(x) = \mathrm{e}^{\mathrm{i}Q_\mu^{(n)}(x)}\, U_\mu^{(n)}(x) . \tag{4.27}$$

The scalar field is APE smeared in our case. After $(n+1)$ APE smearing steps the field is then [107]

$$\phi^{(n+1)}(x) = \frac{1}{7}\left(\phi^{(n)}(x) + \sum_{\mu=1}^{4}\Big[U_\mu^{(n)}(x)\,\phi^{(n)}(x+\hat\mu) + U_\mu^{(n)}(x-\hat\mu)^\dagger\,\phi^{(n)}(x-\hat\mu)\Big]\right) , \tag{4.28}$$

where the n-times stout smeared links $U_\mu^{(n)}(x)$ enter in the smearing procedure of the scalar.

During our analysis up to 10 smearing steps have been performed for operators with the quantum numbers of the vacuum. Usually 3 to 4 smearing steps have been used for the simplest vector operators discussed in Chapter 5.

4.4 Gauge fixing on the lattice

In order to compute the propagators of elementary fields we need to fix a gauge. Without this procedure those propagators would be zero as a consequence of the theorem in [68]. We are interested in the elementary propagators since, in the end, we want to check whether the FMS mechanism produces correct predictions.

We again restrict the discussion on how to fix a gauge on the lattice to the case where we have the gauge group $\mathrm{SU}(3)$ as well as a single scalar field in the fundamental representation.

We fix locally to the Landau gauge in our lattice calculation, which is given by $\partial_\mu A_\mu = 0$ in the continuum. It can be shown that this condition is equivalent with finding the minimal value of the functional

$$\begin{aligned} F_g[U] &= -a^2 \sum_x \mathrm{Re}\,\mathrm{tr}\big[g(x)\,K_g[U](x)\big] , \text{ with} \\ K_g[U](x) &= \sum_{\mu=1}^{4}\Big(U_\mu(x)\,g(x+\hat\mu)^\dagger + U_\mu(x-\hat\mu)^\dagger\,g(x-\hat\mu)^\dagger\Big) , \end{aligned} \tag{4.29}$$

on the lattice for fixed $U_\mu(x)$ as a function of $g(x)$. Since there is more than one local minimum, i.e., Gribov copies [74], it is assumed that unique gauge fixing is accomplished by randomly selecting a Gribov copy for every configuration U. Therefore, this prescription averages over all minima when

one computes correlation functions. This procedure is called minimal Landau gauge [108, 109]. There are several methods on the market to minimize this functional, see, e.g., [110]. We choose the stochastic overrelaxation method in our study [110]. Generally the overrelaxation algorithm optimizes the value of $F_g[U]$ locally, i.e., minimizes $\mathrm{Re}\,\mathrm{tr}[g(x)\,K_g[U](x)]$ for all lattice sites x. Let us discuss the solution to this optimization problem first for the gauge group $\mathrm{SU}(2)$ and then generalize the results to the $\mathrm{SU}(3)$ case: For $\mathrm{SU}(2)$ the normalized product

$$w_g[K](x) = \frac{g(x)\,K_g[U]}{\sqrt{\det\big[g(x)\,K_g[U]\big]}} \in \mathrm{SU}(2)\ , \tag{4.30}$$

is a local solution of the optimization problem. One now iteratively applies this solution to the gauge field configuration as

$$g(x) \to \begin{cases} \big(w_g[K](x)^\dagger\big)^2\, g(x)\ , & \text{with probability } p \\ w_g[K](x)^\dagger \quad g(x)\ , & \text{with probability } 1-p \end{cases}\ , \tag{4.31}$$

where $p \in (0,1)$. In our simulations we adaptively tuned the probability p in order to find as closely as possible the optimal value for every parameter set such that the number of iterations becomes as small as possible.

For the case of gauge group $\mathrm{SU}(3)$ one can use the Cabibbo-Marinari trick to iteratively operate in the three $\mathrm{SU}(2)$ subgroups [111]. We also apply reunitarization using the method of maximal trace as described in [112].

This algorithm allows for a so-called checkerboard decomposition, where we perform the transformations on the even and odd sites separately.

The iteration stops if the quantity $e_6(t)$ defined as [110]

$$\begin{aligned} e_6(t) &= \frac{1}{12\,L}\sum_{\nu=1}^{4}\sum_{c=1}^{8}\sum_{x_\nu=1}^{L}\frac{\Big(Q^c_\nu(x_\nu)-\hat{Q}^c_\nu\Big)^2}{\hat{Q}^{c\ 2}_\nu}\ , \text{ with} \\ \hat{Q}^c_\nu &= \frac{1}{L}\sum_{x_\nu=1}^{L} Q^c_\nu(x_\nu) \quad \text{and} \quad Q^c_\nu(x_\nu) = \sum_{\mu\neq\nu}\sum_{x_\mu=1}^{4} A^c_\nu(x)\ , \end{aligned} \tag{4.32}$$

is smaller than some value ϵ. In our simulations we usually set $\epsilon = 10^{-13}$. However, this quantity is expensive to measure. Therefore, we linearly extrapolate the number of iterations until the next measurement of $e_6(t)$ to the desired accuracy ϵ. The advantage to use this quantity in contrast to others is, that it is sensitive to long-wavelength fluctuations [110].

To accomplish the 't Hooft-Landau gauge condition of Equation (3.1) we have to fix also the global direction of the scalar field. We want to perform a global gauge transformation such that the space-time average $\bar{\phi}$ of the scalar field point into some direction n:

$$g\,\frac{\bar{\phi}}{\big|\,\bar{\phi}\,\big|} = n \quad \text{with} \quad \bar{\phi} = \frac{1}{V}\sum_x \phi(x) \quad \text{and} \quad g \in \mathrm{SU}(3)\ , \tag{4.33}$$

where we set $n_i = \delta_{i,3}$ as discussed in Chapter 3. We use two consecutive $\mathrm{SU}(3)$ rotations, where the first transformation rotates the first component of $\bar{\phi}$ to zero and the second one implements the

rotation such that the vector points into the third real direction as desired. With this procedure g can be constructed from the average $\bar{\phi}$. See Appendix C for the derivation and detailed expressions.

This global gauge transformation is then applied to the scalar field $\phi(x)$ for all x. Of course, the links get transformed accordingly, i.e., $U_\mu(x) \to g\, U_\mu(x)\, g^\dagger$, again for all x. With this the gauge is now completely fixed on the lattice to a so-called minimal 't Hooft Landau gauge.

4.5 Propagators of gauge variant quantities and running coupling

In this section we define all the lattice propagators of the gauge-variant quantities, which are computed on the gauge-fixed configurations according to the procedure described in the last section. We also give a definition of the corresponding Schwinger functions of the propagators. Further, we mention how the running coupling is computed.

4.5.1 Gauge field and scalar propagator

We compute the propagators or correlation functions of the elementary fields in momentum space. Therefore, we directly Fourier-transform the gauge and scalar fields rather than first computing the propagators first in position space and afterwards Fourier-transforming the result. But first, the gauge field A_μ has to be extracted from the link U_μ:

$$\begin{aligned} A_\mu(x) &= \frac{1}{2\,\mathrm{i}\,a}\left(U_\mu(x) - U_\mu(x)^\dagger\right)\Big|_{\text{traceless}} \\ &= \frac{1}{2\,\mathrm{i}\,a}\left(U_\mu(x) - U_\mu(x)^\dagger - \frac{\mathbb{1}}{3}\mathrm{tr}\big[U_\mu(x) - U_\mu(x)^\dagger\big]\right) . \end{aligned} \tag{4.34}$$

The Fourier transformation of the gauge and scalar field is done by [29]

$$A_\mu(p) = \frac{1}{\sqrt{V}}\,\mathrm{e}^{\mathrm{i}\,\frac{p_\mu}{2}} \sum_x \mathrm{e}^{-\mathrm{i}\,a\,p\cdot x}\, A_\mu(x) \quad \text{and} \quad \phi(p) = \frac{1}{\sqrt{V}} \sum_x \mathrm{e}^{-\mathrm{i}\,a\,p\cdot x}\, \phi(x) \ , \tag{4.35}$$

with the lattice momenta $p_\mu = 2\pi k_\mu/(aL)$, where $k_\mu = -L/2+1, \ldots, L/2$, $\mu = 1,2,3,4$, and due to the periodic boundary conditions of the fields in position space, they are also periodic in momentum space, and therefore only the momenta $k_\mu = 0, 1, \ldots, L/2$ are independent. The lattice momenta k_μ are related to physical momenta $\hat{p}$ by

$$\hat{p}_\mu = \frac{2}{a}\,\sin\left(\frac{p_\mu}{2}\right) = \frac{2}{a}\,\sin\left(\frac{\pi}{L}\,k_\mu\right) . \tag{4.36}$$

The gauge-field propagator is given by the expectation value

$$D^{bc}_{\mu\nu}(p^2) = \left\langle A^b_\mu(p)\, A^c_\nu(-p)\right\rangle , \tag{4.37}$$

where the components of the gauge fields are obtained from $A^c_\mu = 2\,\mathrm{tr}[A_\mu\, T^c]$. Due to the isotropic lattice, we can take the trace over the Euclidean Lorentz-indices. Further, the propagator is diagonal in the adjoint indices if we are in the BEH regime, see Chapter 5, and if we fix the gauge as described

in Section 4.4. These considerations yield the gauge-field propagator

$$D^c\big(p^2\big) = \sum_{\mu=1}^{4} \big\langle A^c_\mu(p)\, A^c_\mu(-p)\big\rangle \ , \quad c = 1, 2, \ldots, 8 \ . \tag{4.38}$$

For the scalar propagator we split the field ϕ into its real and imaginary parts and use the notation $\phi = \frac{1}{\sqrt{2}}\big(\phi_1 + \mathrm{i}\,\phi_2, \phi_3 + \mathrm{i}\,\phi_4, \phi_5 + \mathrm{i}\,\phi_6\big)$. Then we define the propagator as

$$D_{ij}\big(p^2\big) = \big\langle \phi_i(p)\, \phi_j(-p)\big\rangle \ , \quad i, j = 1, 2, \ldots, 6 \ . \tag{4.39}$$

Again, in the BEH regime and in the minimial 't Hooft Landau gauge this propagator is diagonal, i.e., $D_{ij}\big(p^2\big) = D_i\big(p^2\big)\delta_{ij}$. Due to the analysis performed in Section 3.1 we expect, for the vev-choice $n_i = \delta_{i,3}$, that only the propagator $D_5(p^2)$ behaves like a massive propagator and the remaining ones correspond to the propagation of massless particles in the Landau gauge.

4.5.2 Definition of the renormalization scheme

Before continuing with the remaining propagator, we need to define a renormalization scheme for the scalar propagator $D_{ij}\big(p^2\big)$. To this end we follow [113]. We assume that the renormalization of the propagator can be done as in the perturbative case [3]. Thus, there are two renormalization constants: The multiplicative wave function renormalization Z_i and an additive mass renormalization δm_i^2. This yields the renormalized scalar propagator in minimal 't Hooft Landau gauge,

$$D^{\mathrm{r}}_i\big(p^2\big) = \frac{1}{Z_i\,\big(p^2 + m_i^{\mathrm{r}\,2}\big) + \Pi_i\big(p^2\big) + \delta m_i^2} \ , \quad i = 1, 2, \ldots, 6 \ , \tag{4.40}$$

where m_i^{r} is the renormalized mass of the ith particle and $\Pi_i\big(p^2\big)$ is the corresponding self energy which is obtained from the unrenormalized propagator (4.39) as

$$\Pi_i\big(p^2\big) = \frac{1 - p^2\, D_i\big(p^2\big)}{D_i\big(p^2\big)} \ . \tag{4.41}$$

Thus, the self energy measures essentially the deviation from the tree-level propagator, i.e.,

$$D_i\big(p^2\big) = \frac{1}{p^2 + \Pi_i\big(p^2\big)} \ . \tag{4.42}$$

Note, that the tree-level mass m_i is implicitly included in the self-energy.

The scheme we use to fix the renormalization constants is

$$D^{\mathrm{r}}_i\big(\mu^2\big) = \frac{1}{\mu^2 + m_i^{\mathrm{r}\,2}} \qquad \text{and} \qquad \left.\frac{\mathrm{d}D^{\mathrm{r}}_i\big(p^2\big)}{\mathrm{d}p}\right|_{p^2=\mu^2} = -\frac{2\mu}{\big(\mu^2 + m_i^{\mathrm{r}\,2}\big)^2} \ , \tag{4.43}$$

where μ is the renormalization scale. Therefore, the renormalized propagator and its derivative are

given by their tree-level values at $p^2 = \mu^2$. Solving those equations for Z_i and δm_i^2 yields

$$Z_i = 1 - \frac{1}{2\mu} \frac{\mathrm{d}\Pi_i(p^2)}{\mathrm{d}p}\bigg|_{p^2=\mu^2} \quad \text{and} \quad \delta m_i^2 = \frac{\mu^2 + m_i^{\mathrm{r}\,2}}{2\mu} \frac{\mathrm{d}\Pi_i(p^2)}{\mathrm{d}p}\bigg|_{p^2=\mu^2} - \Pi_i(\mu^2) \ . \tag{4.44}$$

The renormalization constants are determined numerically by linear interpolation between two physical momenta along the x-axis, with the value of μ inside the interval $(\hat{p}_1, \hat{p}_2)$. The derivative of the self-energy is obtained by analytically deriving the linear interpolation between the momenta points. We only choose values for μ such that $0 < \hat{p}_1 < \mu < \hat{p}_2 < 2/a$.

At this point we want to mention that for the gauge boson propagators the additive mass renormalization vanishes since an appearance of such a counter term in the theory would be inconsistence with the gauge symmetry.

4.5.3 Ghost propagator

Due to the minimal Landau gauge condition, a ghost term to the gauge-fixed action is introduced and thus a propagator G^{ab} for the Graßmann-valued ghost fields c^a and $\bar{c}^a$ can be defined [3]. It can be derived from the Faddeev-Popov operator $M^{ab}(x,y)$, which for linear covariant gauges is in the continuum given by $M^{ab}(x,y) = -\partial_\mu^x D_\mu^{ab}(y)$, with $D_\mu^{ab}(y) = \delta^{ab}\,\partial_\mu^y + g f^{abc} A_\mu^c(y)$, as

$$G^{ab}(x,y) = \left\langle \bar{c}^a(x)\, c^b(y) \right\rangle = \left\langle \left(M^{-1}\right)^{ab}(x,y) \right\rangle \ , \tag{4.45}$$

which is diagonal in the adjoint indices: $G^{ab} = \delta^{ab}\, G^a$. At tree-level, the propagator in Euclidean spacetime is given by

$$G^a(p^2) = \frac{1}{p^2 + \xi \left(M_{\mathrm{A}}^2\right)^a} \ , \tag{4.46}$$

with $\left(M_{\mathrm{A}}^2\right)^a$ being the ath entry of the diagonal gauge boson mass matrix. Therefore, in 't Hooft Landau gauge, where $\xi \to 0$, the propagator behaves as $1/p^2$ at tree-level, i.e., the propagator of a massless particle.

On the lattice the Faddeev-Popov operator can be derived from the inverse of the Hessian of the functional defined in Equation (4.29). It is a linear combination of gauge links mixed with the generators of the gauge group, see, e.g., [114]. A conjugate gradient method is usually used to invert the Faddeev-Popov operator as described in, e.g., [115]. Details on how the ghost propagator is computed can be found in [59].

4.5.4 Schwinger functions

Having now the propagators defined, one can evaluate the so-called Schwinger functions. Quantities such as masses and widths as well as the analytic structure of the elementary fields or particles can be extracted from these objects. The Schwinger function is given by

$$\Delta(t) = \frac{1}{\pi} \int_0^\infty \mathrm{d}p_4 \, \cos\left(p_4\, t\right) D\left(p_4^2\right) \ , \tag{4.47}$$

for a field with propagator $D(p^2)$. Note that, the propagator $D(p_4^2)$ is evaluated at zero spatial momentum, as is indicated by the argument p_4^2. The lattice version of this function is given by [116]

$$\Delta(t) = \frac{1}{a\pi L} \sum_{p_4=0}^{L-1} \cos\left(\frac{2\pi\, p_4}{L}\, t\right) D(p_4^2) \ , \quad t = 0, 1, \ldots, L-1 \ , \tag{4.48}$$

where the sum extends over the whole momentum range including the parts of the propagator reproduced by periodicity.

For a stable particle with pole mass m and an Euclidean propagator $(p^2 + m^2)^{-1}$, the Schwinger function is

$$\Delta(t) = \frac{1}{2m}\, \mathrm{e}^{-m\, t} \ . \tag{4.49}$$

Therefore, an exponential decay is expected in Euclidean time for a massive, stable particle. Beyond tree-level the analysis is more involved but also gives insight into the decay widths of the particles. We refer for an analysis thereof to [109].

4.5.5 Running coupling

Using the gauge field propagator (4.38) and the ghost propagator (4.45) the running coupling α^b can be computed for every value of $b = 1, 2, \ldots, N^2 - 1$. In a momentum subtraction scheme in four dimensions it is given by [109, 117–120]

$$\alpha^b(p^2) = p^6\, \alpha(\mu^2)\, G^b(p^2, \mu^2)^2\, D^b(p^2, \mu^2) \ , \tag{4.50}$$

where μ is again the renormalization scale. Note that, this is a renormalization-scale invariant combination.

The running coupling is computed in the so-called minimal momentum subtraction scheme [120]. We determine the running coupling to see whether the system we focus on is weakly coupled or not, and thus if the lowest order of gauge-invariant perturbation theory is applicable or not.

Chapter 5

SU(3) lattice gauge theory with a fundamental scalar

In this chapter, we discuss the lattice results of an $\mathrm{SU}(3)$ gauge theory with a scalar field in the fundamental representation of the gauge group. This is a special case of the various theories discussed in Chapter 3.

First we discuss how the phase diagram of this theory is obtained and show in which regions Brout-Englert-Higgs physics or QCD-like physics dominates. Next, the physical spectrum, i.e., the spectrum of gauge invariant and thus observable particles, is examined. The last section of this chapter is dedicated to the test of the Fröhlich-Morchio-Strocchi mechanism. It contains a brief recapitulation of the predictions of Section 3.1 for $N = 3$, as well as a detailed comparison of the spectra of the gauge-variant and gauge-invariant states.

Some of the results shown here have been published in [65, 66].

5.1 Phase diagram of the theory

Since the breaking pattern in our case is $\mathrm{SU}(3) \to \mathrm{SU}(2)$ and thus the gauge group is not fully broken, the Osterwalder-Seiler-Fradkin-Shenker construction [54, 121] does not apply. Therefore, this theory may or may not have separated phases and a possibly rich phase structure. We expect (at least) two regions of the phase diagram: Due to the non-Abelian nature of our theory defined in Equation (4.2), a region where QCD-like physics takes place and due to the Higgs sector we also expect a region with Higgs-like physics. Since we are especially interested in a situation with a perturbatively accessible Brout-Englert-Higgs effect [56, 58, 59, 88] we scanned the phase diagram using the quantity [122]

$$\langle \bar{\phi}^2 \rangle = \left\langle \left| \frac{1}{V} \sum_x \phi(x) \right|^2 \right\rangle = \frac{1}{V^2} \sum_{x,y} \langle \phi(x)^\dagger \phi(y) \rangle \ , \tag{5.1}$$

with $\bar{\phi}$ being already defined in Equation (4.33). Of course, this quantity is gauge dependent, and thus we fix to minimal 't Hooft Landau gauge gauge described in Section 4.4 to compute this expectation value.

The two-point function $\langle \phi(x)^\dagger \phi(y) \rangle$, appearing on the right-hand side of Equation (5.1), drops exponentially with the distance $|x - y|$, i.e., $\exp\big(-|x-y|/\xi\big)$, where ξ is the correlation length.

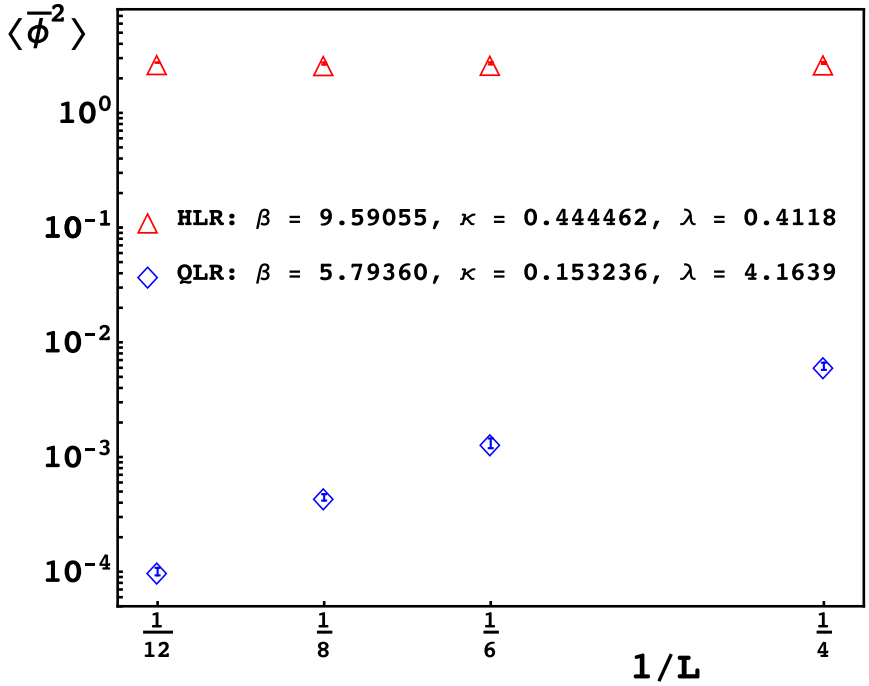

Figure 5.1: Two examples for $\langle\bar{\phi}^2\rangle$ as a function of the inverse lattice size L. The red triangles show a constant behavior signaling a Brout-Englert-Higgs effect, and thus being a point in the Higgs-like region (HLR) of the phase diagram. The blue diamonds go to zero in the infinite volume limit. Therefore, this parameter point belongs to the QCD-like region (QLR) of the phase diagram.

Therefore, $\langle\bar{\phi}^2\rangle$ behaves approximately as

$$\langle\bar{\phi}^2\rangle \approx \frac{\xi}{V} \,. \tag{5.2}$$

In the Higgs-like region the system is strongly correlated, since there exists a preferred relative orientation of the scalar field. This means that $\xi \to \infty$ in the infinite volume limit, and thus $\langle\bar{\phi}^2\rangle \xrightarrow{V\to\infty} \text{const.} > 0$. However, in the QCD-like region the correlation length is finite and thus $\langle\bar{\phi}^2\rangle \sim 1/V \xrightarrow{V\to\infty} 0$.

We show examples for these two different types of behavior in Figure 5.1. There, $\langle\bar{\phi}^2\rangle$ is plotted for two different lattice parameter sets as a function of the inverse of the lattice size L. The red triangles show an example of a parameter point which belongs to the Higgs-like regime since the quantity (5.1) is essentially constant. For a second set of parameters (blue diamonds) the observable $\langle\bar{\phi}^2\rangle$ goes to zero for $L \to \infty$ and the parameter point thus corresponds to the QCD-like phase.

To scan the phase diagram quickly, we performed simulations for $V = 4^4, 6^4, 8^4$, and 12^4 lattices for randomly distributed parameters β, κ, and λ. We measured the quantity defined in Equation (5.1) on 1000 gauge-fixed configurations for each random parameter set and lattice size. Then, the volume dependence of this observable was used to decide to which region the parameter point belongs to.

This procedure yields the phase diagram shown in Figure 5.2. We neither did check or need in what follows if the two regions are separated by a genuine phase transition and are really distinct phases.

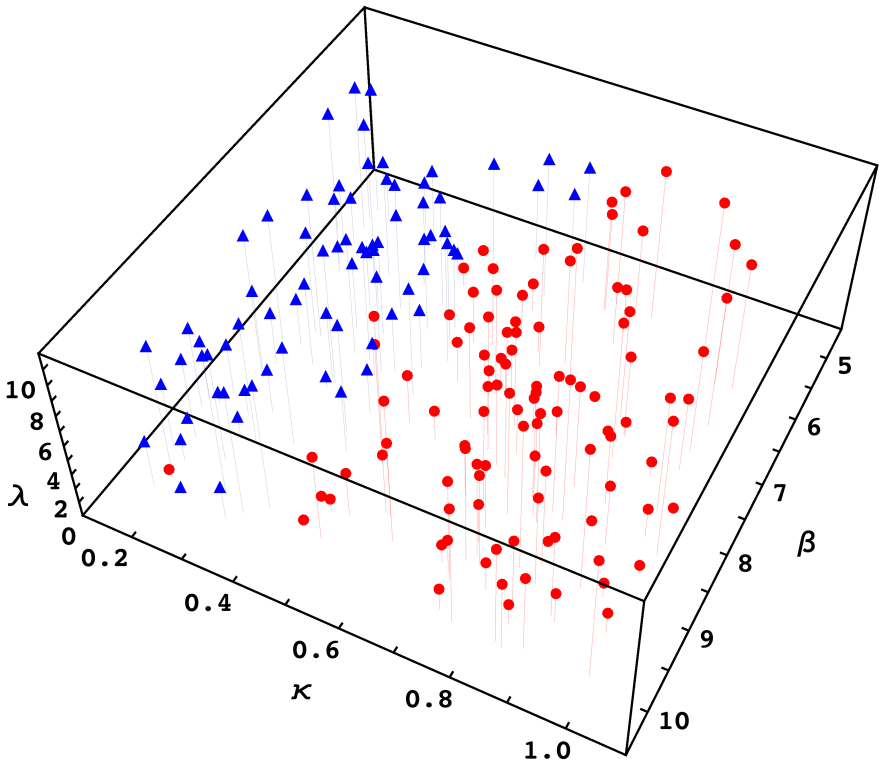

Figure 5.2: The phase diagram of the theory. The red dots show a Brout-Englert-Higgs effect in minimal 't Hooft Landau gauge, putting them in the Higgs-like region, while the blue triangles do not, meaning that they are in the QCD-like region of the phase diagram.

For large values of κ, i.e., large negative tree-level masses and thus a steep potential, a Brout-Englert-Higgs effect is observed in this gauge. Whereas, for small values of κ there is mainly no Brout-Englert-Higgs effect present.

For small values of β, i.e., large values of the gauge coupling g, larger values of κ are needed to get a Brout-Englert-Higgs effect, since bosonic fluctuations force the system into the symmetric phase. Also, for larger values of β and smaller values of λ a Brout-Englert-Higgs effect can be observed (see lower left corner in the QLR of Figure 5.2), which has also been observed in [59] for the $\mathrm{SU}(2)$ case.

5.2 Physical spectrum

In this section, we present results on the gauge-invariant and thus physical spectrum of the $\mathrm{SU}(3)$ gauge theory with a scalar field in the fundamental representation. We use the methods described in Chapter 4, especially the updates described in Section 4.2, to create configurations, and the procedures described in Section 4.3 to perform the spectroscopy.

We usually perform $300 + 10\,L$ updates to drive the system into equilibrium. Between the measurements of the observables we drop $3\,L$ configurations for decorrelation. We also performed sev-

eral independent runs with different random number seeds for each parameter set to further reduce correlations. The integrated autocorrelation time for the plaquette is $\tau_{\text{int}} \approx 1/2$, i.e., close to the minimal value, for the parameter sets we analyzed. Therefore, no significant correlations between subsequent measurements of observables are detected. We usually studied $V = 8^4$, 12^4, 16^4, and 20^4 lattices to perform a finite-size analysis of the resulting masses in several quantum number channels. We typically have $\mathcal{O}\big(10^5\big)$ configurations at hand to compute the correlation functions. The errors of the correlators are computed throughout by a standard Jackknife procedure, and for secondary observables we use the method of error propagation unless stated otherwise.

5.2.1 Definition of interpolators

Before we show results for the spectroscopic analysis, we first define the interpolators used for this purpose. The interpolators we measured in our simulations are listed in Table 5.1 and carry the quan-

Table 5.1: List of interpolators used for our spectroscopic analysis. Definitions of the objects D_μ, $L_\mu^{(1)}$, $L_\mu^{(2)}$, and $L_\mu^{(3)}$ can be found in the main text. We perform a zero-momentum projection for all interpolators.

Name	Interpolator	$J^{\text{PC}}_{\text{U(1)}}$
$O_1^{0_0^{++}}(t)$	$\frac{1}{L^3}\sum_{\boldsymbol{x}} \phi(\boldsymbol{x},t)^\dagger \phi(\boldsymbol{x},t)$	0_0^{++}
$O_2^{0_0^{++}}(t)$	$O_1^{0_0^{++}}(t)\, O_1^{0_0^{++}}(t)$	0_0^{++}
$O_3^{0_0^{++}}(t)$	$\frac{1}{L^3}\sum_{\boldsymbol{x}} \sum_{\mu,\nu=1,\mu<\nu}^{3} \text{Re tr}\big[U_{\mu\nu}(\boldsymbol{x},t)\big]$	0_0^{++}
$O_{1,\mu}^{1_0^{--}}(t)$	$\frac{\mathrm{i}}{L^3}\sum_{\boldsymbol{x}} \phi(\boldsymbol{x},t)^\dagger\, D_\mu\, \phi(\boldsymbol{x},t)$	1_0^{--}
$O_{2,\mu}^{1_0^{--}}(t)$	$O_1^{0_0^{++}}(t)\, O_{1,\mu}^{1_0^{--}}(t)$	1_0^{--}
$O_{3,\mu}^{1_0^{--}}(t)$	$\sum_{\nu=1}^{3}\Big(O_{1,\nu}^{1_0^{--}}(t)\, O_{1,\nu}^{1_0^{--}}(t)\Big)\, O_{1,\mu}^{1_0^{--}}(t)$	1_0^{--}
$O_{4,\mu}^{1_0^{--}}(t)$	$\frac{1}{L^3}\sum_{\boldsymbol{x}} \text{Im}\, L_\mu^{(1)}(\boldsymbol{x},t)$	1_0^{--}
$O_{5,\mu}^{1_0^{--}}(t)$	$\frac{1}{L^3}\sum_{\boldsymbol{x}} \text{Im}\, L_\mu^{(2)}(\boldsymbol{x},t)$	1_0^{--}
$O_{6,\mu}^{1_0^{--}}(t)$	$\frac{1}{L^3}\sum_{\boldsymbol{x}} \text{Im}\, L_\mu^{(3)}(\boldsymbol{x},t)$	1_0^{--}
$O_4^{0_0^{++}}(t)$	$\sum_{\mu,=1}^{3} O_{1,\mu}^{1_0^{--}}(t)\, O_{1,\mu}^{1_0^{--}}(t)$	0_0^{++}
$O^{2_0^{++}}(t)$	$\frac{1}{L^3}\sum_{\boldsymbol{x}} \text{Re tr}\big[U_{12}(\boldsymbol{x},t) + U_{23}(\boldsymbol{x},t) - 2\, U_{13}(\boldsymbol{x},t)\big]$	2_0^{++}
$O^{0_0^{-+}}(t)$	$\frac{1}{L^3}\sum_{\boldsymbol{x}} \sum_{\mu\neq\nu\neq\gamma\neq\rho=1}^{3} \text{tr}\big[U_{\mu\nu}(\boldsymbol{x},t)\, U_{\gamma\rho}(\boldsymbol{x},t)\big]$	0_0^{-+}
$O^{0_1^{++}}(t)$	$\frac{1}{L^3}\sum_{\boldsymbol{x}} \sum_{\mu,\nu=1}^{3} \epsilon_{ijk}\, \Big[\phi_i\, (D_\mu\, \phi)_j\, (D_\mu\, D_\nu\, D_\nu\, \phi)_k\Big](\boldsymbol{x},t)$	0_1^{++}
$O_\mu^{1_1^{--}}(t)$	$\frac{1}{L^3}\sum_{\boldsymbol{x}} \sum_{\nu=1}^{3} \epsilon_{ijk}\, \Big[\phi_i\, (D_\mu\, \phi)_j\, (D_\nu\, D_\nu\, \phi)_k\Big](\boldsymbol{x},t)$	1_1^{--}

tum numbers $J^{PC}_{\mathrm{U}(1)}$, where the lower index is the quantum number of the custodial group $\mathrm{U}(1)$, as already described in Section 3.1. The parity transformation $\mathcal{P}$ acts on the fields as

$$\begin{aligned} \phi(\boldsymbol{x},t) &\xrightarrow{\mathcal{P}} \phi(-\boldsymbol{x},t) \quad , \quad \phi(\boldsymbol{x},t)^\dagger \xrightarrow{\mathcal{P}} \phi(-\boldsymbol{x},t)^\dagger \ , \\ U_\mu(\boldsymbol{x},t) &\xrightarrow{\mathcal{P}} \begin{cases} U_\mu(-\boldsymbol{x}-\hat{\mu},t)^\dagger & , \text{ for } \mu = 1,2,3 \\ U_\mu(-\boldsymbol{x},t) & , \text{ for } \mu = 4 \end{cases} \ , \end{aligned} \tag{5.3}$$

and charge conjugation $\mathcal{C}$ transforms the fields as

$$\phi(x) \xrightarrow{\mathcal{C}} \phi(x)^\dagger \quad , \quad \phi(x)^\dagger \xrightarrow{\mathcal{C}} \phi(x) \quad , \quad U_\mu(x) \xrightarrow{\mathcal{C}} U_\mu(x)^\star = \left(U_\mu(x)^\dagger\right)^T \ . \tag{5.4}$$

The custodial $\mathrm{U}(1)$-group acts on the scalar field ϕ only and dresses the field with a phase, i.e., $\phi(x) \xrightarrow{\mathrm{U}(1)} \mathrm{e}^{\mathrm{i}\,\alpha}\,\phi(x)$, where $\alpha \in [0,2\pi)$, and analogously for the Hermitean-conjugate field, $\phi(x)^\dagger \xrightarrow{\mathrm{U}(1)} \mathrm{e}^{-\mathrm{i}\,\alpha}\,\phi(x)^\dagger$.

The parity P, the charge parity C (using the transformations defined above), and the total angular momentum J, are assigned to the interpolators by their transformation properties under the octahedral symmetry group O_{h}, which is the discrete symmetry group of an isotropic lattice. A method on how these quantum numbers are assigned to the interpolators according to the irreducible representations of the octahedral group can be found in, e.g., [123] and [124].

Note, that we only use the 'spatial'-directions $\mu = 1,2,3$ for the operators, since we are interested in the propagation of the state in Euclidean time-direction $\mu = 4$.

In Table 5.1 several of the interpolators can be viewed as bound states of the scalar and the gauge bosons in the language of a naive constituent interpretation (we only discuss the 'atomic' interpolators here):

- $O^{0_0^{++}}_1$ describes a two-scalar bound state.

- $O^{1_0^{--}}_{1,\mu}$ is a gauge boson dressed with two scalar fields. The gauge bosons appear in the lattice version of the covariant derivative defined as

$$D_\mu\,\phi(x) = \frac{U_\mu(x)\,\phi(x+\hat{\mu}) - U_\mu(x-\hat{\mu})^\dagger\,\phi(x-\hat{\mu})}{2} \ . \tag{5.5}$$

- $O^{0_0^{++}}_3$ is a scalar glueball.

- $O^{1_0^{--}}_{4,5,6,\mu}$ are vector glueball interpolators as defined in [123]. Several definitions are needed to define the spatially summed quantities $L^{(1,2,3)}_\mu$ from Table 5.1. These quantities are built from the Wilson loop operator

$$\begin{aligned} W_{\mu\nu\rho}(x) = \mathrm{tr}\Big[& U_\mu(x)\,U_\mu(x+\hat{\mu})\,U_\nu(x+2\hat{\mu})\,U_\mu(x+\hat{\mu}+\hat{\nu})^\dagger \\ & \times U_\rho(x+\hat{\mu}+\hat{\nu})\,U_\mu(x+\hat{\nu}+\hat{\rho})^\dagger\,U_\rho(x+\hat{\nu})^\dagger\,U_\nu(x)^\dagger\Big] \ , \end{aligned} \tag{5.6}$$

and linear combinations thereof,

$$\begin{aligned}
L^{(1)}_{\mu\nu\rho} &= W_{+\mu+\nu+\rho} + W_{+\mu+\nu-\rho} + W_{+\mu-\nu+\rho} + W_{+\mu-\nu-\rho} \\
&\quad -W_{-\mu+\nu+\rho} - W_{-\mu+\nu-\rho} - W_{-\mu-\nu+\rho} - W_{-\mu-\nu-\rho} \,, \\
L^{(2)}_{\mu\nu\rho} &= W_{+\mu+\nu+\rho} + W_{+\mu+\nu-\rho} + W_{+\mu-\nu+\rho} - W_{+\mu-\nu-\rho} \\
&\quad +W_{-\mu+\nu+\rho} + W_{-\mu+\nu-\rho} - W_{-\mu-\nu+\rho} - W_{-\mu-\nu-\rho} \,, \\
L^{(3)}_{\mu\nu\rho} &= W_{+\mu+\nu+\rho} - W_{+\mu+\nu-\rho} + W_{+\mu-\nu+\rho} - W_{+\mu-\nu-\rho} \\
&\quad +W_{-\mu+\nu+\rho} - W_{-\mu+\nu-\rho} + W_{-\mu-\nu+\rho} - W_{-\mu-\nu-\rho} \,,
\end{aligned} \tag{5.7}$$

where we skipped the spacetime argument x for brevity. The last step is to build the following linear combinations of Equation (5.7) to build the interpolators that give the vector representation, $J = 1$, and negative parity P:

$$\begin{aligned}
L^{(1)} &= \left(L^{(1)}_{123} + L^{(1)}_{132} \,,\, L^{(1)}_{231} + L^{(1)}_{213} \,,\, L^{(1)}_{312} + L^{(1)}_{321} \right) \,, \\
L^{(2)} &= \left(L^{(2)}_{123} + L^{(2)}_{321} \,,\, L^{(2)}_{231} + L^{(2)}_{132} \,,\, L^{(2)}_{312} + L^{(2)}_{213} \right) \,, \\
L^{(3)} &= \left(L^{(3)}_{123} + L^{(3)}_{213} \,,\, L^{(3)}_{231} + L^{(3)}_{321} \,,\, L^{(3)}_{312} + L^{(3)}_{132} \right) \,.
\end{aligned} \tag{5.8}$$

Taking the imaginary parts of these quantities yields interpolators with negative charge parity C. It is trivial to construct a vector glueball interpolator with other P and C quantum numbers from the definitions given above [123]. However, we are particularly interested in the 1^{--}_0 glueball for reasons illustrated in the next subsection where this quantum number channel is discussed.

- $O^{0^{-+}_0}$, and $O^{2^{++}_0}$ are a pseudo-scalar glueball, and a tensor glueball, respectively, see [89].
- $O^{0^{++}_1}$ and $O^{1^{--}_1}_\mu$ are the only interpolators with an open $\mathrm{U}(1)$-quantum number. The continuum versions are discussed in Section 3.1 and the lattice versions are located in Appendix D.

Having defined the interpolators of our choice for the spectroscopy, we now can look at the physical, gauge-invariant spectrum of the theory.

5.2.2 Spectroscopy results

In what follows, we focus on a set of parameters in the Higgs-like region, since our main target is to test the analytical predictions of the FMS mechanism in the end. We choose a point close to the boundary of the two regions of the phase diagram given by $\beta = 6.85535$, $\kappa = 0.456074$, $\lambda = 2.3416$. This choice is motivated by the simulation results of the $\mathrm{SU}(2)$ theory, where the smallest lattice spacings, i.e., the largest cutoffs, have been found [89]. Results for different sets of lattice couplings are listed in Table E.1 in Appendix E.

As already mentioned, we perform simulations for four different lattice sizes: $V = 8^4$ with 320000 configurations, $V = 12^4$ with 240000 configurations, $V = 16^4$ with 120000 configurations, and $V = 20^4$ with 190000 configurations.

In the following, we investigate individually all the quantum number channels which are listed above.

0_0^{++} channel

In this channel, we perform a variational analysis as described in Subsection 4.3.2. We use a set of five operators from Table 5.1 as basis interpolators: [1]

$$\left\{ O^{0_0^{++}}_{1,(10)} \, , \, O^{0_0^{++}}_{2,(10)} \, , \, O^{0_0^{++}}_{3,(10)} \, , \, O^{0_0^{++}}_{4,(4)} \, , \, O^{0_0^{++}}_{4,(5)} \right\} , \tag{5.9}$$

where the number in the brackets of the lower index denotes the smearing levels of the operators. The operators $O_1^{0_0^{++}}$ and $O_2^{0_0^{++}}$, which contain only scalar fields, are smeared ten times as they are statistically very noisy due to the fact that the vacuum carries the same quantum numbers. For the same reason, we smear the glueball operator $O_3^{0_0^{++}}$ ten times. However, we smear the interpolator $O_4^{0_0^{++}}$, which is built form two 1_0^{--} operators, four and five times.

Solving the generalized eigenvalue problem (4.22) for the cross-correlation matrix, built from the set (5.9), yields the energy levels as a function of Euclidean time. This is shown for several lattice volumes in Figure 5.3.

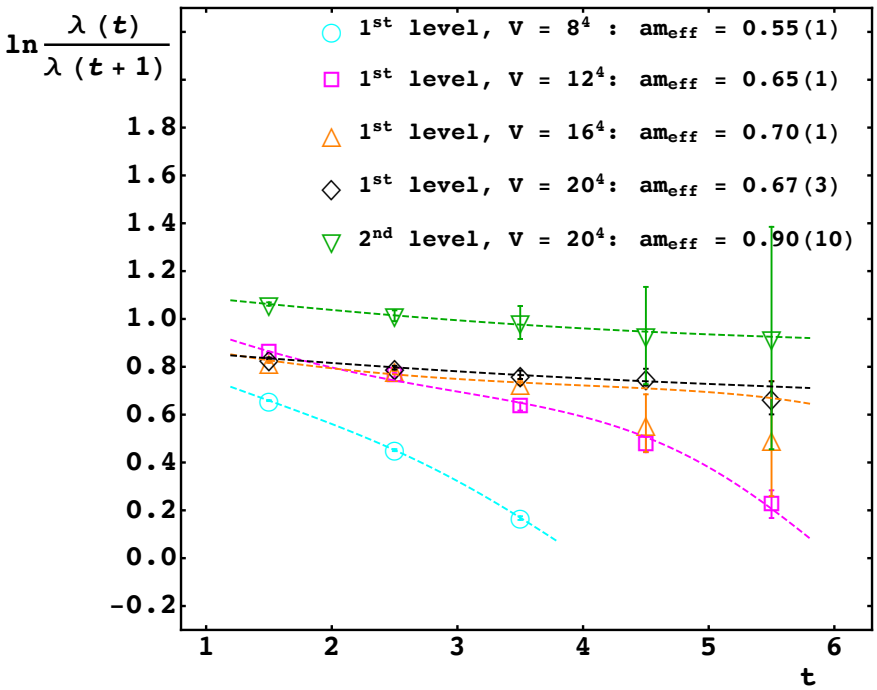

Figure 5.3: Result of the variational analysis for the 0_0^{++}. The first energy levels are shown for the $V = 8^4$, 12^4, 16^4, and 20^4 lattices, whereas the second energy level (green triangles) is only shown for the largest volume for a clear display. The dashed lines are obtained by double-cosh fits of the eigenvalues. The lowest fitted energy values are listed in the legend as effective mass.

We plot the energy of the lowest state (ground state), for each volume, and the second energy level (first excited state) for the largest volume. The effective masses and their errors, listed in the legend of Figure 5.3, are obtained by fitting the the mean, upper, and lower value of the eigenvalues

[1] We also performed our analysis with more operators in the basis set. However, the results did not improve substantially and therefore we do not show them here.

by a double-cosh, see Equation (4.24), for each volume. The resulting fit parameters are listed in Table E.2 in Appendix E. Note, that due to the large fluctuations of the correlation functions from connected contributions at large Euclidean time t, we do not show data points for $t > 6$.

In Figure 5.4, the volume dependence of the ground state mass is plotted. We see that this state has a rather strong dependence on the lattice size. Nevertheless, a fit of the lattice masses as a function of the volume, $am_{0_0^{++}}(V) = am_{0_0^{++}} + \delta\, \mathrm{e}^{-\gamma V}$, can be performed and gives the grey error band (see Table E.4 in Appendix E for the numerical values). We conclude that the dimensionless ground state mass in this channel is $am_{0_0^{++}} = 0.68(2)$ which is below the $2\, am_{1_0^{--}}$ threshold, i.e., the elastic threshold, as it can be seen in the discussion of the 1_0^{--} channel.

The next-level state has an approximated mass of $am^{\star}_{0_0^{++}} \approx 0.9(1)$ which is almost compatible with the $2\, am_{1_0^{--}} = 0.78(2)$ state expected from the process $0_0^{++} \to 1_0^{--} + 1_0^{--}$. However, more statistics for all volumes would be helpful to make a definite statement. Of course, with the available methods we cannot definitely say if this state is a resonance or a scattering state. A Lüscher finite volume scaling analysis [125, 126] would be necessary to make a definite conclusion.

The next expected states are the ones with mass $2\, am_{0_0^{++}}$ and with $2\, am_{0_0^{++}} + p^{\mathrm{rel}}$, where p^{rel} is a relative momentum (a state with relative momentum is discussed below). However, this state is relatively heavy and only noisy signals around this region have been found and thus no definite results are available yet.

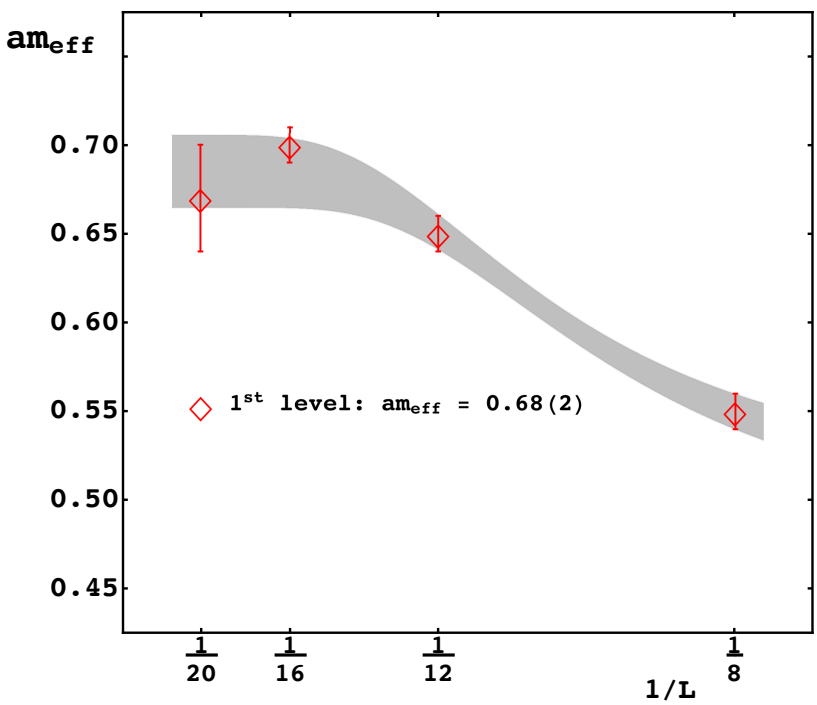

Figure 5.4: First energy level of the 0_0^{++} channel as a function of the inverse lattice size. The grey bands are the error bands obtained by fits of the lower and upper bounds of the masses (see Table E.4 in Appendix E). The extrapolated mass is $am_{0_0^{++}} = 0.68(2)$.

1_0^{--} channel

We use again a variational analysis but this time with a basis of six interpolators (see Table 5.1 for their definition), i.e.,

$$\left\{ O^{1_0^{--}}_{1,\mu,(3)} \,,\, O^{1_0^{--}}_{1,\mu,(4)} \,,\, O^{1_0^{--}}_{2,\mu,(3)} \,,\, O^{1_0^{--}}_{2,\mu,(4)} \,,\, O^{1_0^{--}}_{3,\mu,(3)} \,,\, O^{1_0^{--}}_{3,\mu,(4)} \right\} , \tag{5.10}$$

where the smearing levels are indicated in the brackets of the lower index of each operator. We did not include the vector glueball interpolators $O^{1_0^{--}}_{4,\mu}$, $O^{1_0^{--}}_{5,\mu}$, and $O^{1_0^{--}}_{6,\mu}$ in the basis, since they are too noisy even for the largest used smearing level as can be seen from the effective masses in the first three panels in Figure 5.8. However, those states are very high up in the spectrum and thus it is a justified assumption that they do not alter the infrared spectrum of the theory.

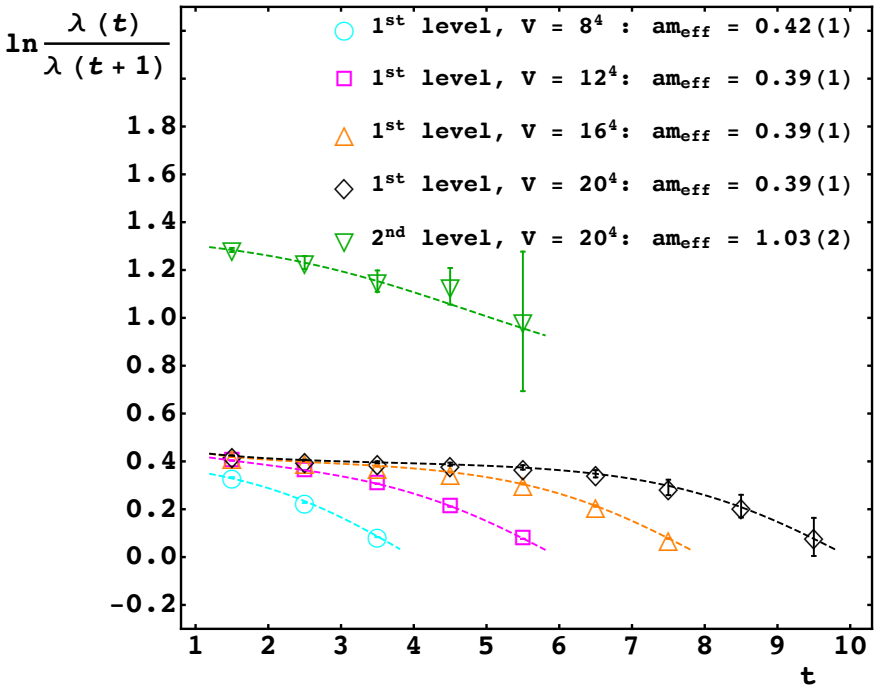

Figure 5.5: Result of the variational analysis in the 1_0^{--} channel. The first energy levels are shown for the $V = 8^4$, 12^4, 16^4, and 20^4 lattices, whereas the second energy level (green triangles) is only shown for the largest volume for a clear display and for $t < 6$. The dashed lines are obtained by double-cosh fits of the eigenvalues except for the smallest volume where we used a single-cosh fit. The lowest extracted fitted energy values are listed in the legend as effective mass.

In Figure 5.5, we show the energy levels obtained from the variational analysis with the cross-correlation matrix built from the basis interpolators (5.10). The lowest energy level is shown for each lattice volume. As in the previous discussion the second energy level is only shown for the largest volume and for $t < 6$. Again we list the effective masses in the legend of this figure, which are obtained by the same fit strategy as in the 0_0^{++} case. The fit parameters can be found in Table E.2 in Appendix E.

The ground state has almost no volume dependence, hence the infinite volume extrapolated ground state mass is $am_{1_0^{--}} = 0.39(1)$, see Figure 5.6 and Table E.2. Hence, the singlet vector state is lighter

than the singlet scalar state, i.e., $m_{1_0^{--}} < m_{0_0^{++}}$ for the investigated set of bare lattice parameters.

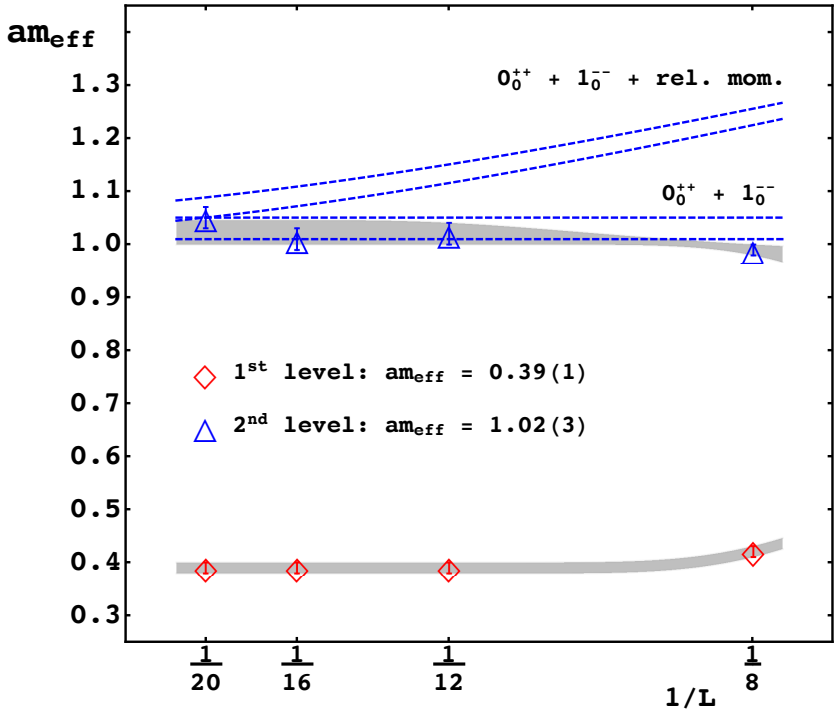

Figure 5.6: First and second energy level of the 1_0^{--} channel as a function of the inverse lattice size. The grey bands are the error bands obtained by fits of the lower and upper bounds of the masses (see Table E.4 in Appendix E). The dashed blue lines are the expected masses of the next-level states $am_{0_0^{++}} + am_{1_0^{--}}$ and $p^{\mathrm{rel}} + am_{0_0^{++}} + am_{1_0^{--}}$, where $\boldsymbol{p}^{\mathrm{rel}} = (2\pi/L, 0, 0)$. The extrapolated masses are $am_{1_0^{--}} = 0.39(1)$ for the ground state, and $am^{\star}_{1_0^{--}} = 1.02(3)$ for the second level.

Next-level states are expected at a mass of $am_{0_0^{++}} + am_{1_0^{--}}$, and at $3\, am_{1_0^{--}}$ for the processes $1_0^{--} \to 0_0^{++} + 1_0^{--}$ and $1_0^{--} \to 1_0^{--} + 1_0^{--} + 1_0^{--}$ respectively. Additionally, one can find states with relative momentum as $p^{\mathrm{rel}} + am_{0_0^{++}} + am_{1_0^{--}}$ and $p^{\mathrm{rel}} + 3\, am_{1_0^{--}}$. This is possible since the zero-momentum projected operators in Table 5.1 allow for two-particle states where the particles have equal and opposite momentum. The energy levels E can be extracted from [123]

$$\sinh^2\left(\frac{E(L,k)}{2}\right) = \sinh^2\left(\frac{m_{2\mathrm{p}}}{2}\right) + \sum_{i=1}^{3} \sin^2\left(\frac{\pi}{L}\, k_i\right) \,, \tag{5.11}$$

where $m_{2\mathrm{p}}$ is the mass of the two-particle state and the relative lattice momentum is $p_i^{\mathrm{rel}} = 2\pi k_i/L$, $k_i = -L/2+1, \ldots, L/2$. In the continuum limit this equation turns into the familiar energy-momentum relation $E(\boldsymbol{p}) = \sqrt{m^2 + \boldsymbol{p}^2}$.

The ordering of the states depends on the value of the masses of the 0_0^{++} and 1_0^{--} states. For the parameter set we study, the $am_{0_0^{++}} + am_{1_0^{--}}$ state should be the lightest next-level state, since $am_{0_0^{++}} + am_{1_0^{--}} = 1.07(3)$, and $3\, am_{1_0^{--}} = 1.17(3)$. Besides the ground state, we also show in Figure 5.6 the volume dependence of the second level (blue triangles) with its error band as well as the expected next-level states $am_{0_0^{++}} + am_{1_0^{--}}$ and $p^{\mathrm{rel}} + am_{0_0^{++}} + am_{1_0^{--}}$ (dashed blue lines,

upper and lower bounds) with $\boldsymbol{p}^{\mathrm{rel}} = (2\pi/L, 0, 0)$, i.e., the smallest possible relative momentum. It seems that the mass of the second state is consistent with the expected $0_0^{++} + 1_0^{--}$ state and is not in agreement with the state including relative momentum. All other energy levels are too noisy to comment on them.

0_0^{-+}, 1_0^{--} *and* 2_0^{++} *glueballs*

Here we show the spectroscopy results of several glueball states. All the results shown below share one feature, the signal is very noisy which makes it rather hard to perform fits in order to extract masses of the states. Furthermore, all the masses seem to be well above the lowest lattice mass in the spectrum, i.e., above $am_{1_0^{--}}$.

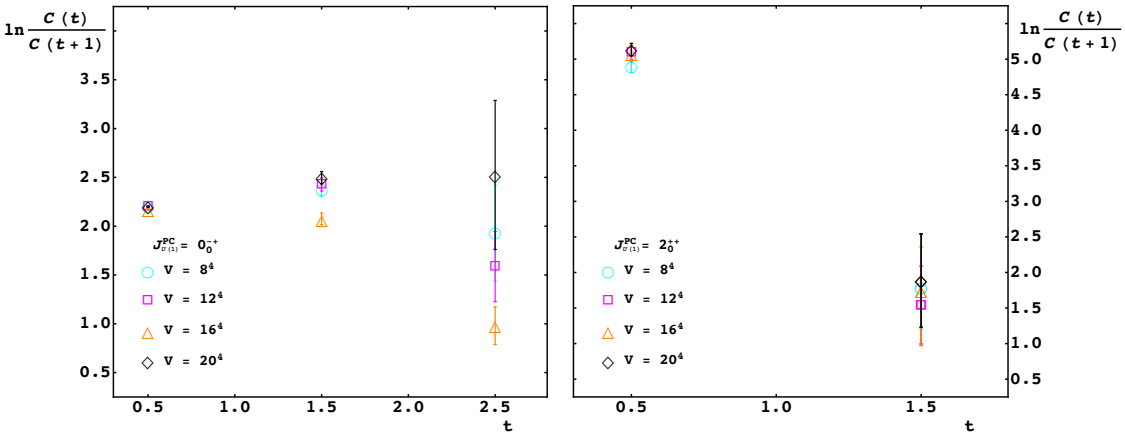

Figure 5.7: On the left-hand side the effective mass of the pseudo-scalar glueball is shown as a function of Euclidean time. On the right-hand side the effective mass of the tensor glueball is plotted. For both, the results are shown for $V = 8^4$, 12^4, 16^4, and 20^4 for 10-times smeared fields.

Figure 5.7 shows the effective masses of the 0_0^{-+} pseudo-scalar glueball on the left-hand side and the 2_0^{++} glueball on the right-hand side as a function of Euclidean time for several lattice volumes. We do not show data points for $t > 3$ and $t > 2$ respectively, since these regions are dominated by noise even though we used 10-times smeared operators.

The effective masses in both channels are around $am_{0_0^{-+}} \approx am_{2_0^{++}} \approx 2.0$, i.e., above the lattice cutoff. These approximate masses are of course just crude estimates.

We also performed a variational analysis with sets of different smeared operators in these channels. However, this procedure did not improve the signal substantially and therefore we do not show the results here.

Some, but not all, possible decay channels for the two states with the available channels are:

- 0_0^{-+} channel: two 1_0^{--} in a p-wave
- 2_0^{++} channel: two 0_0^{++} in a d-wave
  two 1_0^{--} in a s-wave
  1_1^{--} and 1_{-1}^{--} in a s-wave

The masses in both channels are compatible with the last option at both points, i.e., a decay in 1_1^{--} and 1_{-1}^{--} in an s-wave (see below). Nonetheless, this is very speculative since more statistics and more operators including better overlap with the decay channels would be needed to make precise statements. Of course, another option is that those signals are just lattice artifacts.

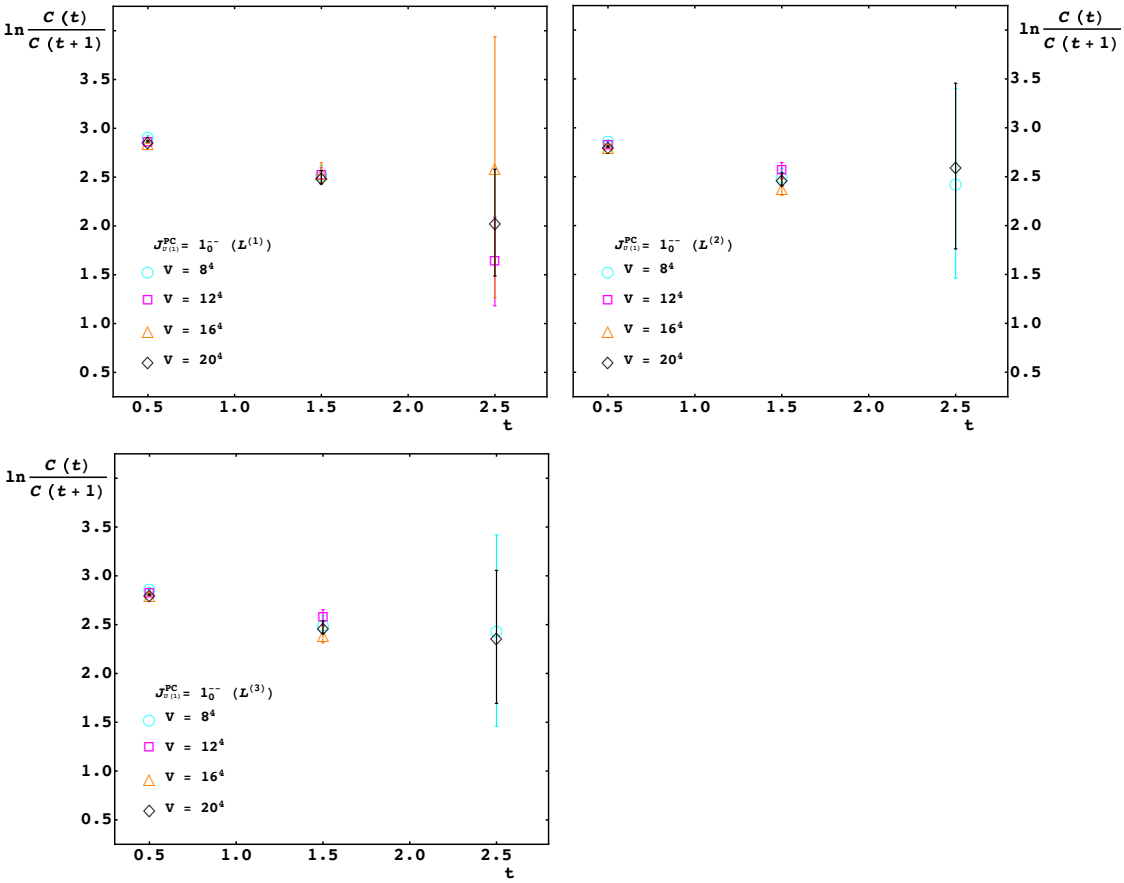

Figure 5.8: The three panels show the effective masses of the 1_0^{--} glueballs $L^{(1)}$, $L^{(2)}$ and $L^{(3)}$ as a function of Euclidean time $t < 3$. The results are shown for $V = 8^4$, 12^4, 16^4, and 20^4 for 10-times smeared fields.

In Figure 5.8 we show the effective masses of the three 1_0^{--} glueballs, $L^{(1)}$, $L^{(2)}$, and $L^{(3)}$, for $V = 8^4$, 12^4, 16^4 and 20^4 lattices. As before, we do not plot the whole time region in all the plots due to the large fluctuations of the correlators and thus the effective masses. The results are shown for 10-times smeared operators as before.

Even though the signals are again noisy we deduce that the effective masses of the three 1_0^{--} glueballs are approximately 7-times larger than the extracted ground state mass in this channel, and thus well above the lattice cutoff. As already argued in the discussion of the 1_0^{--} channel, they do not alter the ground state and thus the infrared spectrum, since they are too high up in the spectrum to generate any significant contribution.

We are well aware that the effective mass plateau of three points which are still inclined, are probably still contaminated by excited state contributions, and higher statistics would be needed.

$0^{++}_{\pm 1}$ *and* $1^{--}_{\pm 1}$ *open* $\mathrm{U}(1)$ *channels*

Finally, we study quantum number channels with an open $\mathrm{U}(1)$ quantum number, i.e., the $0^{++}_{\pm 1}$ and $1^{--}_{\pm 1}$ states. These states are stable since the global custodial quantum number is conserved.

In Figure 5.9 we present results for the effective masses of the $0^{++}_{\pm 1}$ (left plot) and $1^{--}_{\pm 1}$ (right plot) channels for different lattice volumes. In both channels we performed a variational analysis with different smearing levels of the corresponding operators: In the scalar sector the basis consists of 6- to 10-times smeared interpolators, whereas in the vector sector we included 8- to 10-times smeared interpolators in the basis. The effective masses [2] of both states are listed in the legends of the figure and the corresponding values from the fit are given in Table E.4 in Appendix E.

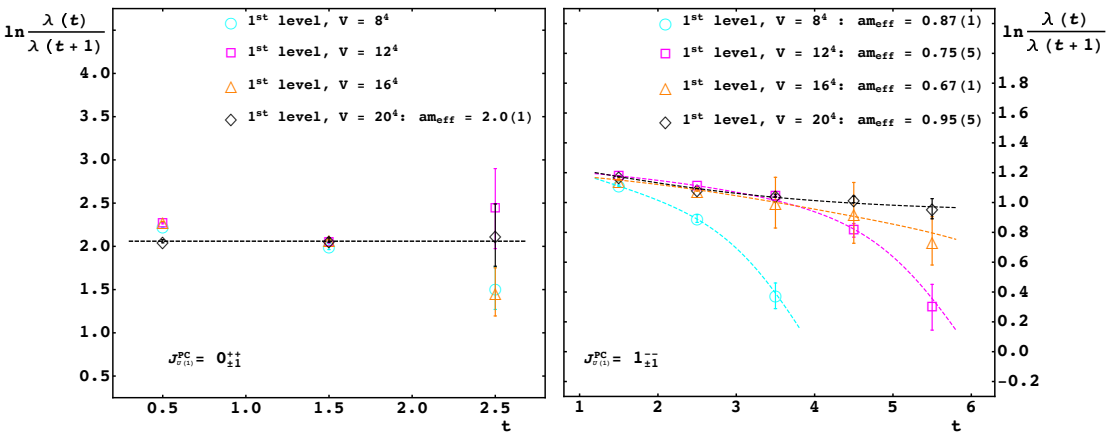

Figure 5.9: On the left-hand side the effective mass of the $0^{++}_{\pm 1}$ state is shown as a function of Euclidean time $t < 3$. On the right-hand side the effective mass of the $1^{--}_{\pm 1}$ state is plotted for $t < 6$. For both, the results are shown for $V = 8^4, 12^4, 16^4$, and 20^4 lattices. The dashed lines in the left and right panels are results of single- and double-cosh fits, respectively.

The scalar sector is dominated by noise and only the points for $t < 3$ are reliable. The mass in this channel is roughly $am_{0^{++}_{\pm 1}} \approx 2$. Of course this is only a coarse estimation and larger statistics as well as larger lattices can alter the result.

The vector channel is not so much dominated by noise and thus, more time slices can be used for the fit ($t < 6$). However, from $V = 8^4$ to $V = 16^4$ the effective mass seems to drop but for the largest lattice slightly rises again. Again, more statistics could still change this behavior. Nonetheless, we estimate a mass of $am_{1^{--}_{\pm 1}} \approx 0.8(2)$.

Besides increasing the statistics [3], also including more operators can have an impact on the result in both cases. For future studies also the lattice version of the operators (3.11) and (3.12) discussed in Subsection 3.1.2 should be included in the basis for a variational analysis.

[2] Note that, $m_{0^{++}_{+1}} = m_{0^{++}_{-1}}$, i.e., particle and anti-particle states. Thus the effective mass given in the left-hand side of Figure 5.9 is the mass of the particle and anti-particle. Certainly, the same is true for the $1^{--}_{\pm 1}$ channel.

[3] Apart from the issues with the ground state, the amount of statistics used here was not enough to extract higher energy levels.

5.3 Test of the Fröhlich-Morchio-Strocchi mechanism

This section is dedicated to test the Fröhlich-Morchio-Strocchi mechanism for the $\mathrm{SU}(3)$ gauge theory with a fundamental scalar on the lattice. We first recapitulate the predictions of this mechanism which is already discussed in Section 3.1 for this special theory. Afterwards the spectrum of gauge-variant quantities, i.e., elementary field propagators are presented. The comparison between this spectrum and the physical spectrum, as examined in the previous section, concludes this section.

5.3.1 Predictions from the FMS mechanism

Specifying the gauge group to $\mathrm{SU}(3)$ the following physical states are predicted according to the FMS procedure (see Subsection 3.1.2): In the 0_0^{++} channel there should be only one ground state with the mass of the elementary scalar field m_h. The ground state in the 1_0^{--} channel has either the mass of the heaviest gauge boson M_A or the mass of the Higgs m_h. For the next-level state it is the other way around. However, the inequality $m_{1_0^{--}} \leq m_{0_0^{++}}$ must hold. The ground state mass of the open $\mathrm{U}(1)$ states is for the scalar and the vector state $2\,m_\mathrm{A}$. The next energy level is predicted to be at $2\,m_\mathrm{A} + M_\mathrm{A}$. The phyiscal (gauge-invariant) as well as the gauge-variant spectrum for this theory is summarized in Table 5.2.

Table 5.2: This table is a special case of Table 3.1.
Left: Gauge-variant spectrum of an $\mathrm{SU}(3)$ gauge theory with a single scalar field in the fundamental representation. We set the direction n of the vev to $n_i = \delta_{i,3}$.
Right: Gauge-invariant (physical) spectrum of the theory. Here m_h denotes the mass of the elementary Higgs field, M_A is the mass of the heaviest elementary gauge boson and m_A the mass of the degenerated lighter massive gauge bosons. We assign a custodial $\mathrm{U}(1)$ charge of $1/3$ to the scalar field ϕ. The column 'next-level state' lists the masses of possible additional bound states or resonances, see the discussion in the main text and in Appendix B. Whether these states are indeed bound states or resonances or only nontrivial scattering states can not be decided here. Trivial scattering states are ignored.

	elementary spectrum			gauge-invariant spectrum				
J^P	Field	Mass	Deg.	$\mathrm{U}(1)$	Op.	Mass	Next-level state	Deg.
0^+	h	m_h	1	0	$O^{0_0^{++}}$	m_h	-	1
				± 1	$O^{0_{\pm 1}^{++}}$	$2\,m_\mathrm{A}$	$2\,m_\mathrm{A} + M_\mathrm{A}$	$1/\bar{1}$
1^-	$A_\mu^{1,2,3}$	0	3	0	$O_\mu^{1_0^{--}}$	M_A	-	1
	$A_\mu^{4,\ldots,7}$	m_A	4	± 1	$O_\mu^{1_{\pm 1}^{--}}$	$2\,m_\mathrm{A}$	$2\,m_\mathrm{A} + M_\mathrm{A}$	$1/\bar{1}$
	A_μ^8	M_A	1					

We focus again on the lattice parameter set $\beta = 6.85535$, $\kappa = 0.456074$, and $\lambda = 2.3416$ for our investigations.

5.3.2 Spectrum of gauge-variant quantities

In order to check the predictions above, masses extracted from the elementary field propagators need to be computed, i.e., the spectrum of the gauge-variant theory needs to be determined.

For this purpose we use for the 8^4 lattice 16000, for the 12^4 lattice 12000, for the 16^4 lattice 4700, and for the 20^4 lattice 5500 gauge-fixed configurations. We fix to the minimal 't Hooft Landau gauge as described in Section 4.4 to measure the propagators.

Let us now focus on the propagator of the gauge bosons $D^c(p^2) = \langle A^c_\mu(p)\, A^c_\mu(-p)\rangle$, $c = 1, 2, \ldots, 8$, defined in Equation (4.38). The lattice momenta $p_\mu = 2\pi k_\mu / L$ are along the links, and along all possible diagonals of the lattice, i.e., $(k, 0, 0, 0)$, $(k, k, 0, 0)$, $(k, k, k, 0)$, and (k, k, k, k), $k = 0, 1, \ldots, L/2$.

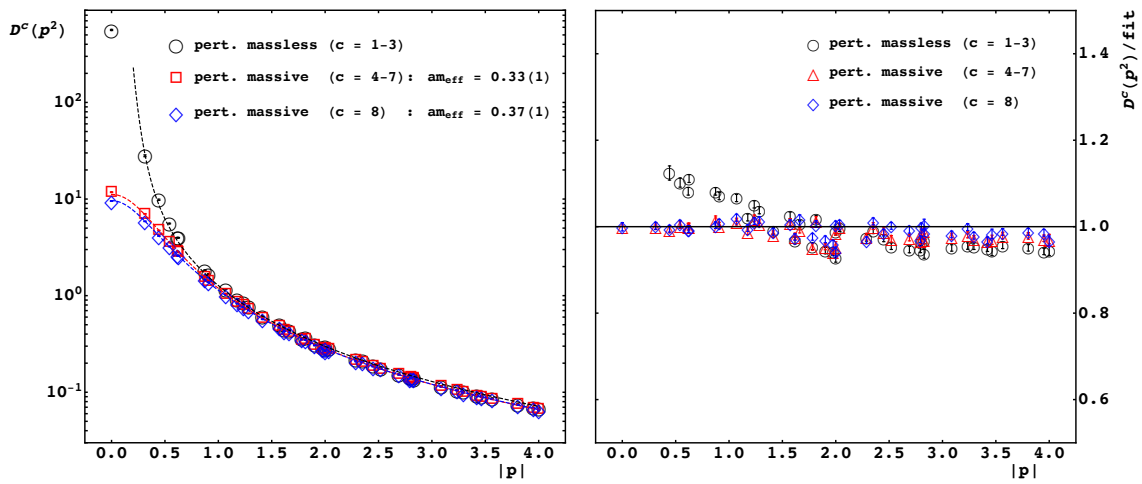

Figure 5.10: Plot of the gauge-boson propagators on a 20^4 lattice for the 3 perturbatively massless modes (black circles), the 4 degenerate perturbatively massive modes (red squares), and the heaviest mode (blue diamonds) as a function of the absolute value of the physical momentum $|p|$ on the left-hand side. The dashed lines are results of the fits described in the main text. On the right-hand side the data points are divided by the corresponding fitted values as a function of $|p|$ and thus shows the quality of the fit.

On the left-hand side of Figure 5.10. we show the propagators, evaluated on a 20^4 lattice, of the perturbatively 3 massless modes ($c = 1, 2, 3$, black circles), of the perturbatively 4 degenerate massive modes ($c = 4, 5, 6, 7$, red squares), and the perturbatively heaviest mode ($c = 8$, blue diamonds). Those are plotted as a function of the absolute value of the physical momentum $|p| \equiv \sqrt{\hat{p}_\mu\, \hat{p}_\mu}$, see Equation (4.36). The degenerate modes are averaged over to improve the statistics.

The dashed lines are fits according to

$$
\begin{aligned}
D^c(p^2) &= \frac{Z}{p^2}\left(\frac{A}{V p^4} + \frac{p^2}{\left(am^c\right)^2 + b^2\, p^2\, \left(1 + d^2 \ln \frac{p^2+\Lambda^2}{\Lambda^2}\right)^\gamma}\right)\,, \quad c = 1, 2, 3\,, \\
D^c(p^2) &= \frac{Z}{p^2 + \ln\left(p^2 + b^2\right)^d + \left(am^c\right)^2}\,, \quad c = 4, 5, \ldots, 8\,,
\end{aligned}
\tag{5.12}
$$

where Z are wave function renormalization constants and am^c is the effective mass in lattice units. The first term in the first line is a pure finite-volume effect. The logarithmic corrections of leading loop-corrections are taken into account for both cases. A list of the fit parameters can be found in Table E.3 in Appendix E. Also fits with the tree-level propagators have been performed but those fit functions did not resolve the UV-behavior well. Only for coarser lattices, i.e., larger $am_{1_0^{--}}$ masses,

the tree-level form is a good fit ansatz at least for the massive modes. Those larger masses dominate, such that the logarithmic corrections only play a minor role, see [65].

The effective masses extracted for the different sectors are listed in the legend of the figure for the 20^4 lattice. The fitted effective masses for the perturbatively massless modes are indeed very small and comparable to zero. This suggests a Coulomb-like behavior, although corrections deep in the infrared may still alter this.

On the right-hand side of Figure 5.10, the data points are divided by fitted values for every momentum $|p|$. The deviation from the value 1 gives access to the quality of the fit for each mode. For the massive modes the fit according to (5.12) shows only small deviations from the data for the whole momentum range, whereas larger deviations for the massless modes are visible for smaller momenta and are getting smaller for larger momenta.

The extracted masses from the fits for $c = 4, 5, 6, 7$ (red diamonds) and $c = 8$ (green triangles) are shown in Figure 5.11 as a function of the inverse lattice size L. The extrapolated infinite volume values are $m_{\mathrm{A}} = 0.32(1)$ for the 4 degenerate massive and $M_{\mathrm{A}} = 0.36(1)$ for the heaviest gauge boson, see the legend in the figure and Table E.4. The ratio of the lighter and heavier mass is $m_{\mathrm{A}}/M_{\mathrm{A}} = 0.89(5)$ which is in good agreement with the tree-level ratio of $\sqrt{3/4} \approx 0.87$, see (3.4). Together with the (almost) masslessness of the propagator in the unbroken sector this implies that the spectrum of the elementary fields coincides with the one expected from perturbation theory, especially of three massless and five massive states.

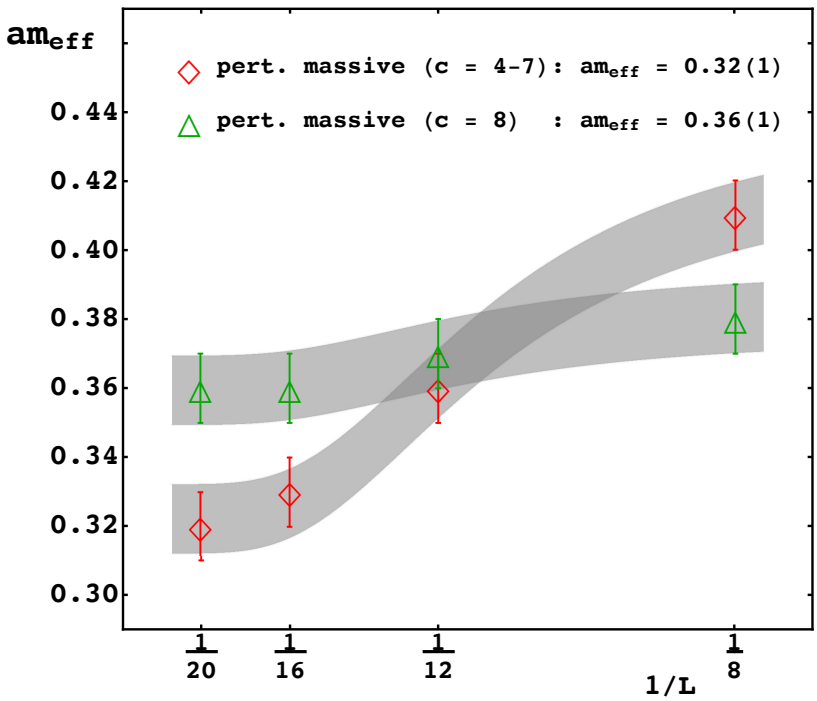

Figure 5.11: Masses of the 4 degenerate massive (red diamonds) and the heaviest (green triangles) gauge bosons as a function of the inverse lattice size L. The grey areas are the corresponding error bands obtained from a fit to $am + \alpha\, \mathrm{e}^{-\gamma V}$, see Table E.4.

We also computed the Schwinger functions $\Delta^c(t)$, $c = 1, 2, \ldots, 8$, as described in Subsection 4.5.4, along the lines of [89]. Again, Schwinger functions where degeneracies are expected, i.e.,

$c = 1, 2, 3$, and $c = 4, 5, 6, 7$, are averaged over. [4] The resulting effective masses obtained from $\ln \Delta^c(t)/\Delta^c(t+1)$ for different lattice volumes are given in Figure 5.12. The errors are computed from the propagators by the method of error propagation. The top left panel shows the effective mass as a function of Euclidean time for the heaviest mode, the top right panel the effective mass of the 4 degenerate massive modes, and the remaining panel shows a plot of the effective mass for the 3 degenerate massless modes. Due to the relatively large error bars for the massive modes for $t > 6$, we do not show those points here.

From the maximum values of the effective mass curves one can deduce the masses for each volume. The results are given in the legend of each plot. Of course, the errors are still too large and more statistics is needed to make a final statement. But the trend is clear and the obtained masses are in agreement within the large error bars with the ones obtained from the fits of the propagators with the functions defined in (5.12). Furthermore, the effective masses of the particles in the unbroken subsector ($c = 1, 2, 3$) tend to go to zero for $V \to \infty$.

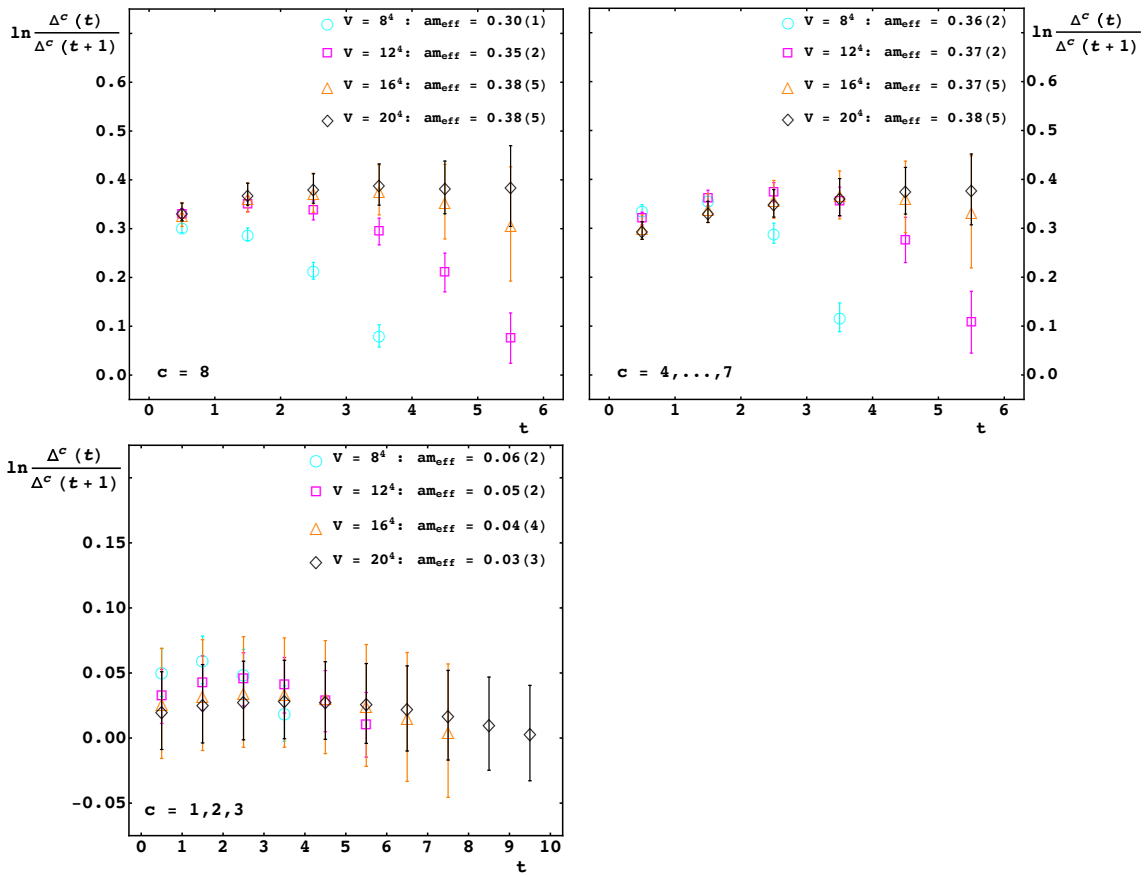

Figure 5.12: Effective masses from Schwinger functions for the heaviest mode (top left panel), the 4 degenerate modes (top right panel), and the 3 massless modes (bottom left panel), for 8^4, 12^4, 16^4, and 20^4 lattices. The masses in the legends in each panel are obtained by taking the maximum value of the functions for each volume.

In the scalar sector we computed the renormalized propagators of the real components of the scalar field $D_i^{\mathrm{r}}(p^2)$, $i = 1, 2, 3, 4, 6$, as described in Subsection 4.5.1 and 4.5.2. We choose the arbitrary di-

[4] These expected degenerate states overlap within error bars.

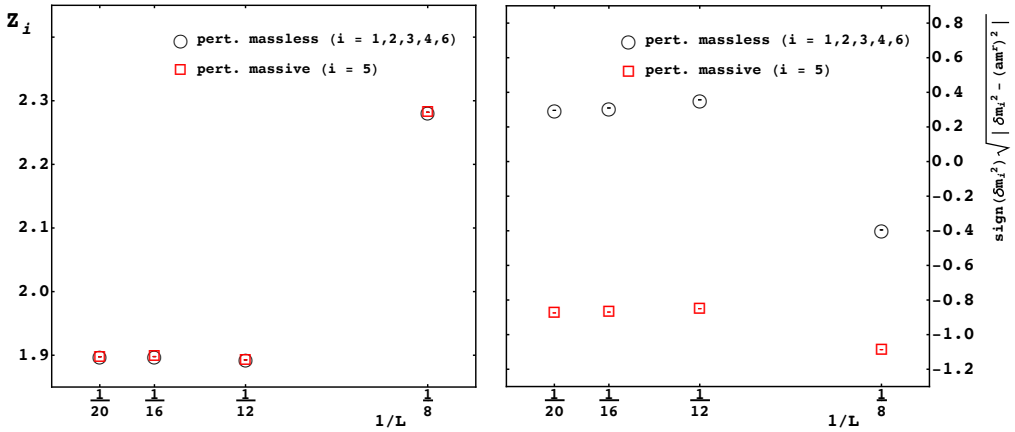

Figure 5.13: Wave function renormalization constant (left panel) and mass renormalization constant (right panel) for the perturbatively massless and the massive modes as a function of the inverse lattice size for $a\mu = 0.85$.

mensionless renormalization scale to be $a\mu = 0.85$ for each propagator. Under the assumption that the pole scheme works [60, 113] we set the renormalized masses m^{r} to $am^{\mathrm{r}} = am_{0_0^{++}}$ for the perturbatively massive propagator ($i = 5$) and to $am^{\mathrm{r}} = 0$ for the perturbatively massless propagators ($i = 1, 2, 3, 4, 6$). The degenerate massless renormalized propagators are averaged over to increase the statistics.

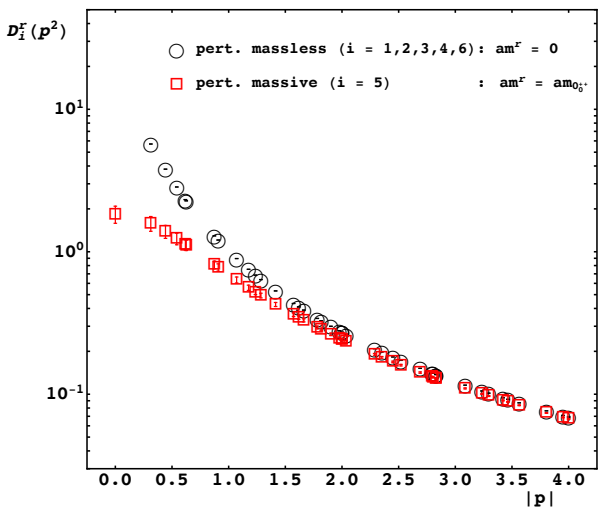

Figure 5.14: Perturbatively massless and massive scalar propagators for a 20^4 lattice and for $a\mu = 0.85$. The renormalized masses are $am^{\mathrm{r}} = 0$ for the (averaged) massless mode and $am^{\mathrm{r}} = am_{0_0^{++}}$ for the massive mode.

In Figure 5.13 the computed renormalization constants Z_i (left panel) and δm_i^2 (right panel), more precisely $\mathrm{sign}(\delta m_i^2)\left(|\delta m_i^2 - (am^{\mathrm{r}})^2|\right)^{1/2}$, $i = 1, 2, \ldots, 6$, are plotted as a function of the inverse lattice size. For both renormalization constants finite volume effects are clearly visible for the smallest volume. For larger volumes the values for the perturbatively massless (black circles) as well as for the massive (red squares) modes converge to constants relatively fast.

Having determined both renormalization constants, the renormalized propagator D_i^{r} can be computed. The result is shown in Figure 5.14, where again both, the perturbatively massless (black circles) and massive (red squares) modes are shown. Both propagators show the expected behaviors, namely the ones of a massless and a massive propagator.

In order to extract the effective masses, Schwinger functions need to be computed. Unfortunately, the statistics is too low at this point and thus the error bars too large to extract the effective mass from the Schwinger functions. Therefore, no results on this are presented here. However, in [59] [5] it is shown that the effective mass is of the order of the renormalized mass as long as the renormalized mass is large enough. Thus, by adjusting the renormalized mass one can control the effective mass to almost every value desired.

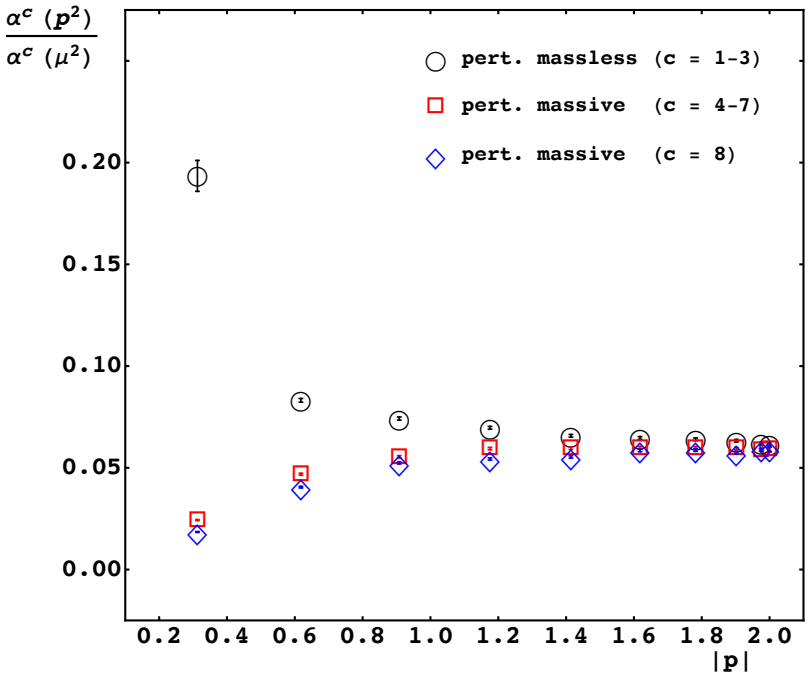

Figure 5.15: Renormalized running coupling for the three different sectors. The renormalization has been performed such that the couplings agree with the perturbative one for large momenta, see [59] for details. The lattice couplings are in this case $\beta = 10.05222$, $\kappa = 0.420352$, and $\lambda = 0.717362$.

Finally, we show the renormalized running coupling $\alpha^c(p^2)/\alpha^c(\mu^2)$ for the different sectors in Figure 5.15: The perturbatively massless sector (black circles), the sector with the 4 degenerate massive modes (red squares), and the sector with the heaviest mode (blue diamonds). The massless modes behave QCD-like as expected, since these modes live in the unbroken non-Abelian subsector. All the modes show perturbative behavior in the UV and vanish for large momenta, even though not visible due to the small lattices and thus small lattice momenta. The couplings stay relatively small throughout the whole momentum range, signaling that the tree-level expansion in the FMS mechanism applicable.

[5] An SU(2) gauge theory with a fundamental scalar was used there.

5.3.3 Comparison between the spectra

From the findings of the previous subsection and the predictions of the gauge-invariant physical spectrum, we are able to check the predictions of the FMS mechanism explicitly now.

In the 0_0^{++} channel we found one stable state with a mass of $am_{0_0^{++}} = 0.68(2)$ which is the one that we expect to find from the Schwinger function of the renormalized scalar propagator. However, more statistics is needed to accomplish this. The remaining states in this channel are high up in the spectrum and most likely scattering states.

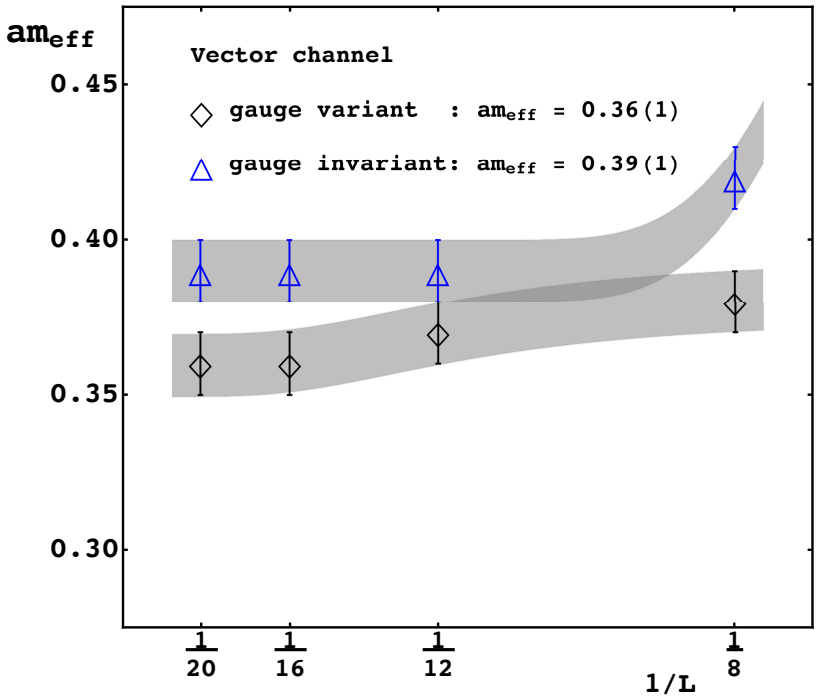

Figure 5.16: Effective masses of the singlet vector channel obtained from the gauge-variant propagator and from a variational analysis of gauge-invariant operators as a function of the inverse lattice size. The discrepancy of the infinite volume extrapolated values is discussed in the main text.

In the 1_0^{--} channel we extracted a ground state lattice mass of $am_{1_0^{--}} = 0.39(1)$. The mass extracted from the heaviest gauge boson is $aM_{\mathrm{A}} = 0.36(1)$. The volume dependence of these masses is shown in Figure 5.16. According to the FMS mechanism those masses should be equal but there is a slight discrepancy between them. There are several explanations for that: First, the FMS prediction, see Equation 3.9, relies on the smallness of the Higgs fluctuations and on the applicability of standard perturbation theory. Of course, nonperturbative effects could explain this deviation even though the running coupling is relatively small but probably still slightly large in this case, see Figure 5.15.

Another possibility is that this discrepancy of the masses could stem from finite volume and discretization effects. We observe that the larger the mass of the lightest state is[6], i.e., the larger the lattice spacing a is and thus the larger the physical volume is, the better is the agreement with the vector boson mass, see Figure 5.17 and [65].

[6] Which is the singlet vector state mass in our case.

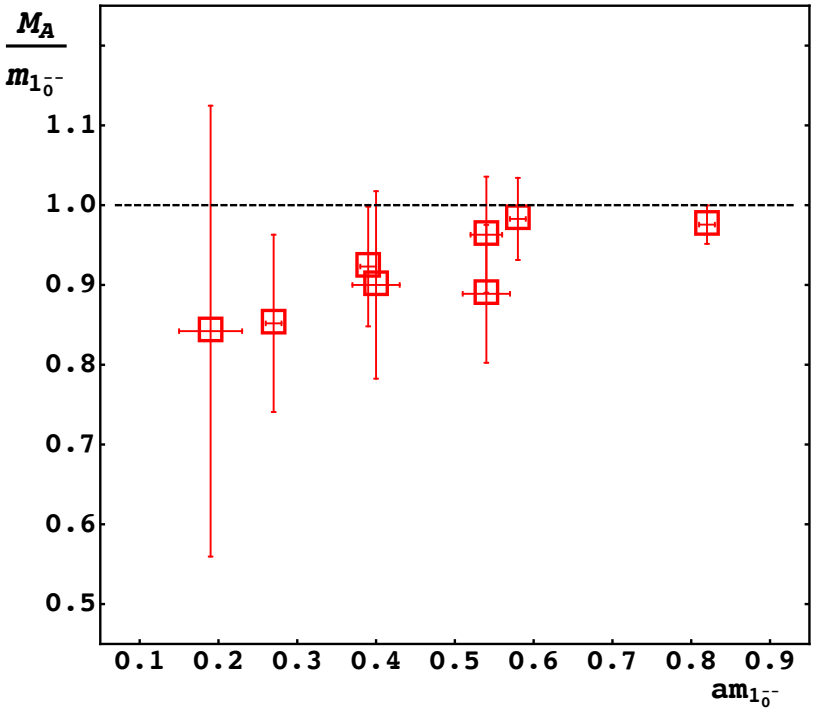

Figure 5.17: Ratio of the heaviest vector boson mass M_{A} and the ground state mass in the 1_0^{--} channel, $m_{1_0^{--}}$, as a function of the lattice mass $am_{1_0^{--}}$. The points are obtained from simulations at points in the phase diagram in the Higgs-like region, see Table E.1. The dashed line is the FMS prediction.

Lastly, also the infinite volume extrapolation we used, see Table E.4, does not take into account that the broken sector of the theory still interacts weakly with the unbroken sector, i.e., the sector of massless particles. The extrapolation we used does not take this into account and more sophisticated fitting procedures could change the results slightly.

The open $\mathrm{U}(1)$ quantum number channels, i.e., the $0_{\pm 1}^{++}$ and $1_{\pm 1}^{--}$ channels, still suffer from too low statistics. The extracted ground state of the vector state would be consistent with both, the ground state, $2\,am_{\mathrm{A}} = 0.64(2)$, and the predicted next-level state, $am_{\mathrm{A}} + aM_{\mathrm{A}} = 1.00(3)$ since $am_{1_{\pm 1}^{--}} \approx 0.8(2)$. The scalar state has a mass of $am_{0_{\pm 1}^{++}} \approx 2.0(1)$ and is relatively high up in the spectrum. Thus, we neither can confirm nor disprove the FMS prediction in these channels. Nevertheless, these masses are smaller than one would naively expect from a simple constituent model.

In Figure 5.17, we summarize our findings in the singlet vector channel for all the simulations we performed for points in the phase diagram where the system is in the Brout-Englert-Higgs phase, see Table E.1. In this plot the dimensionless ratio of the vector boson mass M_{A} to the singlet vector mass $m_{1_0^{--}}$ as a function of the lattice singlet vector mass $am_{1_0^{--}}$ is shown. The dashed line at $M_{\mathrm{A}}/m_{1_0^{--}} = 1$ reflects agreement with the FMS prediction in the vector channel. All in all, a good correspondence to the FMS prediction is found in particular for larger lattice spacings a, i.e., larger lattice masses of the singlet vector state, and thus larger physical volumes. For smaller masses finite volume effects are expected to play a role.

The confirmation of the FMS mechanism for this theory makes us confident to apply and eventually confirm this mechanism for theories with scalars in other representations, as discussed, e.g., in Section 3.2, using the same strategy as discussed here.

Chapter 6

Conclusions

In this thesis, we first studied an $\mathrm{SU}(N > 2)$ gauge theory with a scalar field in the fundamental representation of the gauge group in Section 3.1. This theory exhibits an additional global $\mathrm{U}(1)$ custodial symmetry. In a standard perturbative treatment the gauge group breaks 'spontaneously' to $\mathrm{SU}(N-1)$. While the number of massless as well as the number of massive gauge bosons increase with increasing N, the number of Higgs bosons remain the same. In fact only a single massive Higgs boson is predicted. This is the spectrum of gauge-variant, elementary and thus non-observable fields. Applying the FMS prescription to gauge-invariant bound states in distinct quantum number channels reveals that the observable, physical spectrum only consists of one massive $\mathrm{U}(1)$-singlet vector state with the mass of the perturbative heaviest gauge boson, one massive $\mathrm{U}(1)$-singlet scalar state with the mass of the perturbative Higgs, as well as two $\mathrm{U}(1)$-non-singlet scalar states and two $\mathrm{U}(1)$-non-singlet vector states with masses of $(N-1)$ times the mass of the perturbative lightest, non-massless gauge boson. On top of that a variety of next-level states is predicted which are resonances and/or additional bound states as well as trivial scattering states.

The case of an $\mathrm{SU}(N)$ gauge theory with an adjoint scalar field is due to its structure more involved than the case with a fundamental scalar as presented in Section 3.2. The reason is that there is no unique breaking pattern anymore. There exist $\lfloor N/2 \rfloor$ different breaking patterns which are given by $\mathrm{SU}(N) \to \mathrm{S}\big(\mathrm{U}(P) \times \mathrm{U}(N-P)\big)$ for $P < N$. Thus, the complexity of the spectrum of elementary fields for these kind of theories increases rapidly with increasing N.

We focused for most of the time on $\mathbb{Z}_2$-symmetric theories. Therefore, gauge-invariant operators can be classified in $\mathbb{Z}_2$ even and odd states. The predicted spectrum from gauge-invariant perturbation theory depends on the actual physical realization of the theory as discussed in Appendix A. However, we predicted always two massless vector states for $N > 2$. For $N = 2$, all $\mathbb{Z}_2$ even vector operators vanish identically, and thus only one massless vector state is predicted. We discussed the cases $N = 2, 3$, and 4 in detail. We elaborated different breaking patterns for $N = 3, 4$ and discussed the effects of a $\mathbb{Z}_2$ breaking term in the potential for the $\mathrm{SU}(3)$ case. The spectrum of scalar states depends on the breaking pattern and whether there is a $\mathbb{Z}_2$ symmetry or not.

Having explored the cases with only a single scalar field in the fundamental and adjoint representation of the gauge group, we studied structures with multiple scalar fields as well.

Based on the arguments of gauge-invariant perturbation theory the usual construction of $\mathrm{SU}(5)$ as an extension of the standard model would be ruled out already on structural grounds as a possible candidate for a grand-unified theory, see Section 3.3, even if it would not be ruled out for quantitative reasons [3, 127, 128]. Besides the actual particle spectrum, our investigations demonstrate that, for instance, the computation of a possible proton decay has to be rethought.

We also studied an $\mathrm{SU}(3)$ gauge theory with two different fundamental scalar fields in Section 3.4. The spectrum of the theory depends on the alignment of the two vacuum expectation values. The breaking pattern is $\mathrm{SU}(3) \to \mathrm{SU}(2) \to 1$ if they are non-parallel and $\mathrm{SU}(3) \to \mathrm{SU}(2)$ if they are parallel. We used the multiplet structure of the $\mathrm{SU}(2) \times \mathrm{U}(1)$ global custodial group for the construction of the gauge-invariant, physical states. We again found discrepancies between the spectrum of elementary fields and the spectrum of the bound states using the FMS mechanism for the two breaking patterns.

The predictions for the gauge-invariant physical states can be checked using non-perturbative methods. Of course, once the mechanism has been established, analytic predictions for other theories can be made with similar ease, and confidence, as in ordinary perturbation theory.

Checks of the FMS mechanism have been made for the $\mathrm{SU}(2)$-gauge-Higgs sector of the standard model [58, 59, 65]. Hints of a massless vector state as predicted by the mechanism for an adjoint scalar with gauge group $\mathrm{SU}(2)$ have been found in [98] in an exploratory lattice study for small lattice volumes.

In this work, we checked this mechanism for an $\mathrm{SU}(3)$ gauge theory with a fundamental scalar equipped with a custodial $\mathrm{U}(1)$ symmetry using lattice methods in Chapter 5. We first performed a scan of the phase diagram of this theory searching especially for regions with a Brout-Englert-Higgs effect.

The spectrum of gauge-invariant states has been computed using spectroscopic methods as outlined in Chapter 4. Especially, we analyzed the scalar and vector $U(1)$-singlet and $\mathrm{U}(1)$-non-singlet states, see Section 5.2. Those are the states for which we predicted ground state as well as next-level state masses using the FMS mechanism. We presented results for the effective masses of these states for a distinct lattice parameter set.

Then, we determined the gauge-variant spectrum by analyzing gauge-fixed configurations and extracting the poles from fits to the gauge-boson and the scalar propagators in Section 5.3. The propagators showed good agreement with the expectations from perturbation theory. Also, the gauge interaction remained weak in the broken as well as in the unbroken subsector over the whole momentum range we studied, signaling that gauge-invariant perturbation theory is applicable.

Our results support the predictions of the FMS mechanism, including non-trivial relations between the masses in different channels.

Of course larger volumes, larger parts of the parameter space, and higher statistics is needed to improve the support in the non-singlet channels and will also help to substantiate our findings in the singlet channels. Also multilevel algorithms [129–131] could help to reduce fluctuations of the correlation functions.

However, the qualitative features of the spectrum are already in agreement with the predictions, and this makes it somewhat unlikely that quantitative corrections will be able to alter the result substantially. We could show that standard perturbation theory fails to predict the correct spectrum and only the FMS mechanism in gauge-invariant perturbation theory fixes this and predicts the correct spectrum of states.

The findings from our simulations are important since the FMS mechanism has been applied and confirmed for a theory where a conflict between the spectrum of elementary fields and the spectrum of gauge-invariant, composite states arises. This will probably have impact for current and future candidates for beyond the standard model theories with a Brout-Englert-Higgs effect and could rule out some of them [63]. Especially, we could show that the standard constructions of GUTs do not work since the gauge-invariant spectrum of these theories do not provide the necessary low-energy spectrum of the standard model. The only possibility to overcome this problem, is to enhance the

global symmetry group of the theory, and thus adding more scalar fields, such that more gauge-invariant, observable states can be constructed. This procedure might yield the correct low-energy spectrum at least in the bosonic sector.

A next logical step, besides continuing checks on the lattice, would be to investigate current candidates for beyond the standard model physics, including also the fermionic sector along the lines of [56, 57, 62], to see whether conflicts arise for some of them as well. This does not need to be the case, as the explicit example of 2HDMs shows [64], but may happen as have been seen here. It would also be desirable to further develop the tools designed here to allow a quicker assessment of which theories may harbor conflicts, and which not.

Appendix A

The structure of the state space

When considering the adjoint case in Section 3.2 an additional complication arose.

This complication arose in the following way. In the fundamental case, every gauge orbit is either only zero field, or belongs to an orbit with symmetry group $\mathrm{SU}(N-1)$, as always a gauge transformation exists which rotates a given scalar field locally into a vector with only a single non-zero component. These two distinct classes are called strata, and the corresponding symmetry groups, $\mathrm{SU}(N)$ for zero scalar field and $\mathrm{SU}(N-1)$ otherwise, are the little groups [93]. Thus, in this case there is only a single special orbit, the vacuum, and all others behave in the same way.

When moving outside this case, the situation becomes more complex. In the following the $\mathrm{SU}(3)$ case with an adjoint scalar field will be used as an example, and the most general case has not yet been solved in a constructive way, to the knowledge of the author. Note, however, that the ranks of the little groups, and thus the size of the Cartans, play an important role in determining the number of different little groups [93].

In the general case, there are not only two strata and little groups, but more. For instance, for the $\mathrm{SU}(3)$ case with adjoint Higgs there are three: $\mathrm{SU}(3)$, $\mathrm{SU}(2)\times\mathrm{U}(1)$, and $\mathrm{U}(1)\times\mathrm{U}(1)$. Any value of the Higgs field can have only one of these little groups as invariance groups, and the set of all such orbits is again the corresponding stratum of the little group. Thus, there is no gauge transformation moving a value of the Higgs field from one stratum to another, and belonging to a stratum is a gauge-independent statement. Thus, corresponding gauge-invariant quantities to state this fact exists, these are merely the invariant polynomials of the group and the representation [93]. For instance, Equation (3.27) yields to which stratum a field locally belongs for the $\mathrm{SU}(3)$ case.

There is now a twist to this group-theoretical problem in a field theory. The distinction is local. The scalar field is a field, and its value changes from point to point. Especially, a scalar field can belong to any stratum at different space-time points. Thus, the distinction is not meaningful in a global way. Still, because a gauge transformation acts on the Higgs field locally, this feature is again locally gauge-invariant. Thus, the function (3.27) locally characterizes in the example the stratum of the scalar field.

Likewise, it is possible to characterize the space-time average of any scalar field configuration by the stratum to which it belongs. This will be independent under global gauge transformations.

The question is now how this affects the main part of the text.

First of all, this does not affect perturbation theory. Because perturbation theory is a small field expansion, perturbation theory will stay inside a given stratum, by definition, as the characterization in terms of invariants is discontinuous [93].

However, this is a problem when attempting to fix the gauge (3.16) beyond perturbation theory. If the vector Σ_0^a belongs to a given stratum, and the Higgs field at a point x belongs to a different

stratum, then the term $[\Sigma_0, \Sigma]$ vanishes at this point. [1] Thus, at this point the gauge condition degenerates to the covariant gauge condition. However, the gauge was chosen such that the gauge condition rotates the space-time average of the Higgs field into the direction of Σ_0, which is part of a fixed stratum. This is impossible, as noted above, if the average of a gauge orbit belongs to a different stratum. Thus, the gauge condition is not fulfilled on this gauge orbit. Instead, the orientation within the stratum is not affected, and thus ultimately still an average over the directions inside the stratum is performed, yielding again a zero expectation value for this gauge orbit. Hence, on such a gauge orbit the gauge condition (3.16) degenerates into the covariant gauge condition.

The path integral therefore decomposes into a sum of distinct parts. One contains the orbits for which the gauge condition in terms of the space-time average can be fulfilled, and the remainder contains the strata where this is not the case, and the vacuum expectation value vanishes. Consequently, the vacuum expectation value will still be the desired one, as the second part does not contribute, provided the measure of gauge orbits in the first part is not of size zero.

Unfortunately, this implies also that it is not possible to distinguish between strata using expectation values. Though, e.g., Equation (3.27) is gauge-invariant, its actual value is determined by weighting the value for every gauge orbit by the exponentiated action, and averaging over the orbits of the different strata. Its expectation value is therefore possibly continuous throughout the phase diagram of the theory.[2]

For the calculation of the spectrum using the FMS mechanism this has the following consequence. Given the arguments above, the vacuum expectation has still the same direction. However, fields belonging to a different stratum do not have a small fluctuation around this vacuum expectation value. Thus, for correlators holds, symbolically,

$$\begin{aligned}\left\langle O(x)\, O^\dagger(y)\right\rangle &= \int \mathcal{D}[A] \left(\int\limits_{\text{selected stratum}} \mathcal{D}[\phi]\, O(x)\, O^\dagger(y)\, \mathrm{e}^{\mathrm{i}\, S[\phi,A]} \right. \\ &\qquad \left. + \int\limits_{\text{other strata}} \mathcal{D}[\phi]\, O(x)\, O^\dagger(y)\, \mathrm{e}^{\mathrm{i}\, S[\phi,A]} \right) \\ &= \left\langle O(x)\, O^\dagger(y)\right\rangle_{\mathrm{e}} + \left\langle O(x)\, O^\dagger(y)\right\rangle_{\mathrm{n}} ,\end{aligned} \tag{A.1}$$

i.e., it decomposes into two correlators, of which one is meaningfully expendable (index e) around the vacuum expectation value, while the other is not (index n). The latter can, in principle, have any arbitrary pole structure, since no meaningful perturbative expansion is possible.

For the purpose of the main text there are two possible sets of assumptions for proceeding:

- There are no non-trivial (non-scattering) pole structures in the second correlator, and thus the pole structure of the first term, determined using the FMS expansion, completely describes the physics. This does not imply that if the physical spectrum differs for different choices of expansion strata this gives rise to a physical distinction. The different results are not changing the multiplicity, and the change can come about by gradual degeneracies.

[1] Note that the global $\mathbb{Z}_2$ symmetry, if not explicitly broken, is broken by the gauge condition, yielding a diagonal $\mathbb{Z}_2$ subgroup.

[2] This is not necessarily so. But there is always also the QCD-like phase, which technically belongs to the full group, as no direction is preferred. However, the corresponding stratum has measure zero, it is only the vacuum, and it can thus not arise by any other means than cancellation.

- The second correlator harbors the pole structures which would be obtained when fixing the gauge based on the other stratas. Then the physical spectrum would be obtained by the union of all spectra obtained by using the FMS mechanism around every possible vacuum expectation value.

At the current time we do not have arguments in favor of either possibility. It is quite possible that this is dynamically decided. Note, e.g., that if the global $\mathbb{Z}_2$ parity is explicitly broken, the absolute minimum always favors the maximal little group for $\mathrm{SU}(3)$ [93]. Thus, it is entirely possible that if the potential spontaneously breaks this global symmetry the first case may be appropriate, and then only one of the strata contributes to the spectrum, and otherwise the second. This will require a full non-perturbative investigation of the spectrum and the phase diagram to understand better. In the main text we therefore discuss all possible spectra.

Appendix B

Analysis of open U(1) states

In this appendix, we sketch the computation of the bound state spectrum regarding operators with open $\mathrm{U}(1)$ quantum numbers for a Higgs field in the fundamental representation. We again choose the convenient gauge in which $n_i = \delta_{i,N}$. In order to keep the computation transparent, we introduce the following abbreviations for the gauge fields,

$$A_\mu = A_\mu^a \, T^a \equiv \begin{pmatrix} \tilde{\mathbf{A}}_\mu^{\mathbf{0}} & X_\mu^+ \\ X_\mu^- & Z'_\mu \end{pmatrix} \, . \tag{B.1}$$

The matrix $\tilde{\mathbf{A}}_\mu^{\mathbf{0}}$ is the $(N-1) \times (N-1)$ submatrix containing the $\big((N-1)^2 - 1\big)$ massless gauge fields, $\tilde{\mathbf{A}}_\mu^{\mathbf{0}} = A_\mu^a \, \tilde{T}^a$ with $\tilde{T}$ the generators of the $\mathrm{SU}(N-1)$ subgroup. The abbreviation X_μ^+ contains the gauge fields in the Nth column of A_μ except for the Nth element, thus forming an $(N-1)$ component complex column vector

$$X_\mu^+ \equiv \begin{pmatrix} X_{\mu,1}^+ \\ \vdots \\ X_{\mu,N-1}^+ \end{pmatrix} = \frac{1}{2} \begin{pmatrix} A_\mu^{(N-1)^2} - \mathrm{i} \, A_\mu^{(N-1)^2+1} \\ \vdots \\ A_\mu^{N^2-3} - \mathrm{i} \, A_\mu^{N^2-2} \end{pmatrix} \, , \tag{B.2}$$

and $X_\mu^- = \big(X_\mu^+\big)^\dagger$. The fields X_μ^+ and X_μ^- encode the $2(N-1)$ degenerated massive gauge bosons with mass m_{A}. Finally, Z'_μ is a short cut for the $N \times N$ element of A_μ given by $Z'_\mu = -\frac{1}{2} \sqrt{2/N} \, A_\mu^{N^2-1}$ and encodes the heaviest gauge boson with mass M_{A}.

With this reformulation of the gauge boson matrix, it is straightforward to analyze the spectrum of the operators in the open $\mathrm{U}(1)$ channel. Starting with the vector operator (3.11), we obtain in leading order in the FMS expansion,

$$O_{1_1^-}^\mu = \mathrm{i}g \left(\frac{v}{\sqrt{2}}\right)^N \epsilon_{i_1 \ldots i_N} \, n_{i_1} \, \big(A_{\nu_1} \, n\big)_{i_2} \, \big(F^{\nu_1}{}_{\nu_2} \, n\big)_{i_3} \, \ldots \, \big(F^{\nu_{N-2}\mu} \, n\big)_{i_N} + \mathcal{O}(\varphi) \, . \tag{B.3}$$

In order to obtain the elementary field content of the gauge invariant operator, we have to compute the components of the $\mathrm{SU}(N)$-vectors $A^\mu \, n$ and $F^{\mu\nu} \, n$. They read,

$$A^\mu \, n = \begin{pmatrix} X_\mu^+ \\ Z'_\mu \end{pmatrix} \, , \tag{B.4}$$

and

$$F_{\mu\nu}\, n = \begin{pmatrix} \partial_\mu\, X^+_\nu - \partial_\nu\, X^+_\mu \\ \partial_\mu\, Z'_\nu - \partial_\nu\, Z'_\mu \end{pmatrix} + 2\,\mathrm{i}\, g \begin{pmatrix} \tilde{\mathbf{A}}^{\mathbf{0}}_{[\mu}\, X^+_{\nu]} + X^+{}_{[\mu}\, Z'_{\nu]} \\ X^-_{[\mu}\, X^+_{\nu]} \end{pmatrix} . \tag{B.5}$$

The right-hand side of Equation (B.3) is nonvanishing, only if the $(N-1)$-tuple $(i_2, i_3, \ldots, i_N)$ is given by $(1, 2, \cdots, N-1)$ or a permutation of these numbers due to the antisymmetry of the epsilon tensor and $n_{i_1} = \delta_{i_1,N}$. Neglecting for a moment the contribution from the commutator of $F_{\mu\nu}$, $O^\mu_{1^-_1}$ contains schematically the product $X^+_1\, X^+_2\, \ldots\, X^+_{N-1}$ of the $(N-1)$ different fields stored in X^+ at leading order in the FMS expansion.

Computing the propagator and employing the simple constituent model, we predict at tree level that the mass of the operator (3.11) is given as the sum of the masses of the $(N-1)$ elementary massive gauge fields, $m_{1^-_1} = (N-1)m_{\mathrm{A}}$.

Moreover, the investigated operator contains an excitation at mass $m^\star_{1^-_1} = (N-1)m_{\mathrm{A}} + M_{\mathrm{A}}$. This can be seen from the last term in Equation (B.5) coming from the commutator of the two gauge fields in $F_{\mu\nu}$. From this additional term, we can read of that the correlator of the gauge-invariant bound state operator also contains at next-to-leading order in the gauge fields the propagation of the different $(N-1)$ fields X^+_μ and an elementary gauge boson which is either one of the massless gauge fields stored in $\tilde{\mathbf{A}}^{\mathbf{0}}_\mu$ or the heaviest gauge boson described by Z'. For $M_{\mathrm{A}} < m_{\mathrm{h}}$, the latter predicts the first next-level state of $O^\mu_{1^-_1}$. In case $M_{\mathrm{A}} > m_{\mathrm{h}}$, this state will be either a trivial scattering state of the ground state with the bound state of the scalar singlet or a resonance which can decay to the ground state and the bound state of the scalar singlet, $(1^-_1)^\star \to 1^-_1 + 0^+_0$.

As the operator $O^\mu_{1^-_1}$ is build from $F^{\mu\nu}\, n$ precisely $(N-2)$ times, we get similarly excited states with mass $(N-1)m_{\mathrm{A}} + 2M_{\mathrm{A}}, \ldots, (N-1)m_{\mathrm{A}} + (N-2)M_{\mathrm{A}}$ as we have schematically $X^+ \left(X^+ + \tilde{\mathbf{A}}^{\mathbf{0}}\, X^+ + X^+\, Z'\right)^{N-2}$. These are trivial scattering states (or might be resonances) of the ground state (or its first excitation) and the vector or scalar singlets regarding the $\mathrm{U}(1)$ independent of the relation between m_{h} and M_{A}. For instance the state with mass $(N-1)m_{\mathrm{A}} + 2M_{\mathrm{A}}$ can be viewed as a scattering state of the ground state of $O^\mu_{1^-_1}$ and two ground states of $O^\mu_{1^-_0}$.

In addition, the next-to-leading order contribution in the FMS expansion $\sim \varphi$ contributes also to the spectrum with mass $(N-1)m_{\mathrm{A}} + m_{\mathrm{h}}$ but is likely to be always a trivial scattering state of the ground state of $O^\mu_{1^-_1}$ and $O^\mu_{0^+_0}$ within our first order approximation.

In full analogy, the ground state spectrum as well as the higher excitations of the scalar operator with open $\mathrm{U}(1)$ quantum number $O_{0^+_1}$, see Equation (3.12), can be derived. The ground state has mass $(N-1)m_{\mathrm{A}}$ and possible additional particles might be encoded in the next-level state with mass $(N-1)m_{\mathrm{A}} + M_{\mathrm{A}}$ for $M_{\mathrm{A}} < m_{\mathrm{h}}$.

Appendix C

Global gauge transformation for the space-time averaged scalar field

In this appendix, we give the explicit form of the transformation matrix responsible for rotating the space-time averaged scalar field $\bar{\phi}$ into the third real direction for an $\mathrm{SU}(3)$ gauge theory with the scalar transforming in the fundamental representation of the gauge group.

We start with Equation (4.33) and express the total transformation g as a sequence of two consecutive $\mathrm{SU}(3)$ rotations, i.e.,

$$g\,\bar{\phi} = g_2\,g_1\,\bar{\phi} = n\ , \quad g_1, g_2 \in \mathrm{SU}(3)\ , \tag{C.1}$$

where $n = (0,0,1)$ and without loss of generality we assume a normalized vector $|\,\bar{\phi}\,| = 1$. The first transformation g_1 has the task to rotate the first component of $\bar{\phi}$ to zero:

$$g_1\,\bar{\phi} = \begin{pmatrix} g_1^{11} & g_1^{12} & 0 \\ -\left(g_1^{12}\right)^\star & \left(g_1^{11}\right)^\star & 0 \\ 0 & 0 & 1 \end{pmatrix} \begin{pmatrix} \bar{\phi}_1 \\ \bar{\phi}_2 \\ \bar{\phi}_3 \end{pmatrix} = \begin{pmatrix} 0 \\ \bar{\phi}_2' \\ \bar{\phi}_3' \end{pmatrix} = \bar{\phi}'\ \ ,\ \left|\,g_1^{11}\,\right|^2 + \left|\,g_1^{12}\,\right|^2 = 1\ . \tag{C.2}$$

The second transformation g_2 then rotates the second component of $\bar{\phi}'$ to zero:

$$g_2\,\bar{\phi}' = \begin{pmatrix} 1 & 0 & 0 \\ 0 & g_2^{11} & g_2^{12} \\ 0 & -\left(g_2^{12}\right)^\star & \left(g_2^{11}\right)^\star \end{pmatrix} \begin{pmatrix} 0 \\ \bar{\phi}_2' \\ \bar{\phi}_3' \end{pmatrix} = \begin{pmatrix} 0 \\ 0 \\ \bar{\phi}_3'' \end{pmatrix} = \bar{\phi}''\ \ ,\ \left|\,g_2^{11}\,\right|^2 + \left|\,g_2^{12}\,\right|^2 = 1\ . \tag{C.3}$$

Solving these equations for the matrix elements g_i^{nm} with the normalization constraint gives the desired transformation matrix g. To summarize, the following steps have to be performed:

1. Normalize $\bar{\phi}$, $\left|\,\bar{\phi}\,\right| = 1$.

2. Compute

$$g_1^{11} = \left(1 + \frac{\left|\,\bar{\phi}_1\,\right|^2}{\left|\,\bar{\phi}_2\,\right|^2}\right)^{-\frac{1}{2}} \quad , \quad g_1^{12} = -\frac{\bar{\phi}_1\,\bar{\phi}_2^\star}{\left|\,\bar{\phi}_2\,\right|^2}\ . \tag{C.4}$$

3. Compute

$$\begin{aligned} \mathrm{Re}\, g_2^{11} &= \frac{1}{1+\frac{\left|\bar{\phi}_2\right|^2}{\left|\bar{\phi}_3\right|^2}} \left[\mathrm{Re}\left[\bar{\phi}_3\right] \left(1 + \frac{\mathrm{Im}\left[\bar{\phi}_3\right]^2}{\mathrm{Re}\left[\bar{\phi}_3\right]^2} \right) \right]^{-1} \quad , \quad \mathrm{Im}\, g_2^{11} = \frac{\mathrm{Im}\,\bar{\phi}_3}{\mathrm{Re}\,\bar{\phi}_3}\, \mathrm{Re}\, g_2^{11} \ , \\ g_2^{12} &= -\frac{\bar{\phi}_3^\star}{\left|\,\bar{\phi}_3\,\right|^2} \frac{\left(g_1^{11}\right)^\star}{\left|\,g_1^{11}\,\right|^2}\, \bar{\phi}_2\, g_2^{11} \ . \end{aligned} \tag{C.5}$$

4. Construct $g = g_2\, g_1$ from the previous steps.

5. Apply the global gauge transformations to the scalar and gauge fields:

$$\phi(x) \to g\, \phi(x) \quad , \quad U_\mu(x) \to g\, U_\mu(x)\, g^\dagger \quad , \quad \forall\, x, \mu \ . \tag{C.6}$$

Appendix D

Lattice versions of the open $\mathrm{U}(1)$ operators

Here we show the explicit lattice versions of the operators with an open $\mathrm{U}(1)$ quantum number mentioned in Section 5.2.1 for an $\mathrm{SU}(3)$ gauge theory with a fundamental scalar.

- Scalar operator

$$
\begin{aligned}
O^{0_1^{++}}(t) &= \frac{1}{L^3} \sum_{\boldsymbol{x}} \sum_{\mu,\nu=1}^{3} \epsilon_{ijk} \left[\phi_i \, (D_\mu \, \phi)_j \, (D_\mu \, D_\nu \, D_\nu \, \phi)_k \right] (\boldsymbol{x}, t) \\
&= \frac{1}{16 \, L^3} \sum_{\boldsymbol{x}} \sum_{\mu,\nu=1}^{3} \epsilon_{ijk} \, \phi_i(\boldsymbol{x}, t) \\
&\quad \times \Big(U_\mu(\boldsymbol{x}, t) \, \phi(\boldsymbol{x} + \hat{\mu}, t) - U_\mu(\boldsymbol{x} - \hat{\mu}, t)^\dagger \, \phi(\boldsymbol{x} - \hat{\mu}, t) \Big)_j \\
&\quad \times \Big(U_\mu(\boldsymbol{x}, t) \, U_\nu(\boldsymbol{x} + \hat{\mu}, t) \, U_\nu(\boldsymbol{x} + \hat{\mu} + \hat{\nu}, t) \, \phi(\boldsymbol{x} + \hat{\mu} + 2\hat{\nu}, t) \\
&\quad - \quad U_\mu(\boldsymbol{x} - \hat{\mu}, t)^\dagger \, U_\nu(\boldsymbol{x} - \hat{\mu}, t) \, U_\nu(\boldsymbol{x} - \hat{\mu} + \hat{\nu}, t) \, \phi(\boldsymbol{x} - \hat{\mu} + 2\hat{\nu}, t) \\
&\quad + \quad U_\mu(\boldsymbol{x}, t) \, U_\nu(\boldsymbol{x} + \hat{\mu} - \hat{\nu}, t)^\dagger \, U_\nu(\boldsymbol{x} + \hat{\mu} - 2\hat{\nu}, t)^\dagger \, \phi(\boldsymbol{x} + \hat{\mu} - 2\hat{\nu}, t) \\
&\quad - \quad U_\mu(\boldsymbol{x} - \hat{\mu}, t)^\dagger \, U_\nu(\boldsymbol{x} - \hat{\mu} - \hat{\nu}, t)^\dagger \, U_\nu(\boldsymbol{x} - \hat{\mu} - 2\hat{\nu}, t)^\dagger \, \phi(\boldsymbol{x} - \hat{\mu} - 2\hat{\nu}, t) \Big)_k
\end{aligned}
\tag{D.1}
$$

- Vector operator: $\mu = 1, 2, 3$

$$
\begin{aligned}
O_{\mu}^{1_1^{--}}(t) &= \frac{1}{L^3} \sum_{\boldsymbol{x}} \sum_{\nu=1}^{3} \epsilon_{ijk} \Big[\phi_i \, (D_\mu \, \phi)_j \, (D_\nu \, D_\nu \, \phi)_k \Big] (\boldsymbol{x}, t) \\
&= \frac{1}{8 \, L^3} \sum_{\boldsymbol{x}} \sum_{\nu=1}^{3} \epsilon_{ijk} \, \phi_i(\boldsymbol{x}, t) \\
&\quad \times \Big(U_\mu(\boldsymbol{x}, t) \, \phi(\boldsymbol{x} + \hat{\mu}, t) - U_\mu(\boldsymbol{x} - \hat{\mu}, t)^\dagger \, \phi(\boldsymbol{x} - \hat{\mu}, t) \Big)_j \\
&\quad \times \Big(U_\nu(\boldsymbol{x}, t) \, U_\nu(\boldsymbol{x} + \hat{\nu}, t) \, \phi(\boldsymbol{x} + 2\hat{\nu}, t) \\
&\quad + \quad U_\nu(\boldsymbol{x} - \hat{\nu}, t)^\dagger \, U_\nu(\boldsymbol{x} - 2\hat{\nu}, t)^\dagger \, \phi(\boldsymbol{x} - 2\hat{\nu}, t) \Big)_k
\end{aligned}
\tag{D.2}
$$

Appendix E

Data and fit tables

In this appendix, we collect all the parameter sets of the phase diagram points were we performed simulations for different lattice sizes in order to obtain data for spectroscopy and for propagators of gauge-variant fields. Additionally, we list the fit parameters which we obtained and which are used in the figures shown in Section 5.2 and 5.3 .

E.1 Numerical values

Here, we provide the numerical values for the ground state energy levels in the vector singlet channel in lattice units $am_{1_0^{--}}$, the mass of the heaviest vector state aM_{A} also in lattice units, and the average plaquette defined for gauge group $\mathrm{SU}(3)$ as

$$U_{\mathrm{P}} = \frac{1}{18\,V} \sum_{x} \sum_{\mu<\nu} \mathrm{Re}\,\mathrm{tr}\big[U_{\mu\nu}(x)\big] \ , \tag{E.1}$$

where $U_{\mu\nu}(x)$ is defined in Equation (4.3), for several values of the lattice couplings β, κ and λ. Only such values are examined for which a BEH-effect was found.

Table E.1: Numerical values of the ground state energy level in the 1_0^{--} channel, the mass of the gauge-variant vector state aM_{A}, and the plaquette expectation value for various values of β, κ, and λ in the Higgs-like region of the phase diagram.

β	κ	λ	$am_{1_0^{--}}$	aM_{A}	$\langle U_{\mathrm{P}} \rangle$
5.798500	0.419035	1.259900	0.54(3)	0.48(2)	0.5832(1)
6.855350	0.456074	2.341600	0.39(1)	0.36(1)	0.6674(1)
7.912200	0.493113	3.423300	0.39(1)	0.36(1)	0.7204(1)
8.172900	0.490558	6.483650	0.27(1)	0.23(2)	0.7291(1)
8.433600	0.488003	9.544000	0.19(4)	0.16(2)	0.7382(1)
9.590550	0.444462	0.411800	0.82(1)	0.80(1)	0.7844(1)
9.607400	0.174193	0.030100	0.54(2)	0.52(2)	0.7786(1)
10.05222	0.420352	0.717362	0.58(1)	0.57(1)	0.7896(1)

We do not list higher energy levels in this channel as well as the lattice masses in the scalar singlet channel, since only for the main simulation point defined in Subsection 5.2.2 enough statistics was gained. There, the mass $am_{0_0^{++}}$ was below the elastic threshold and also the higher levels were not to noisy to draw conclusions. Also, points have not been included where no BEH-effect was found and/or where the singlet vector mass was above 1 in lattice units.

The errors listed in Table E.1 are obtained by fitting the lower and upper bounds of the eigenvalues for the gauge-invariant case and of the propagators in the gauge-variant case. Subsequently, the method of error propagation is used. Systematic errors are not included.

E.2 Tables of fit parameters

In this section we show the fit parameters used in the figures shown in Section 5.2 and 5.3 for the parameter values $\beta = 6.855350$, $\kappa = 0.456074$, and $\lambda = 2.341600$. All the errors are obtained as described previously. We use fit routines provided by `Mathematica` [132] throughout.

Table E.2: Fit parameters from a double-cosh fit of the eigenvalues, $\lambda(t) = A\cosh\left(am_{\text{eff}}^{(1)}(t-L/2)\right) + B\cosh\left(am_{\text{eff}}^{(2)}(t-L/2)\right)$, obtained from a variational analysis for several lattice volumes $V = L^4$ in the scalar and vector channels. The dash indicates that only a single-cosh fit has been used.

J_{U1}^{PC}	V	Level	Fit-range $[t_{\text{min}}, t_{\text{max}}]$	$am_{\text{eff}}^{(1)}$	$am_{\text{eff}}^{(2)}$	A	B
0_0^{++}	8^4	1st	$[1,4]$	0.55(1)	1.44(1)	0.1156(3)	0.0031(1)
	12^4	1st	$[1,6]$	0.65(1)	1.55(1)	0.0180(4)	0.0009(1)
	16^4	1st	$[1,6]$	0.70(1)	1.45(3)	0.0044(1)	0.000007(2)
	20^4	1st	$[2,7]$	0.67(3)	1.08(5)	0.0010(1)	0.00003(2)
	8^4	2nd	$[1,4]$	0.95(4)	1.4(2)	0.0282(2)	0.002(1)
	12^4	2nd	$[1,6]$	0.80(1)	1.4(2)	0.0045(5)	0.00030(15)
	20^4	2nd	$[2,6]$	0.90(10)	1.3(1)	0.00013(6)	0.000003(2)
1_0^{--}	8^4	1st	$[2,4]$	0.42(1)	–	0.337(1)	–
	12^4	1st	$[2,6]$	0.39(1)	1.50(4)	0.159(1)	0.0003(1)
	16^4	1st	$[2,8]$	0.39(1)	1.5(2)	0.072(1)	0.000003(2)
	20^4	1st	$[2,9]$	0.39(1)	1.4(1)	0.033(1)	0.0000005(5)
	8^4	2nd	$[2,4]$	0.99(1)	–	0.026(1)	–
	12^4	2nd	$[2,4]$	1.02(2)	1.7(2)	0.018(1)	0.00026(1)
	16^4	2nd	$[2,6]$	1.01(1)	1.9(2)	0.0010(1)	0.0000003(2)
	20^4	2nd	$[2,6]$	1.03(2)	1.4(1)	0.0003(1)	0.000002(1)
$0_{\pm1}^{++}$	20^4	1st	$[1,3]$	2.0(1)	–	$2.3(1)\cdot10^{-9}$	–
$1_{\pm1}^{--}$	8^4	1st	$[2,6]$	0.87(1)	1.65(1)	0.0236(1)	0.0017(1)
	12^4	1st	$[2,6]$	0.75(5)	1.35(5)	0.0025(1)	0.0005(2)
	16^4	1st	$[2,6]$	0.67(1)	1.27(2)	0.0007(1)	0.00006(1)
	20^4	1st	$[2,6]$	0.95(5)	1.60(5)	0.00006(6)	0.00000002(1)

Table E.3: Fit parameters from a fit of the perturbatively massless and massive propagators for several lattice volumes V. The fit functions are:

- $D^c(p^2) = \frac{Z}{p^2}\left(\frac{A}{Vp^4} + \frac{p^2}{\left(am^c\right)^2 + b^2\, p^2\, \left(1+d^2 \ln[1+p^2/\Lambda^2]\right)^\gamma}\right)\,,\ c = 1,2,3\,,$
- $D^c(p^2) = Z\left(p^2 + \ln\left(p^2+b^2\right)^d + \left(am^c\right)^2\right)^{-1}\,,\ c = 4,5,6,7,8\,.$

Perturbatively massless ($c = 1,2,3$)

V	Z	A/V	b	d^2	Λ^2	γ	am^c
8^4	1	0.445(2)	0.8	0.4	0.18	0.25	0.26(2)
12^4	1	0.120(4)	0.8	0.4	0.18	0.25	$\sim 10^{-10}$
16^4	1	0.030(3)	0.8	0.4	0.18	0.25	$\sim 10^{-10}$
20^4	1	0.013(1)	0.8	0.4	0.18	0.25	$\sim 10^{-10}$

Perturbatively massive ($c = 4,5,6,7$)

V	Z	b	c	γ	am^c
8^4	1.33(1)	1.044(1)	1	0.249(1)	0.41(1)
12^4	1.28(1)	1.013(4)	1	0.199(1)	0.36(1)
16^4	1.27(1)	1.027(3)	1	0.166(1)	0.34(1)
20^4	1.26(1)	0.997(1)	1	0.249(1)	0.33(1)

Perturbatively massive ($c = 8$)

V	Z	b	c	γ	am^c
8^4	1.33(1)	1.419(4)	1	0.244(2)	0.38(1)
12^4	1.34(1)	1.449(3)	1	0.249(1)	0.37(1)
16^4	1.29(4)	1.134(8)	1	0.152(1)	0.36(1)
20^4	1.25(1)	1.040(4)	1	0.135(1)	0.36(1)

Table E.4: Infinite volume extrapolations of the gauge-invariant singlet scalar ($am_{0_0^{++}}$) and vector ($am_{1_0^{--}}$) lattice masses, as well as the extrapolation of the gauge-variant lattice masses of the gauge-boson propagator $D^c(p^2)$. In all those cases the fit function is $am_{\text{eff}}(V) = am + \alpha\, \mathrm{e}^{-\gamma\, V}$.

State	am	δ	γ
0_0^{++}	0.68(2)	−0.140(5)	0.00007(5)
1_0^{--}	0.39(1)	0.8701(1)	0.000822(1)
$c = 4,\ldots,7$	0.33(1)	0.106(1)	0.000048(1)
$c = 8$	0.36(1)	0.248(1)	0.000043(1)

Appendix F

Determining critical exponents and Wilson coefficients for clock models

This appendix is dedicated to a project I worked on during a stay abroad at the Friedrich-Schiller-University Jena.[1] The project is summarized here.

F.1 Introduction

The conformal bootstrap method [133, 134] is very successful [135–137] in determining critical exponents as well as Wilson coefficients of conformal theories to high accuracy. [2] The drawback of this method is, that in order to determine those quantities to high precision, rather accurate input values are needed. This is due to the fact that the parameter space to bound conformal bootstrap data is so big, and thus makes this method computationally demanding.

The aim of this project is to produce input values for the conformal bootstrap program, i.e., critical exponents and Wilson coefficients, with Monte Carlo methods, as outlined in, e.g., [140–143], for so-called clock models.

F.2 The q-states clock-model

The Hamiltonian for a spin system in 3-dimensional space with a nearest neighbor interaction J and an external magnetic field $\vec{\mu}$ is given by, see, e.g., [144],

$$H[\vec{S}] = -\sum_x \left(J \sum_{\nu=1}^{3} \vec{S}_x \cdot \vec{S}_{x+\hat{\nu}} + \vec{\mu} \cdot \vec{S}_x \right) , \tag{F.1}$$

where the first sum runs over the sites x of a 3-dimensional lattice, the second sum is over the 3 directions $\nu = 1, 2, 3$, and $\hat{\nu}$ denotes the unit vector in ν-direction. Here, the dynamical degrees of freedom are real-valued, 2-dimensional spins $\vec{S}_x$, with $|\vec{S}_x| = 1$, located at the sites of the lattice. They can be parameterized by $\vec{S}_x = (\cos\theta_x, \sin\theta_x)$. Therefore, it is convenient to express the

[1] Besides that, also most of the results presented in Chapter 3 have been obtained during this stay.

[2] For an introduction to conformal field theory and the conformal bootstrap method see [138, 139].

Hamiltonian (F.1) in terms of the angles θ_x, i.e.,

$$H[\theta] = -\sum_x \left(J \sum_{\nu=1}^{3} \cos\left(\theta_x - \theta_{x+\hat{\nu}}\right) + \mu \cos\theta_x \right) , \tag{F.2}$$

where we chose $\vec{\mu} = (\mu, 0)$, without loss of generality.

In case of the q-states clock-model the angles θ_x are discrete, i.e., $\theta_x = \frac{2\pi}{q} n_x, n_x = 0, 1, \ldots, q-1$. The Hamiltonian (F.2) is then only for $\mu = 0$ invariant under the change $\theta_x \to \theta_x + \frac{2\pi}{q} k$, $k = 0, 1, \ldots, q-1$, and therefore exhibits a $\mathbb{Z}_q$ symmetry. If one considers the xy-model, the spins $\vec{S}_x$ are continuous and thus $\theta_x \in [0, 2\pi)$. Therefore, the Hamiltonian (F.2) would be $O(2)$-symmetric, again for vanishing external magnetic field only. However, a non-vanishing external field $\mu \neq 0$ breaks the $\mathbb{Z}_q$ symmetry of the clock-model as well as the $O(2)$ symmetry of the xy-model and no phase transition can occur.

The partition sum of the spin systems discussed above is given by

$$Z = \sum_{\{\theta\}} \mathrm{e}^{-\beta H[\theta]} = \sum_{\{\theta\}} \mathrm{e}^{\sum_x \left(K \sum_{\nu=1}^{3} \cos(\theta_x - \theta_{x+\hat{\nu}}) + h \cos\theta_x \right)} , \tag{F.3}$$

where $\sum_{\{\theta\}}$ is the sum over all configurations of discrete angles, i.e., $\prod_x \frac{1}{q} \sum_{n_x=0}^{q-1}$ in case of the clock-model, and the integral over all configurations of continuous angles, $\prod_x \int_0^{2\pi} \frac{d\theta_x}{2\pi}$ in case of the xy-model. In the first exponent appears the inverse temperature β which in the second exponent is absorbed in the the re-scaled coupling $K = \beta J$ and re-scaled external field $h = \beta\mu$.

F.3 Generating configurations

Since we want to extract critical exponents for the systems discussed above we have to simulate the system close to the critical coupling K_c (and $h = 0$), i.e., close to the phase transition. Of course, the system exhibits a real phase transition only in the infinite volume.

We want to study systems with a second order phase transition, where the system becomes conformal invariant. [3] Therefore, we study models for $q > 3$, since $q = 2$ is equivalent to the well studied 3-dimensional Ising model (with its well known second order phase transition), and $q = 3$ can be mapped to a 3-states Potts model, see, e.g., [144], which has a first order phase transition [146]. The transition for $q = 4$ is second order, since this model can be mapped to twice the Ising model. The xy-model for $J > 0$ in three dimensions has a second order transition as well [147]. The xy-model is of special interest to us, since a comparison to other works [136, 148] is feasible.

Due to critical slowing down a Metropolis algorithm is not efficient and more sophisticated methods such as cluster algorithms should be used. In the following we use the Wolff algorithm [149] which employs as an update strategy a reflection of the spins with respect to a hyperplane orthogonal to a unit vector $\vec{r} = (\cos\theta_r, \sin\theta_r)$, i.e.,

$$\vec{S}_x \longrightarrow \vec{S}_x - 2(\vec{S}_x \cdot \vec{r})\, \vec{r} \quad \Rightarrow \quad \theta_x \longrightarrow 2\theta_r - \theta_x + \pi \ . \tag{F.4}$$

[3] To be more precise: The system becomes scale invariant at the phase transition. However, in two dimensions it can be proven that scale invariance implies conformal invariance. For higher dimensional systems there is no proof, but no example has been found yet where a scale invariant theory was non-conformal [145].

We describe the algorithm using pseudocode below. In our code `uni()` denotes a random number generator that provides uniformly distributed random numbers in the interval $[0, 1)$. The array `stack` stores all sites which are added to the cluster and `stackpos` is the current position in `stack`. The array `mark` is a Boolean array which keeps track of the sites added to the cluster. The sites are added to the cluster with probability

$$P(\theta_x, \theta_y, \theta_r) = 1 - \exp\left[2K\cos\left(\theta_x - \theta_r\right)\cos\left(\theta_y - \theta_r\right) + 2h\cos\left(\theta_y - \theta_r\right)\cos\theta_r\right] . \quad \text{(F.5)}$$

The code can be fully vectorized in the form given below [150].

Pseudocode for the Wolff algorithm:

```
randomly select a lattice site x_0
stack[0] = x_0
θ_r = 2π rand()
θ_{x_0} ← 2θ_r − θ_{x_0} + π
mark[x_0] = true
set stackpos = 1
while stackpos > 0
    x_0 = stack[−−stackpos]
    for ν = ±1 ⟶ ±3
        if mark[x_0 + ν̂] = false
            compute P(θ_{x_0}, θ_{x_0+ν̂}, θ_r)
            if rand() < min { P(θ_{x_0}, θ_{x_0+ν̂}, θ_r) , 1 } then
                θ_{x_0+ν̂} ← 2θ_r − θ_{x_0+ν̂} + π
                mark[x_0 + ν̂] = true
                stack[stackpos++] = x_0 + ν̂
            end if
        end if
    end for
end while
```

If one considers discrete clock-model the angles θ_x can be replaced by integer-valued numbers $n_x = 0, 1, \ldots, q-1$ as discussed in Section F.2 . Due to ergodicity one has to distinguish between even and odd values of q. Therefore, the random angles θ_r have to be of the form [151]

$$\theta_r = \frac{\pi}{q}\begin{cases} n_r & \text{, for } q \text{ even} \\ n_r + \frac{1}{2} & \text{, for } q \text{ odd} \end{cases} \quad , \quad n_r = 0, 1, \ldots, 2q-1 . \quad \text{(F.6)}$$

The updates of the n_x then are [151]

$$n_x \longrightarrow \left(2q + n_r - n_x + \begin{cases} \frac{q}{2} & \text{, for } q \text{ even} \\ \frac{q+1}{2} & \text{, for } q \text{ odd} \end{cases}\right) \bmod q \ . \tag{F.7}$$

F.4 Observables

Several observables which are considered in our simulations are listed here. In the list below $V = L^3$ denotes the volume of the lattice, where L is the lattice extent, and $\langle \mathcal{O} \rangle$ denotes the expectation value of the observable $\mathcal{O}$.

- Energy density: $E = \frac{1}{3V} \sum_x \sum_{\nu=1} \vec{S}_x \cdot \vec{S}_{x+\hat{\nu}} = \frac{1}{3V} \sum_x \sum_{\nu=1} \cos\left(\theta_x - \theta_{x+\hat{\nu}}\right)$
- Heat capacity: $C = \langle E^2 \rangle - \langle E \rangle^2$
- Magnetization: $\vec{M} = \frac{1}{V} \sum_x \vec{S}_x = \frac{1}{V} \sum_x \begin{pmatrix} \cos\theta_x \\ \sin\theta_x \end{pmatrix}$
- Magnetic susceptibility: $\chi/V = \langle \vec{M}^2 \rangle$
- Binder cumulant: $U_\mathrm{B} = 1 - \frac{\langle \vec{M}^4 \rangle}{3\langle \vec{M}^2 \rangle^2}$
- Correlation length: $\xi = \frac{1}{2\sin\frac{\pi}{L}} \sqrt{\frac{\chi}{F} - 1}$ with $F = \frac{1}{V} \left\langle \left| \sum_x e^{i\frac{2\pi}{L}x_1} \vec{S}_x \right|^2 \right\rangle$
- Derivatives: $\frac{\partial U_\mathrm{B}}{\partial K}$ and $\frac{\partial \ln \langle \vec{M}^2 \rangle}{\partial K}$ with $\frac{\partial \langle \vec{M}^{2n} \rangle}{\partial K} = \langle E \vec{M}^{2n} \rangle - \langle E \rangle \langle \vec{M}^{2n} \rangle$

The following results have been obtained by generating spin configurations according to the Wolff algorithm described in Section F.3. Before taking measurements of observables $5 \cdot 10^5$ configurations have been dropped for equilibration. Also in between measurements 20 for the smallest and 70 for the largest lattice configurations have been dropped do decorrelate the system. Here we only present results for a vanishing external field, $h = 0$ and for six different lattice sizes: $L = 40, 60, 80, 100, 120, 140$. We focus on $q = 4$ and the xy-model below. The number of configurations for computing the expectation values is $5 \cdot 10^5$ for the xy-model and 10^6 for the $q = 4$ clock model.

In Figure F.1 results of the observables discussed above are shown for the xy-model. [4]

[4] We do not show the plots of the observables for the $q = 4$ clock model, since they look very similar to the ones shown in Figure F.1 for the xy-model.

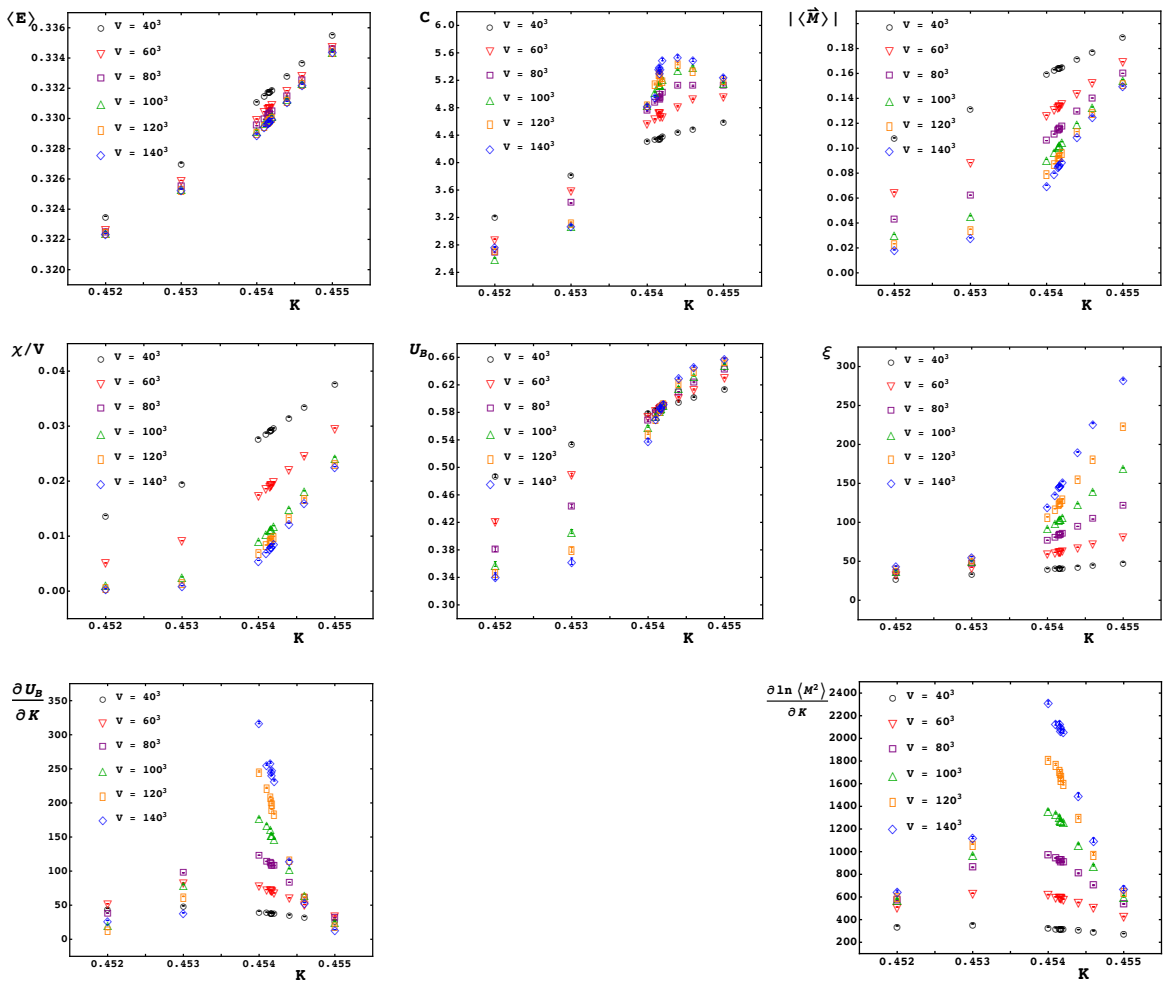

Figure F.1: Plots of the expectation values in the beginning of this section are shown as a function of the coupling K and $h = 0$ for several lattice volumes V for the xy-model.

F.5 Critical couplings

At the critical point, the Binder cumulant U_B and the ratio ξ/L are invariant under renormalization group transformations. For computing the critical couplings K_c we use the Binder crossing method: The value of U_B at K_c is independent of the system size L. This means that as a function of K the Binder cumulant U_B must intersect at a single point $K = K_\mathrm{c}$ for all values of L.

From Figure F.2 we can estimate the critical coupling K_c for the xy-model. In Table F.1 we list our results of K_c for $q = 4$ states clock-models and the xy-model.

The value obtained for the $q = 4$ states clock model is approximately twice as large as the one given in [154]. This is expected, since the $q = 4$ states clock model is essentially the Ising model with a twice as large coupling constant. The value of the critical coupling constant for the xy-model is in good agreement with the one obtained in [148].

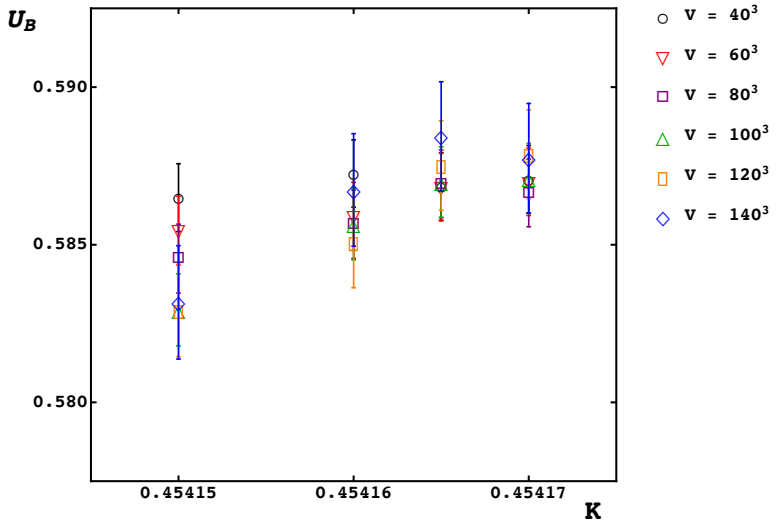

Figure F.2: Results of the Binder crossing method.. The region in K where the error bars overlap give an estimate of the critical coupling K_c.

Table F.1: Estimates of the critical couplings K_c for the $q = 4$ states clock-models and the xy-model are listed here. K_c is obtained by the Binder crossing method. We compare our values to literature values.

q	K_c	$K_c^{\text{Ref.}}$	Ref.
4	0.44330(5)	0.4541659(10)	[152]
∞	0.454165(5)	0.4403388(6)	2×[153]

F.6 Critical exponents and finite size scaling

For magnetic systems the critical exponents can be estimated from the behavior of several observables close to the critical temperature T_c. They behave as a function of the reduced temperature $t = T/T_c - 1$ as

$$\begin{aligned} M &\sim (-t)^{\beta} \quad , \quad C \sim |t|^{-\alpha} \quad , \quad \chi \sim |t|^{-\gamma} \, , \\ M &\sim h^{1/\delta} \quad , \quad \xi \sim |t|^{-\nu} \quad , \quad G(x) \sim \frac{1}{|x|^{d-2-\eta}} \, , \end{aligned} \tag{F.8}$$

where $G(x)$ is the two-point correlation function $\langle S_x S_0 \rangle - \langle S_0 \rangle^2$ and d the dimension of the system.

To extract the critical exponents, it is necessary to perform a finite size scaling (FSS) analysis. In finite systems there is no phase transition and thus the correlation length ξ is finite. However, ξ is finite if one simulates the system not exactly at the critical temperature T_c and therefore the interactions do not feel the finite size of the system. If the size is larger than ξ it behaves like an infinite system. FSS studies how the behavior changes with the system size L. The FSS hypothesis states the following: The ratio of thermodynamic quantities (M, χ, etc.) in the finite size system and in the infinite system is a function of ξ/L only, i.e., $O_L(t)/O_\infty(t) = F(L/\xi(t))$. Since $\xi(t) \sim t^{-\nu}$ one

finds the following FSS behavior of the observables:

$$\chi = L^{\gamma/\nu} F_\chi\big(L^{1/\nu} t\big) \quad , \quad C = L^{\alpha/\nu} F_C\big(L^{1/\nu} t\big) \quad , \quad M = L^{-\beta/\nu} F_M\big(L^{1/\nu} t\big) \; . \tag{F.9}$$

The strategy is as follows: Compute the observables $\mathcal{O}_L$ for different system sizes L for some value t close to zero, i.e., close to T_c or close to K_c respectively. From a fit of $\ln O_L(t) = \mathrm{const.} + \frac{\rho}{\nu} \ln L$ we extract the ratio ρ/ν. The remaining problem is to find the exponent ν. From the scaling of the derivatives of the Binder cumulant and of $\ln\langle \vec{M}^2 \rangle$, i.e.,

$$\frac{\partial U_\mathrm{B}}{\partial K} = a L^{1/\nu}(1 + b L^{-\omega}) = \frac{\partial \ln \langle \vec{M}^2 \rangle}{\partial K} \; , \tag{F.10}$$

we can find the critical exponent ν. The remaining critical exponents can be found by scaling and hyperscaling relations of the other exponents. The most prominent ones are

$$\begin{aligned} \alpha + 2\beta + \gamma = 2 \quad &, \quad 2 - \alpha = d\nu \; , \\ \beta(\delta - 1) = \gamma \quad &, \quad 2 - \eta = \frac{\gamma}{\nu} \; . \end{aligned} \tag{F.11}$$

In Figure F.3 we show results obtained by the procedure described above for the critical exponent ν for the xy-model. We obtain the value $\nu = 0.68 \pm 0.1$, where the error is a statistical error. In Table F.2 we list our critical exponents for the xy-model and the $q = 4$ clock model. We compare these values to the ones given in [148] and [155], respectively. Note that, the results of [155] are obtained from a conformal bootstrap of the 3d Ising model, which is in the same universality class of the $q = 4$ clock model.

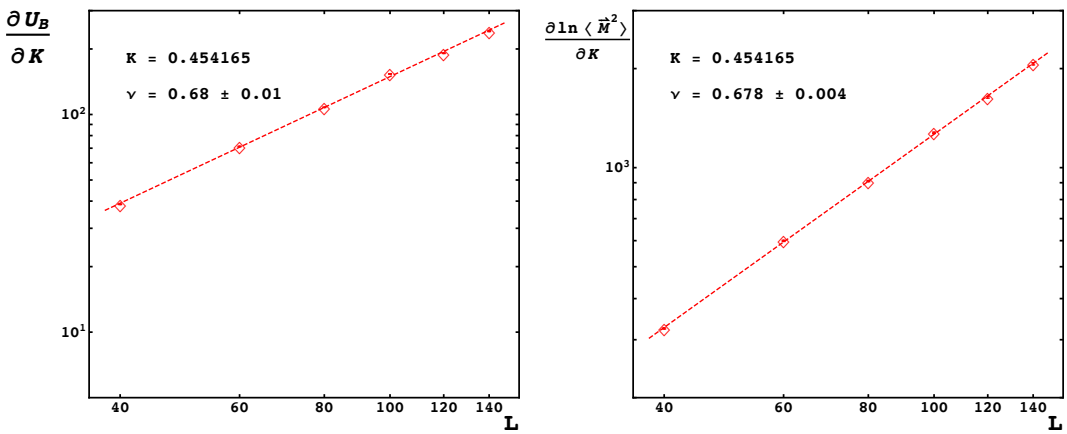

Figure F.3: The observables $\partial U_\mathrm{B}/\partial K$ and $\partial \ln \langle \vec{M}^2 \rangle / \partial K$ as a function of the lattice size L for $K = 0.454165 \approx K_\mathrm{c}$ is shown for the xy-model. The dashed lines are fits according to Equation (F.10) neglecting the correction term $L^{-\omega}$.

All in all our critical exponents are comparable with the ones from the literature, only the exponent η relatively far off the literature values for both models we studied. Converging towards the literature values for the exponent η is desirable to determine scaling dimensions of fields. This issue is discussed in the following section.

However, larger statistics and larger lattices are needed to obtain more accurate values for the crit-

Table F.2: Table of the critical exponents of the xy-model and the $q = 4$-states clock model extracted as described in the main text. We compare our results to [148] and [155].

	xy		$q = 4$	
Exponent	Our result	Result from [148]	Our result	Result from [155]
ν	0.68(1)	0.6717(1)	0.63(1)	0.629971(4)
η	0.028(2)	0.0381(2)	0.08(2)	0.036298(2)
γ	1.34(2)	1.3178(2)	1.220(2)	1.237075(10)
β	0.350(6)	0.3486(1)	0.330(4)	0.326419(3)

ical exponents. Of course, an improvement of the fitting procedure is desirable. Methods like histogram reweighting along the lines of [156] could improve the results as well.

F.7 Wilson coefficients

This part follows closely [141–143].

Consider a complete set of operators of the conformal theory, $\{O_i \mid i = 1, 2, \dots\}$, which for simplicity we assume to be spinless. The operator product expansion (OPE) states that

$$O_i(x_1)\, O_j(x_2) = \sum_k C_{ijk}(x_{12}, \partial_2)\, O_k(x_2)\ , \tag{F.12}$$

where $x_{ij} = |x_i - x_j|$ and $\partial_i = \frac{\partial}{\partial x_i}$. The so-called Wilson coefficients C_{ijk} can be obtained from 3-point functions as

$$\begin{aligned}\big\langle O_i(x_1)\, O_j(x_2)\, O_k(x_3)\big\rangle &= \sum_{k'} C_{ijk'}(x_{12}, \partial_2)\, \big\langle O_{k'}(x_2)\, O_k(x_3)\big\rangle \\ &= \sum_{k'} C_{ijk'}(x_{12}, \partial_2)\, \frac{\delta_{k,k'}}{x_{23}^{2\Delta_k}} = C_{ijk}(x_{12}, \partial_2)\, \frac{1}{x_{23}^{2\Delta_k}} \\ &= \frac{f_{ijk}}{x_{12}^{\Delta_i+\Delta_j-\Delta_k}\, x_{23}^{\Delta_j+\Delta_k-\Delta_i}\, x_{13}^{\Delta_k+\Delta_i-\Delta_j}}\ ,\end{aligned} \tag{F.13}$$

where only connected expectation values are considered. Several steps have been performed here: In the first line the OPE of the operators $O_i(x_1)$ and $O_j(x_2)$ was used. In the second line we used the fact that the operator set is complete as well as the form of the 2-point function in the conformal window, see also the correlation function in Equation (F.8). The last line is the exact form of the 3-point function at conformality [138]. The exponents Δ_i are the so-called scaling dimensions of the operators O_i. They are related to the critical exponents η_i by $\Delta_i = \frac{d-2-\eta_i}{2}$ in d dimensions. The numbers f_{ijk} are real constants. From Equation(F.13) we find that the Wilson coefficient is proportional to f_{ijk} times some differential operator.

The most naive approach to obtain the Wilson coefficients is to compute the 3-point function directly. However, the problem with this procedure is that, if one computes the connected correlator one has to subtract 2-point components which leads to a mix of contributions with similar exponents.

Instead one may studies perturbed 2-point functions [141] close to the critical point,

$$\left\langle O_i(x)\, O_j(0)\right\rangle_h = \sum_k C_{ijk}(|x|, h)\, \left\langle O_k(0)\right\rangle_h \,, \tag{F.14}$$

where the expectation value is computed with respect to an action or Hamiltonian with external field h. We outline the method using the clock-model (F.2). The perturbed action of the continuum clock-model in three dimensions is

$$S = S_{\mathrm{CFT}} + \int \mathrm{d}^3x\, \vec{s}(x) \cdot \vec{h} \,, \tag{F.15}$$

where the action of the conformal theory S_{CFT} describes the system at criticality. The only relevant fields or operators at the conformal point are the energy $E(x)$ and the spin field $s(x)$, where $s(x) = \vec{s}(x) \cdot \vec{h}/|\vec{h}|$.

The expectation values of these fields hence depend on h. Using renormalization group arguments yields

$$\left\langle s\right\rangle = A_s\, h^{\frac{\Delta_s}{\Delta_h}} \quad , \quad \left\langle E\right\rangle = A_E\, h^{\frac{\Delta_E}{\Delta_h}} \,, \tag{F.16}$$

where the scaling dimensions Δ_s, Δ_E can be obtained by determining the critical exponents η_s, η_E of the 2-point correlators of the corresponding the fields. The scaling dimension Δ_h is fixed by dimensional arguments to $\Delta_h = 3 - \Delta_s$. The amplitudes A_s and A_E are real constants.

We introduce the following notation:

$$\begin{aligned} C_{ijk} &= \lim_{|x|\to\infty} C_{ijk}(|x|, 0)\, |x|^{\dim C_{ijk}(|x|,0)} \,, \\ \partial_h C_{ijk} &= \lim_{|x|\to\infty} \partial_h C_{ijk}(|x|, 0)\, |x|^{\dim \partial_h C_{ijk}(|x|,0)} \,. \end{aligned} \tag{F.17}$$

Then the short distance expansions of the correlators are [141]:

$$\begin{aligned} |x|^{2\Delta_s} \left\langle s(x)\, s(0)\right\rangle &= C_{ss1} + A_E\, C_{ssE}\, t^{\frac{\Delta_E}{\Delta_h}} + A_s\, \partial_h C_{sss}\, t^{\frac{\Delta_s}{\Delta_h}+1} + \mathcal{O}\big(t^2\big) \,, \\ |x|^{\Delta_s+\Delta_E} \left\langle s(x)\, E(0)\right\rangle &= A_s\, C_{sEs}\, t^{\frac{\Delta_s}{\Delta_h}} + \partial_h C_{sE1}\, t + A_E\, \partial_h C_{sEE}\, t^{\frac{\Delta_E}{\Delta_h}+1} + \mathcal{O}\Big(t^{\frac{\Delta_s}{\Delta_h}+1}\Big) \,, \\ |x|^{2\Delta_E} \left\langle E(x)\, E(0)\right\rangle &= C_{EE1} + A_E\, C_{EEE}\, t^{\frac{\Delta_E}{\Delta_h}} + A_s\, \partial_h C_{EEs}\, t^{\frac{\Delta_s}{\Delta_h}+1} + \mathcal{O}\big(t^2\big) \,, \end{aligned} \tag{F.18}$$

where we used the scaling variable $t = |h|\, |x|^{\Delta_h}$. We set $C_{ss1} = C_{EE1} = 1$, which is the standard normalization. Here, we are only interested in the coefficients C_{ssE}, C_{sEs}, and C_{EEE}, i.e., in the ones that appear at order $t^{\Delta_{s,E}/\Delta_h}$.

Until now the discussion was in the continuum formulation. We now discuss how to obtain the

normalizations from a lattice formulation. The partition function at the conformal point is

$$Z = \sum_{\{\theta\}} \mathrm{e}^{K_\mathrm{c} \sum_{x,\nu} \cos(\theta_x - \theta_{x+\hat{\nu}}) + h^\mathrm{l} \sum_x \cos\theta_x} \ , \tag{F.19}$$

where we distinguish between the continuum external field h and the lattice version h^l. We use $s_x \equiv \cos\theta_x$ in the following. The spin average s is on the lattice naturally $s^\mathrm{l} = \frac{1}{V}\sum_x s_x$, and the energy operator is $E^\mathrm{l} = \frac{1}{3V}\sum_{x,\nu}\cos(\theta_x - \theta_{x+\hat{\nu}}) - E^\mathrm{cr}$, where E^cr is the energy at criticality.

Note, that if one measures the expectation values (F.16) and the correlators (F.18) on the lattice, the lattice versions of the Wilson coefficients C and the amplitudes A, i.e., C^l and A^l, are found. The relation to the continuum quantities can be obtained as follows: From

$$\left\langle s_x \, s_y \right\rangle = \frac{R_s^2}{|x-y|^{2\Delta_s}} \ , \tag{F.20}$$

one gets $s = R_s^{-1}\, s^\mathrm{l}$, where we assume the standard normalization of the 2-point correlator in the continuum. Similarly, we get $E = R_E^{-1}\, E^\mathrm{l}$. From a dimensional analysis of the continuum and lattice perturbed action one obtains $h = R_s\, h^\mathrm{l}$. The constants R_s and R_E can be obtained from a finite size scaling analysis. Note that the external field should be small in order to keep the correlation length large.

The lattice amplitudes $A^\mathrm{l}_{s,E}$ are obtained from the lattice version of the expectation values and their dependence on the external field $h^\mathrm{l} = R_s^{-1} h$. Then, from this equation we get

$$A_s = R_s^{\frac{\Delta_h}{\Delta_s}-1}\, A^\mathrm{l}_s \quad , \quad A_E = R_s^{\frac{\Delta_h}{\Delta_E}}\, R_E^{-1}\, A^\mathrm{l}_E \ , \tag{F.21}$$

and from Equation (F.18) the desired matching factors for the Wilson coefficients are obtained:

$$C_{ssE} = R_E\, C^\mathrm{l}_{ssE} \quad , \quad C_{sEs} = R_s\, C^\mathrm{l}_{sEs} \quad , \quad C_{EEE} = R_E\, C^\mathrm{l}_{EEE} \ . \tag{F.22}$$

However, the determination of these Wilson coefficients contains several steps, as seen above. All these steps add statistical as well as systematic error contributions to the final result. Unfortunately, we have not yet succeeded to control those errors in order to produce reliable estimates for the Wilson coefficients and the scaling dimensions of the operators.

References

[1] S. Weinberg, *The Quantum theory of fields. Vol. 1: Foundations*. Cambridge University Press, Cambridge, 1995. Cambridge, UK: Univ. Pr. (1995) 609 p.

[2] S. Weinberg, *The quantum theory of fields. Vol. 2: Modern applications*. Cambridge University Press, Cambridge, 1996. Cambridge, UK: Univ. Pr. (1996) 489 p.

[3] M. Böhm, A. Denner, and H. Joos, *Gauge theories of the strong and electroweak interaction*. Teubner, Stuttgart, 2001. Stuttgart, Germany: Teubner (2001) 784 p.

[4] M. E. Peskin and D. V. Schroeder, *An Introduction to quantum field theory*. Addison-Wesley, Reading, USA, 1995.

[5] LHCb Collaboration, R. Aaij *et al.*, "Measurement of the ratio of branching fractions $\mathcal{B}(B_c^+ \to J/\psi\tau^+\nu_\tau)/\mathcal{B}(B_c^+ \to J/\psi\mu^+\nu_\mu)$," `arXiv:1711.05623 [hep-ex]`.

[6] ATLAS Collaboration, M. Aaboud *et al.*, "Search for new phenomena in high-mass diphoton final states using 37 fb^{-1} of proton–proton collisions collected at $\sqrt{s} = 13$ TeV with the ATLAS detector," *Phys. Lett.* B775 (2017) 105–125, `arXiv:1707.04147 [hep-ex]`.

[7] CMS Collaboration, V. Khachatryan *et al.*, "Search for high-mass diphoton resonances in proton–proton collisions at 13 TeV and combination with 8 TeV search," *Phys. Lett.* B767 (2017) 147–170, `arXiv:1609.02507 [hep-ex]`.

[8] A. Einstein, "The Foundation of the General Theory of Relativity," *Annalen Phys.* 49 no. 7, (1916) 769–822. [Annalen Phys.14,517(2005)].

[9] K. Becker, M. Becker, and J. H. Schwarz, *String theory and M-theory: A modern introduction*. Cambridge University Press, 2006.

[10] D. Z. Freedman, P. van Nieuwenhuizen, and S. Ferrara, "Progress Toward a Theory of Supergravity," *Phys. Rev.* D13 (1976) 3214–3218.

[11] T. Thiemann, *Modern canonical quantum general relativity*. Cambridge University Press, 2008. `arXiv:gr-qc/0110034 [gr-qc]`.

[12] S. Weinberg, "Critical Phenomena for Field Theorists," in *14th International School of Subnuclear Physics: Understanding the Fundamental Constitutents of Matter Erice, Italy, July 23-August 8, 1976*, p. 1. 1976.

[13] L. Glaser and R. Loll, "CDT and Cosmology," *Comptes Rendus Physique* 18 (2017) 265–274, `arXiv:1703.08160 [gr-qc]`.

[14] S. Tomonaga, "On a relativistically invariant formulation of the quantum theory of wave fields," *Prog. Theor. Phys.* 1 (1946) 27–42.

[15] J. S. Schwinger, "On Quantum electrodynamics and the magnetic moment of the electron," *Phys. Rev.* 73 (1948) 416–417.

[16] J. S. Schwinger, "Quantum electrodynamics. I A covariant formulation," *Phys. Rev.* 74 (1948) 1439.

[17] R. P. Feynman, "Space - time approach to quantum electrodynamics," *Phys. Rev.* 76 (1949) 769–789.

[18] R. P. Feynman, "The Theory of positrons," *Phys. Rev.* 76 (1949) 749–759.

[19] R. P. Feynman, "Mathematical formulation of the quantum theory of electromagnetic interaction," *Phys. Rev.* 80 (1950) 440–457.

[20] T. Aoyama, M. Hayakawa, T. Kinoshita, and M. Nio, "Tenth-Order QED Contribution to the Electron g-2 and an Improved Value of the Fine Structure Constant," *Phys. Rev. Lett.* 109 (2012) 111807, `arXiv:1205.5368 [hep-ph]`.

[21] T. Aoyama, M. Hayakawa, T. Kinoshita, and M. Nio, "Tenth-Order Electron Anomalous Magnetic Moment — Contribution of Diagrams without Closed Lepton Loops," *Phys. Rev.* D91 no. 3, (2015) 033006, `arXiv:1412.8284 [hep-ph]`. [Erratum: Phys. Rev.D96,no.1,019901(2017)].

[22] D. Hanneke, S. F. Hoogerheide, and G. Gabrielse, "Cavity Control of a Single-Electron Quantum Cyclotron: Measuring the Electron Magnetic Moment," *Phys. Rev.* A83 (2011) 052122, `arXiv:1009.4831 [physics.atom-ph]`.

[23] W. Greiner, S. Schramm, and E. Stein, *Quantum chromodynamics*. Springer, Berlin 2002.

[24] D. J. Gross and F. Wilczek, "Ultraviolet Behavior of Nonabelian Gauge Theories," *Phys. Rev. Lett.* 30 (1973) 1343–1346.

[25] K. G. Wilson, "Confinement of Quarks," *Phys. Rev.* D10 (1974) 2445–2459. [,45(1974)].

[26] J. Greensite, "Some current approaches to the confinement problem," *Acta Phys. Polon.* B40 (2009) 3355–3408.

[27] J. Greensite and K. Matsuyama, "A confinement criterion for gauge theories with matter fields," `arXiv:1708.08979 [hep-lat]`.

[28] I. Montvay and G. Münster, *Quantum fields on a lattice*. Cambridge University Press, Cambridge, 1994. Cambridge, UK: Univ. Pr. (1994) 491 p. (Cambridge monographs on mathematical physics).

[29] H. J. Rothe, *Lattice gauge theories: An Introduction*. World Sci. Lect. Notes Phys., 2005.

[30] C. Gattringer and C. B. Lang, *Quantum chromodynamics on the lattice: An Introductory Presentation*. Lect. Notes Phys., Springer, Berlin Heidelberg 2010.

[31] Particle Data Group Collaboration, C. Patrignani *et al.*, "Review of Particle Physics," *Chin. Phys.* C40 no. 10, (2016) 100001.

[32] S. L. Glashow, "Partial Symmetries of Weak Interactions," *Nucl. Phys.* 22 (1961) 579–588.

[33] A. Salam, "Weak and Electromagnetic Interactions," *Conf. Proc.* C680519 (1968) 367–377.

[34] S. Weinberg, "A Model of Leptons," *Phys. Rev. Lett.* 19 (1967) 1264–1266.

[35] F. Englert and R. Brout, "Broken Symmetry and the Mass of Gauge Vector Mesons," *Phys. Rev. Lett.* 13 (1964) 321–323.

[36] P. W. Higgs, "Broken symmetries, massless particles and gauge fields," *Phys. Lett.* 12 (1964) 132–133.

[37] P. W. Higgs, "Broken Symmetries and the Masses of Gauge Bosons," *Phys. Rev. Lett.* 13 (1964) 508–509.

[38] P. W. Higgs, "Spontaneous Symmetry Breakdown without Massless Bosons," *Phys. Rev.* 145 (1966) 1156–1163.

[39] G. S. Guralnik, C. R. Hagen, and T. W. B. Kibble, "Global Conservation Laws and Massless Particles," *Phys. Rev. Lett.* 13 (1964) 585–587.

[40] ATLAS Collaboration, G. Aad *et al.*, "Observation of a new particle in the search for the Standard Model Higgs boson with the ATLAS detector at the LHC," *Phys. Lett.* B716 (2012) 1–29, `arXiv:1207.7214 [hep-ex]`.

[41] CMS Collaboration, S. Chatrchyan *et al.*, "Observation of a new boson at a mass of 125 GeV with the CMS experiment at the LHC," *Phys. Lett.* B716 (2012) 30–61, `arXiv:1207.7235 [hep-ex]`.

[42] K. G. Wilson and J. B. Kogut, "The Renormalization group and the epsilon expansion," *Phys. Rept.* 12 (1974) 75–200.

[43] D. J. E. Callaway, "Triviality Pursuit: Can Elementary Scalar Particles Exist?," *Phys. Rept.* 167 (1988) 241.

[44] M. Lüscher and P. Weisz, "Scaling Laws and Triviality Bounds in the Lattice phi**4 Theory. 2. One Component Model in the Phase with Spontaneous Symmetry Breaking," *Nucl. Phys.* B295 (1988) 65–92.

[45] M. Lüscher and P. Weisz, "Scaling Laws and Triviality Bounds in the Lattice phi**4 Theory. 3. N Component Model," *Nucl. Phys.* B318 (1989) 705–741.

[46] A. Hasenfratz, K. Jansen, C. B. Lang, T. Neuhaus, and H. Yoneyama, "The Triviality Bound of the Four Component phi**4 Model," *Phys. Lett.* B199 (1987) 531–535.

[47] A. Hasenfratz and P. Hasenfratz, "The Continuum Limit of an SU(2) Gauge Theory With a Scalar Doublet," *Phys. Rev.* D34 (1986) 3160.

[48] H. Georgi and S. L. Glashow, "Unity of All Elementary Particle Forces," *Phys. Rev. Lett.* 32 (1974) 438–441.

[49] R. Shrock, "Some recent results on models of dynamical electroweak symmetry breaking," in *The origin of mass and strong coupling gauge theories. Proceedings, 5th International Workshop, SCGT'06, Nagoya, Japan November 21-24, 2006*, pp. 227–241. 2007. `arXiv:hep-ph/0703050 [hep-ph]`.

[50] M. Schmaltz and D. Tucker-Smith, "Little Higgs review," *Ann. Rev. Nucl. Part. Sci.* 55 (2005) 229–270, `arXiv:hep-ph/0502182 [hep-ph]`.

[51] R. Foot and S. Vagnozzi, "Dissipative hidden sector dark matter," *Phys. Rev.* D91 (2015) 023512, `arXiv:1409.7174 [hep-ph]`.

[52] R. Haag, *Local quantum physics: Fields, particles, algebras*. Springer, Berlin, 1992. Berlin, Germany: Springer (1992) 356 p. (Texts and monographs in physics).

[53] G. 't Hooft, "Why do we need local gauge invariance in theories with vector particles? An introduction," *NATO Adv.Study Inst.Ser.B Phys.* 59 (1980) 101.

[54] K. Osterwalder and E. Seiler, "Gauge Field Theories on the Lattice," *Annals Phys.* 110 (1978) 440.

[55] T. Banks and E. Rabinovici, "Finite Temperature Behavior of the Lattice Abelian Higgs Model," *Nucl.Phys.* B160 (1979) 349.

[56] J. Fröhlich, G. Morchio, and F. Strocchi, "Higgs phenomenon without a symmetry breaking order parameter," *Phys.Lett.* B97 (1980) 249.

[57] J. Fröhlich, G. Morchio, and F. Strocchi, "Higgs phenomenon without a symmetry breaking order parameter," *Nucl.Phys.* B190 (1981) 553–582.

[58] A. Maas, "Bound-state/elementary-particle duality in the Higgs sector and the case for an excited 'Higgs' within the standard model," *Mod.Phys.Lett.* A28 (2013) 1350103, `arXiv:1205.6625 [hep-lat]`.

[59] A. Maas and T. Mufti, "Two- and three-point functions in Landau gauge Yang-Mills-Higgs theory," *JHEP* 1404 (2014) 006, `arXiv:1312.4873 [hep-lat]`.

[60] A. Maas, "Brout-Englert-Higgs physics: From foundations to phenomenology," `arXiv:1712.04721 [hep-ph]`.

[61] P. Törek and A. Maas, "Testing gauge-invariant perturbation theory," *PoS* LATTICE2016 (2016) 203, `arXiv:1610.04188 [hep-lat]`.

[62] L. Egger, A. Maas, and R. Sondenheimer, "Pair production processes and flavor in gauge-invariant perturbation theory," `arXiv:1701.02881 [hep-ph]`.

[63] A. Maas, "Field theory as a tool to constrain new physics models," *Mod. Phys. Lett.* A30 no. 29, (2015) 1550135, `arXiv:1502.02421 [hep-ph]`.

[64] A. Maas and L. Pedro, "Gauge invariance and the physical spectrum in the two-Higgs-doublet model," *Phys. Rev.* D93 no. 5, (2016) 056005, `arXiv:1601.02006 [hep-ph]`.

[65] A. Maas and P. Törek, "Predicting the singlet vector channel in a partially Higgsed gauge theory," *Phys. Rev.* D95 no. 1, (2017) 014501, `arXiv:1607.05860 [hep-lat]`.

[66] A. Maas, R. Sondenheimer, and P. Törek, "A study of how the particle spectra of SU(N) gauge theories with a fundamental Higgs emerge," 2017. `arXiv:1710.01941 [hep-lat]`.

[67] M. Shifman, *Advanced topics in quantum field theory: A lecture course*. Cambridge University Press, 2012.

[68] S. Elitzur, "Impossibility of Spontaneously Breaking Local Symmetries," *Phys. Rev.* D12 (1975) 3978–3982.

[69] L. Faddeev and V. Popov, "Feynman Diagrams for the Yang-Mills Field," *Phys.Lett.* B25 (1967) 29–30. Faddeev-Popov ghosts.

[70] B. Lee and J. Zinn-Justin, "Spontaneously broken gauge symmetries ii. perturbation theory and renormalization," *Phys.Rev.* D5 (1972) 3137–3155.

[71] B. Lee and J. Zinn-Justin, "Spontaneously Broken Gauge Symmetries. 1. Preliminaries," *Phys.Rev.* D5 (1972) 3121–3137. Renormalization Yang-Mills.

[72] B. Lee and J. Zinn-Justin, "Spontaneously broken gauge symmetries. 3. Equivalence," *Phys.Rev.* D5 (1972) 3155–3160. Unitary gauge 't Hooft gauge equivalence.

[73] L. O'Raifeartaigh, "Hidden gauge symmetry," *Rept.Prog.Phys.* 42 (1979) 159.

[74] V. N. Gribov, "Quantization of non-Abelian gauge theories," *Nucl. Phys.* B139 (1978) 1.

[75] I. M. Singer, "Some Remarks on the Gribov Ambiguity," *Commun. Math. Phys.* 60 (1978) 7–12.

[76] F. Lenz, J. W. Negele, L. O'Raifeartaigh, and M. Thies, "Phases and residual gauge symmetries of Higgs models," *Annals Phys.* 285 (2000) 25–60, `arXiv:hep-th/0004200 [hep-th]`.

[77] M. Capri, D. Dudal, M. Guimaraes, I. Justo, S. Sorella, *et al.*, "The (IR-)relevance of the Gribov ambiguity in SU(2) x U(1) gauge theories with fundamental Higgs matter," *Annals Phys.* 343 (2013) 72–86, `arXiv:1309.1402 [hep-th]`.

[78] A. Maas, "Accessing directly the properties of fundamental scalars in the confinement and Higgs phase," *Eur. Phys. J.* C71 (2011) 1548, `arXiv:1007.0729 [hep-lat]`.

[79] T. Heinzl, A. Ilderton, K. Langfeld, M. Lavelle, and D. McMullan, "The Ice-limit of Coulomb gauge Yang-Mills theory," *Phys. Rev.* D78 (2008) 074511, `arXiv:0807.4698 [hep-lat]`.

[80] J. M. Frere and P. Nicoletopoulos, "Gauge Invariant Content of the Effective Potential," *Phys. Rev.* D11 (1975) 2332.

[81] A. Ilderton, M. Lavelle, and D. McMullan, "Colour, copies and confinement," *JHEP* 03 (2007) 044, `arXiv:hep-th/0701168 [hep-th]`.

[82] F. Strocchi, "An introduction to non-perturbative foundations of quantum field theory," *Int. Ser. Monogr. Phys.* 158 (2013) 1–272.

[83] F. Strocchi, "Symmetries, Symmetry Breaking, Gauge Symmetries," `arXiv:1502.06540 [physics.hist-ph]`.

[84] A. Djouadi, "The Anatomy of electro-weak symmetry breaking. I: The Higgs boson in the standard model," *Phys. Rept.* 457 (2008) 1–216, `arXiv:hep-ph/0503172 [hep-ph]`.

[85] E. Seiler, "On the Higgs-Confinement Complementarity," `arXiv:1506.00862 [hep-lat]`.

[86] R. Alkofer and L. von Smekal, "The infrared behavior of QCD Green's functions: Confinement, dynamical symmetry breaking, and hadrons as relativistic bound states," *Phys. Rept.* 353 (2001) 281, `arXiv:hep-ph/0007355`.

[87] P. Hoyer, "Bound states - from QED to QCD," 2014. `arXiv:1402.5005 [hep-ph]`.

[88] A. Maas, "(non-)aligned gauges and global gauge symmetry breaking," *Mod. Phys. Lett.* A27 no. 38, (2012) 1250222.

[89] A. Maas and T. Mufti, "A spectroscopical analysis of the phase diagram of Yang-Mills-Higgs theory," *Phys. Rev.* D91 no. 11, (2015) 113011, `arXiv:1412.6440 [hep-lat]`.

[90] F. Csikor, Z. Fodor, and J. Heitger, "Perturbative and nonperturbative studies of the SU(2) Higgs model on lattices with asymmetric lattice spacings," *Phys. Rev.* D58 (1998) 094504, `arXiv:hep-lat/9804026 [hep-lat]`.

[91] M. Einhorn and D. Jones, "The Effective potential and quadratic divergences," *Phys.Rev.* D46 (1992) 5206–5208. Higg pole mass renormalization scheme.

[92] H. G. Evertz, J. Jersak, C. B. Lang, and T. Neuhaus, "SU(2) Higgs boson and vector boson masses on the lattice," *Phys. Lett.* B171 (1986) 271.

[93] L. O'Raifeartaigh, *Group structure of gauge theories*. Cambridge University Press, Cambridge, 1986. Cambridge, UK: Univ. Pr. (1986) 172 P. (Cambridge Monographs On Mathematical Physics).

[94] L.-F. Li, "Group Theory of the Spontaneously Broken Gauge Symmetries," *Phys. Rev.* D9 (1974) 1723–1739.

[95] H. Ruegg, "Extremas of SU(N) Higgs Potentials and Symmetry Breaking Pattern," *Phys. Rev.* D22 (1980) 2040.

[96] T. Murphy and L. O'Raifeartaigh, "Effect of the Renormalization Group on the Symmetry Breaking Patterns of SU(N) Higgs Potentials," *Nucl. Phys.* B229 (1983) 509–527.

[97] P. Langacker, "Grand Unified Theories and Proton Decay," *Phys. Rept.* 72 (1981) 185. GUT.

[98] I.-H. Lee and J. Shigemitsu, "Spectrum Calculations in the Lattice Georgi-glashow Model," *Nucl. Phys.* B263 (1986) 280–294.

[99] P. Törek and A. Maas, "Towards the spectrum of a GUT from gauge invariance," *PoS* LeptonPhoton2015 (2016) 073, `arXiv:1509.06497 [hep-ph]`.

[100] N. Metropolis, A. W. Rosenbluth, M. N. Rosenbluth, A. H. Teller, and E. Teller, "Equation of state calculations by fast computing machines," *J. Chem. Phys.* 21 (1953) 1087–1092.

[101] T. DeGrand and C. E. Detar, *Lattice methods for quantum chromodynamics.* World Scientific, New Jersey, 2006. New Jersey, USA: World Scientific (2006) 345 p.

[102] P. Gerhold, *Upper and lower Higgs boson mass bounds from a chirally invariant lattice Higgs-Yukawa model.* PhD thesis, Humboldt U., Berlin, 2009. `arXiv:1002.2569 [hep-lat]`.

[103] C. Michael, "Adjoint Sources in Lattice Gauge Theory," *Nucl. Phys.* B259 (1985) 58–76.

[104] M. Lüscher and U. Wolff, "How to Calculate the Elastic Scattering Matrix in Two-dimensional Quantum Field Theories by Numerical Simulation," *Nucl. Phys.* B339 (1990) 222–252.

[105] B. Blossier, M. Della Morte, G. von Hippel, T. Mendes, and R. Sommer, "On the generalized eigenvalue method for energies and matrix elements in lattice field theory," *JHEP* 04 (2009) 094, `arXiv:0902.1265 [hep-lat]`.

[106] C. Morningstar and M. J. Peardon, "Analytic smearing of SU(3) link variables in lattice QCD," *Phys. Rev.* D69 (2004) 054501, `arXiv:hep-lat/0311018 [hep-lat]`.

[107] O. Philipsen, M. Teper, and H. Wittig, "On the mass spectrum of the SU(2) Higgs model in (2+1)- dimensions," *Nucl.Phys.* B469 (1996) 445–472, `arXiv:hep-lat/9602006 [hep-lat]`.

[108] E.-M. Ilgenfritz, C. Menz, M. Muller-Preussker, A. Schiller, and A. Sternbeck, "SU(3) Landau gauge gluon and ghost propagators using the logarithmic lattice gluon field definition," *Phys.Rev.* D83 (2011) 054506, `arXiv:1010.5120 [hep-lat]`.

[109] A. Maas, "Describing gauge bosons at zero and finite temperature," *Phys. Rep.* 524 (2013) 203, `arXiv:1106.3942 [hep-ph]`.

[110] A. Cucchieri and T. Mendes, "Critical Slowing-Down in SU(2) Landau Gauge-Fixing Algorithms," *Nucl. Phys.* B471 (1996) 263–292, `arXiv:hep-lat/9511020`.

[111] N. Cabibbo and E. Marinari, "A New Method for Updating SU(N) Matrices in Computer Simulations of Gauge Theories," *Phys. Lett.* B119 (1982) 387–390.

[112] H. Suman and K. Schilling, "A Comparative study of gauge fixing procedures on the connection machines CM2 and CM5," `arXiv:hep-lat/9306018`.

[113] A. Maas, "The quenched SU(2) fundamental scalar propagator in minimal Landau gauge," *Eur. Phys. J.* C76 no. 7, (2016) 366, `arXiv:1603.07525 [hep-lat]`.

[114] A. Sternbeck, E. M. Ilgenfritz, M. Müller-Preussker, and A. Schiller, "Going infrared in SU(3) Landau gauge gluodynamics," *Phys. Rev.* D72 (2005) 014507, `arXiv:hep-lat/0506007`.

[115] A. Cucchieri, "Gribov copies in the minimal Landau gauge: The influence on gluon and ghost propagators," *Nucl. Phys.* B508 (1997) 353–370, `arXiv:hep-lat/9705005`.

[116] A. Cucchieri, T. Mendes, and A. R. Taurines, "Positivity violation for the lattice Landau gluon propagator," *Phys. Rev.* D71 (2005) 051902, `arXiv:hep-lat/0406020`.

[117] L. von Smekal, R. Alkofer, and A. Hauck, "The infrared behavior of gluon and ghost propagators in Landau gauge QCD," *Phys. Rev. Lett.* 79 (1997) 3591–3594, `arXiv:hep-ph/9705242`.

[118] L. von Smekal, A. Hauck, and R. Alkofer, "A solution to coupled Dyson-Schwinger equations for gluons and ghosts in Landau gauge," *Ann. Phys.* 267 (1998) 1, `arXiv:hep-ph/9707327`.

[119] J. C. R. Bloch, A. Cucchieri, K. Langfeld, and T. Mendes, "Propagators and running coupling from SU(2) lattice gauge theory," *Nucl. Phys.* B687 (2004) 76–100, `arXiv:hep-lat/0312036`.

[120] L. von Smekal, K. Maltman, and A. Sternbeck, "The strong coupling and its running to four loops in a minimal MOM scheme," *Phys. Lett.* B681 (2009) 336–342, `arXiv:0903.1696 [hep-ph]`.

[121] E. H. Fradkin and S. H. Shenker, "Phase Diagrams of Lattice Gauge Theories with Higgs Fields," *Phys. Rev.* D19 (1979) 3682–3697.

[122] W. Caudy and J. Greensite, "On the Ambiguity of Spontaneously Broken Gauge Symmetry," *Phys. Rev.* D78 (2008) 025018, `arXiv:0712.0999 [hep-lat]`.

[123] M. Wurtz and R. Lewis, "Higgs and W boson spectrum from lattice simulations," *Phys.Rev.* D88 (2013) 054510, `arXiv:1307.1492 [hep-lat]`.

[124] B. Berg and A. Billoire, "Glueball Spectroscopy in Four-Dimensional SU(3) Lattice Gauge Theory. 1.," *Nucl. Phys.* B221 (1983) 109–140.

[125] M. Lüscher, "Volume Dependence of the Energy Spectrum in Massive Quantum Field Theories. 1. Stable Particle States," *Commun.Math.Phys.* 104 (1986) 177.

[126] M. Lüscher, "Volume Dependence of the Energy Spectrum in Massive Quantum Field Theories. 2. Scattering States," *Commun.Math.Phys.* 105 (1986) 153–188.

[127] H. Georgi, H. R. Quinn, and S. Weinberg, "Hierarchy of Interactions in Unified Gauge Theories," *Phys. Rev. Lett.* 33 (1974) 451–454.

[128] Super-Kamiokande Collaboration, H. Nishino *et al.*, "Search for Proton Decay via $p \to e + \pi^0$ and $p \to \mu + \pi^0$ in a Large Water Cherenkov Detector," *Phys. Rev. Lett.* 102 (2009) 141801, `arXiv:0903.0676 [hep-ex]`.

[129] M. Lüscher and P. Weisz, "Locality and exponential error reduction in numerical lattice gauge theory," *JHEP* 09 (2001) 010, `arXiv:hep-lat/0108014 [hep-lat]`.

[130] H. B. Meyer, "Locality and statistical error reduction on correlation functions," *JHEP* 01 (2003) 048, `arXiv:hep-lat/0209145 [hep-lat]`.

[131] M. Della Morte and L. Giusti, "Exploiting symmetries for exponential error reduction in path integral Monte Carlo," *Comput. Phys. Commun.* 180 (2009) 813–818.

[132] Wolfram Research, Inc., "Mathematica, Version 11.1.". Champaign, IL, 2017.

[133] R. Rattazzi, V. S. Rychkov, E. Tonni, and A. Vichi, "Bounding scalar operator dimensions in 4D CFT," *JHEP* 12 (2008) 031, `arXiv:0807.0004 [hep-th]`.

[134] F. Caracciolo and V. S. Rychkov, "Rigorous Limits on the Interaction Strength in Quantum Field Theory," *Phys. Rev.* D81 (2010) 085037, `arXiv:0912.2726 [hep-th]`.

[135] S. El-Showk, M. F. Paulos, D. Poland, S. Rychkov, D. Simmons-Duffin, and A. Vichi, "Solving the 3D Ising Model with the Conformal Bootstrap," *Phys. Rev.* D86 (2012) 025022, `arXiv:1203.6064 [hep-th]`.

[136] F. Kos, D. Poland, D. Simmons-Duffin, and A. Vichi, "Bootstrapping the O(N) Archipelago," *JHEP* 11 (2015) 106, `arXiv:1504.07997 [hep-th]`.

[137] F. Kos, D. Poland, D. Simmons-Duffin, and A. Vichi, "Precision Islands in the Ising and $O(N)$ Models," *JHEP* 08 (2016) 036, `arXiv:1603.04436 [hep-th]`.

[138] D. Simmons-Duffin, "The Conformal Bootstrap," in *Proceedings, Theoretical Advanced Study Institute in Elementary Particle Physics: New Frontiers in Fields and Strings (TASI 2015): Boulder, CO, USA, June 1-26, 2015*, pp. 1–74. 2017. `arXiv:1602.07982 [hep-th]`.

[139] J. D. Qualls, "Lectures on Conformal Field Theory," `arXiv:1511.04074 [hep-th]`.

[140] D. Landau and K. Binder, *A Guide to Monte Carlo Simulations in Statistical Physics*. Cambridge University Press, New York, NY, USA, 2005.

[141] M. Caselle, G. Costagliola, and N. Magnoli, "Numerical determination of the operator-product-expansion coefficients in the 3D Ising model from off-critical correlators," *Phys. Rev.* D91 no. 6, (2015) 061901, `arXiv:1501.04065 [hep-th]`.

[142] M. Caselle, G. Costagliola, and N. Magnoli, "Conformal perturbation of off-critical correlators in the 3D Ising universality class," *Phys. Rev.* D94 no. 2, (2016) 026005, `arXiv:1605.05133 [hep-th]`.

[143] G. Costagliola, "Operator product expansion coefficients of the 3D Ising model with a trapping potential," *Phys. Rev.* D93 no. 6, (2016) 066008, `arXiv:1511.02921 [hep-th]`.

[144] A. Wipf, "Statistical approach to quantum field theory," *Lect. Notes Phys.* 864 (2013) pp.1–390.

[145] Y. Nakayama, "Scale invariance vs conformal invariance," *Phys. Rept.* 569 (2015) 1–93, `arXiv:1302.0884 [hep-th]`.

[146] W. Janke and R. Villanova, "Three-dimensional three state Potts model revisited with new techniques," *Nucl. Phys.* B489 (1997) 679–696, `arXiv:hep-lat/9612008 [hep-lat]`.

[147] A. P. Gottlob and M. Hasenbusch, "Critical behavior of the 3-D XY model: A Monte Carlo study," `arXiv:cond-mat/9305020 [cond-mat]`.

[148] M. Campostrini, M. Hasenbusch, A. Pelissetto, and E. Vicari, "The Critical exponents of the superfluid transition in He-4," *Phys. Rev.* B74 (2006) 144506, `arXiv:cond-mat/0605083 [cond-mat]`.

[149] U. Wolff, "Collective Monte Carlo Updating for Spin Systems," *Phys. Rev. Lett.* 62 (1989) 361.

[150] H. G. Evertz, "Vectorized cluster search," *Nucl. Phys. Proc. Suppl.* 26 (1992) 620–622, `arXiv:hep-lat/9112001 [hep-lat]`.

[151] R. P. H. Wu, V. cheong Lo, and H. Huang, "Critical behavior of two-dimensional spin systems under the random-bond six-state clock model," *Journal of Applied Physics* 112 no. 6, (2012) 063924.

[152] Y. J. Deng, H. W. J. Blote, and M. P. Nightingale, "Surface and bulk transitions in three-dimensional O(n) models," *Phys. Rev.* E72 (2005) 016128–016138.

[153] A. L. Talapov and H. W. J. Blote, "The Magnetization of the 3-D Ising model," *J. Phys.* A29 (1996) 5727–5734, `arXiv:cond-mat/9603013 [cond-mat]`.

[154] M. Hasenbusch, K. Pinn, and S. Vinti, "Critical exponents of the three-dimensional Ising universality class from finite-size scaling with standard and improved actions," *Phys. Rev.* B59 (1999) 11471–11483, `arXiv:hep-lat/9806012 [hep-lat]`.

[155] S. El-Showk, M. F. Paulos, D. Poland, S. Rychkov, D. Simmons-Duffin, and A. Vichi, "Solving the 3d Ising Model with the Conformal Bootstrap II. c-Minimization and Precise Critical Exponents," *J. Stat. Phys.* 157 (2014) 869, `arXiv:1403.4545 [hep-th]`.

[156] K. Kajantie, L. Karkkainen, and K. Rummukainen, "Tension of the interface between two ordered phases in lattice SU(3) gauge theory," *Nucl. Phys.* B357 (1991) 693–712.

Acknowledgements

Over the last years I have received a lot of support from many people and organizations I feel deeply indebted to. Here, I would like to take the opportunity to express my gratitude to each of them individually.

First of all, I would like to thank my advisor Axel Maas for giving me the opportunity to research on such an interesting and challenging topic the past three years. His experience was extremely helpful and had direct impact on the outcome of this work, of course. I am thankful for his patience and his guidance, especially during the time I wrote the simulation code. Furthermore, I am grateful to him giving me the opportunity to participate in international conferences.

During my stay abroad for six months at the Friedrich-Schiller University in Jena, Germany, I worked under the supervision of Andreas Wipf on a different project. I am grateful for his hospitality and for giving me the possibility to profit from his practically endless knowledge. I received a lot of warm and friendly support from the local group members and collaborators, among them Martin Ammon and André Sternbeck.

Also, I want to thank Christian Kohlführst for all the afternoons and evenings he spent with me in Jena, discussing about my work and listening to my problems.

Moreover, I would like to acknowledge the mobility grant of the University of Graz for supporting me during my research stay in Jena. I also want to express my gratitude for the support of the FWF doctoral school W1203-N16.

The use of HPC resources provided by ZID at University of Graz and Graz University of Technology, and the Vienna Scientifc Cluster are acknowledged as well. All the lattice results presented here have been obtained using these resources.

Special thanks go to René Sondenheimer, with whom I worked on a project during my stay abroad, which turned out to be one of the main parts of the thesis. I am grateful for the many fruitful and helpful discussions we had. Also, I want to thank him for proofreading this thesis and substantially improving the content.

I am grateful to Christof Gattringer for being my mentor during the time of my PhD studies, and for always having an open ear for my problems. I am indebted to him for proofreading parts of this thesis as well.

Also, I would like to express my gratitude to all of the professors of the University of Graz for the many excellent lectures from which I profited a lot.

During my daily work time I always felt surrounded by friendly and cooperative colleagues, which I want to mention here: Adrian Blum, Angel Miramontes Lopez, Carlotta Marchis, Christian Rohrhofer, Daniel Göschl, Mario Giuliani, Jordi Paris Lopez, Marco Catillo, Mario Mitter, Oliver Orasch, and Walid Ahmed Mian. Especially, I want to thank my former office workmate and friend Markus Pak, from whom I learned a lot.

I am grateful for my friends outside of the theory department of the University, who have been very close friends of mine since I started studying physics in Graz. I am especially thankful to Robert Seebacher and Pamina Winkler.

I would like to thank my close friends Alexander Gortischnig and Stefan Kofler for many delightful and amusing times we had in- and outside of University. I am thankful to them for always listening to my problems, giving me a lot of good advice and supported me when I strongly doubted myself.

I am grateful to my family, in particular my parents Susanne and Christian Törek as well as my sister Tanja Törek, for encouraging and supporting me in all my decisions over the past years.

Last but not least, I would like to thank my fiancee Hanna Brindl the most, for the many beautiful moments, and especially for her never ending patience during all the years of my studies and especially during the time I wrote this thesis. I love you.

Thank you!